# STUDIES ON Bi-Sr-Ca-Cu-0 GLASSES AND SUPERCONDUCTING GLASS CERAMICS

A thesis submitted for the award of
the degree of
Doctor of Philosophy

by
ELIZABETH ZACHARIAS


School of Physics
University of Hyderabad
Hyderabad-500 134
India
March 1995

## CERTIFICATE

SCHOOL OF PHYSICS
UNIVERSITY OF HYDERABAD
HYDERABAD 500 134

Dated: 16 MARCH 1995.

This is to certify that **I, Elizabeth Zacharias** have carried out the research embodied in the present thesis titled **STUDIES ON Bi-Sr-Ca-Cu-O GLASSES AND SUPERCONDUCTING GLASS CERAMICS** for the full period prescribed under the Ph.D. ordinances of the University.

I declare to the best of my knowledge that no part of this thesis was earlier submitted for the award of research degree of any University.

Elizabeth
candidate
**(Elizabeth Zacharias)**

Roll No: **LP 4401**

Rajender Singh
Supervisor
**(Dr. RAJENDER SINGH)**

A.P.Pathak 16/3/95
Dean of the School
**(Prof. A. P. PATHAK)**

## ACKNOWLEDGEMENTS

It has been a great privilege to carry out this work under the able, inspiring and encouraging guidance of Dr. Rajender Singh.

I express my sincere thanks to Prof. S. R. Shenoy and Prof. A. P. Pathak, the deans, school of Physics, during the course of my Ph.D for all the facilities extended from the school.

I am also indebted to those faculty members and research scholars without whose help I could not have succeeded in completing my work. Here I would specially mention Ms. I). Ramasita, Mr. J. S. Chakravarthy, Ms. Shoba Rani and many others for their constant encouragement and help during the course of my Ph.D work.

I am grateful to Dr. Rajasekharan, school of Chemistry, for his useful guidance and discussions. I also thank Mr. Prasad, Ms. S. Ammeerunisa and my other friends in the school of Chemistry who have extended their cooperation during my work.

I am grateful to the Principal Scientific Officer Dr. K. V. Reddy and all the employees of CIL for their assistance in carrying out various measurements.

My special thanks to my friends Mr. S. Manjunath, Ms. D. Ramasita, Mr. S. Srinath, Ms. S. Jayasree, Dr. M. Ram ac hand ran, Dr. D. Palaniappan and Dr. Najmul Hassan who helped me personally in ever so many ways during my stay here.

Financial assistance from the Department of Atomic Energy (DAE), Council of Scientific and Industrial Research (CSIR) and the Department of Science and Tecnology (DST) is gratefully acknowledged.

I also thank God for giving me such wonderful parents and sister who are responsible for this day.

Lastly, words are insufficient to describe what my husband Dr. P. Murali's constant help and encouragement means to me in the completion of this thesis.

**ELIZABETH ZACHARIAS**

*Dedicated to my Parents-in-law*
*and parents*

## Table of Contents

# Chapter 1

# INTRODUCTION

The discover}' of superconductivity in La-Ba-Cu 0 with critical transition temperature of 30 K by Bednorz and Miiller in 1986 led to tremendous amount of research activity in the field of High Temperature Superconductivity. A brief out line of the historical landmarks in the area of superconductivity in general and various developments in the field of high $T_c$ superconductivity is given in the following pages. A review of various studies reported in the literature on Bi-Sr-Ca Cu-O superconductors synthesised by the glass ceramic technique is undertaken. This chapter covers the back ground and the motivation for studies presented in this thesis.

## 1.1 Historical background on superconductors:

Twenty one years after the discovery of Helium on earth, Kamrnerling Onnes in 1908, succeeded in liquifying Helium gas at 4 K. Using this new low temperature range, he studied the electrical resistivity of various metals as a function of temperature and came across the first superconductor mercury in 1911 [1]. The absence of resistivity below a certain temperature was called 'superconductivity' and that temperature the 'critical temperature[1] $T_c$. In 1933, Meissner and Ochenfield [2] demonstrated the 'Miessner effect' i.e. the expulsion of the applied magnetic field by the material in the superconducting state.

Thus superconductors are those materials which show zero electrical resistivity and Miessner effect below the critical temperature.

Several metals and metallic alloys like Nb and $Nb_3Ge$ were found to be superconducting after Hg.

A number of experimental studies were carried out to study the electrical and magnetic properties of the superconductors. From magnetization studies it was found that certain types of materials show a sudden and complete disappearance of diamagnetic signal above a certain field called the 'critical field' $H_c(T)$ and this class of materials are called the type-I superconductors. In another class of superconductors called the type-II, the material show complete diamagnetism below a field $H_{c1}(T)$ and between $H_{c1}(T)$ and a higher field $H_{c2}(T)$, they show a decreasing diamagnetic signal or are in a 'vortex state' and show zero diamagnetic signal above $H_{c2}(T)$. $H_{c1}(T)$ and $H_{c2}(T)$ are called the lower and the upper critical fields and are dependent on the temperature and the material under investigation.

Much of the understanding of superconductors has been derived from the measurements of their specific heat as a function of temperature in the superconducting and in the normal state. The specific heat in the superconducting state was found to be of an exponential form with an argument proportional to $-1/T$ suggestive of excitation of electrons across the energy gap [3].

Thermodynamic arguments were used to derive and to explain some of the properties of superconductors. From the entropy derivation in the normal and the superconducting state, and the gap in the specific heat measurement observed at $T_c$, it was deduced that

the superconducting-normal state transition at $T_c$ in the absence of a magnetic field is a second order phase transition, while it is a first order transition in the presence of a magnetic field.

London, by placing restrictions on the ordinary Maxwell's equations, introduced the London's equations [4] so that the behaviour deduced from these agree with that observed experimentally. The London's equations describe the electrodynamics of superconductivity - the resistanceless property and diamagnetism. They however fail to 'explain' the occurance of superconductivity. When a superconductor is placed in a uniform magnetic field, London's equations predicts that the flux density dies away exponentially inside the superconductor, falling to $1/\exp$ of its value at a distance called the penetration depth.

Ginzburg and Landau derived another phenomenological model by assuming that the superconducting order parameter is a complex wave function and introduced a new parameter called the 'coherence length' [3].

The basis of a quantum theory of superconductivity was laid by Bardeen, Cooper and Schrieffer in 1957. This theory postulates an attractive interaction between electrons to form Cooper pairs [5] and the effective unit of charge is 2e rather than e. Like in conventional superconductors it has been established by Cough et.al. [6] that the effective unit of charge in High-$T_c$ superconductors is 2e.

## 1.2 High Temperature superconductors:

The first of the oxide superconductors $BaPb_{1-x}Bi_xO_3$ was prepared in 1975 [7]. It has a $T_c$ of 13 K. The discovery of La-Ba-Cu-O superconductor with $T_c$ of 30 K by Bednorz

and Müller in 1986 [8] led to the discovery of many oxide superconductors with $T_c$ above liquid nitrogen temperature. The exact composition of the superconducting phase was found by Uchida et al [9] and Takagi et al [10]. The crystal structure of this phase was reported by Jorgenson et al [11] and it was seen that this structure had copper ions coordinated to four oxygen in a square plane and 2 0 atoms along c-axis to form an octahedral coordination. Substitutional studies of other 3d transition metal ions at Cu site were carried out on this system and the sharp depression in $T_c$ suggests the important role of Cu-0 planes in superconductivity [12,13].

Superconductivity in $YBa_2Cu_3O_{(7-\delta)}$ (1-2-3 superconductors) with $T_c$ about 90 K was first reported by Wu et al [14]. The superconducting properties of this system of superconductors are very sensitive to the value of *S* [15, 16].

The crystal structure of superconducting and nonsuperconducting Y-Ba-Cu-0 compound has been reported by many groups [17-20], and it was found that the superconducting phase has an orthorhombic structure while it is tetragonal for the nonsuperconducting phase. The presence of Cu in two sites chains and planes was also reported.

The complete substitution of Yttrium by other rare earth elements except Pr, Ce and Tb, did not affect the superconducting properties of this system of superconductors [21-25]. Substitutional studies of 3d Transition Metal (TM) ions at Cu site in Y-Ba-Cu-0 system drastically decreased $T_c$ and transformed the structure to tetragonal [26-31].

Recently two other superconducting phases namely $YBa_2Cu_4O_y$ (1-2-4 superconductors) [32-34] and $Y_2Ba_4Cu_7O_y$ (2-4-7 superconductors) [35] with $T_c$'s 80 and 40 K respectively, have been identified and their crystal structures reported [36].

Rare earth free Bi-Sr-Cu-0 system was found to show superconductivity at 20 K [37]. Maeda et al [38] found indications of superconductivity even above 100 K in Bi-Sr-Ca-Cu-0 systems. This system has three superconducting phases with the general formula $Bi_2Sr_2Ca_{n-1}Cu_nO_y$ with n = 1, 2, 3 and having $T_c$s 10, 85 and 110 K respectively [39-43].

Takano et al [44 (a)] and Cava et al [44 (b)] demonstrated that partial substitution of Pb for Bi in Bi Sr-Ca-Cu-O promotes the formation of 110 K phase superconductors. Following this, a lot of studies have been carried out with various starting compositions and preparation methods to achieve higher $T_c$ [46- 50].

Tl based superconductors were first reported by Sheng and Herman [51]. Two series $Tl_2Ba_2Ca_{n-1}Cu_nO_{2n+1}$ [52-55] and $TlBa_2Ca_{n-1}Cu_nO_{2n+3}$ [56-58], n = 1, 2, 3 have been reported. The structures of the Tl compounds are similar to that of the Bi-compounds except for the c-axis lengths.

Another family of superconductors $Pb_2ASr_2Cu_3O_{8+\delta}$ (A = rare earths, Ca) with $T_c$ around 70 K has been reported by Cava et al [59].

A new family of superconductors $Nd_{2-x}Ce_xCuO_4$ with $T_{c(onset)}$ at around 25 K was found by Tokura et al [60]. This family of superconductors have electrons as the charge carriers unlike other Cu-oxide based superconductors in which holes are the charge carriers.

Another recent development in the area of superconductivity is **the** discovery of superconductivity at 20-30 K in Potassium and Cerium doped $C_{60}$ [61-62].

$HgBa_2CuO_4$ was reported to become superconductor at 94 K [63] and Hg-Ba-Ca-Cu-0 shows $T_c$ *as* high as 134 K [64].

## 1.3 Bi-Sr-Ca-Cu-O superconductors:

The structural details of Bi-Sr-Ca-Cu-O system is very complicated and different types of unit cells with different unit cell parameters have been reported [65-70]. Tarascon [42] reported the crystal structure of the Bi-2201, Bi-2212 and Bi-2223 superconducting phases assuming a pseudo tetragonal symmetry (fig -1.1). The $a = 6 \approx 5.4$ *A* and does not vary for the three phases. The c-parameters are 24.6, 30.6 and 37.1 *A* for the 10, 85 and 110 K phases respectively.

The 2201 superconductor has Cu in an elongated octahedral symmetry. One Cu atom is square coordinated by 4 oxygen atoms with a Cu-0 bond length equal to 1.94 *A*. The two remaining oxygen atoms are bonded to Cu at a bond length of 2.6 *A*. The 2201 structure has one $CuO_2$ layer between two $SrO_2$ layers (fig-1.1(A)). Strontium has nine nearest oxygen atoms with an average Sr-O distance of $\sim 2.7$ *A*.

The 2212 structure as shown in fig-l.l(B) has $CuO_2/Ca/CuO_2$ replacing the CuO plane in the Bi-2201 structure. Ca has a coordination of eight and has no O in its plane. Cu has only five nearest neighbours in square pyramidal coordination unlike the elongated octahedral symmetry in Bi-2201.

The Bi-2223 structure is similar to the 2212 phase but has additional Ca and CuO planes (fig-l.l(C)).

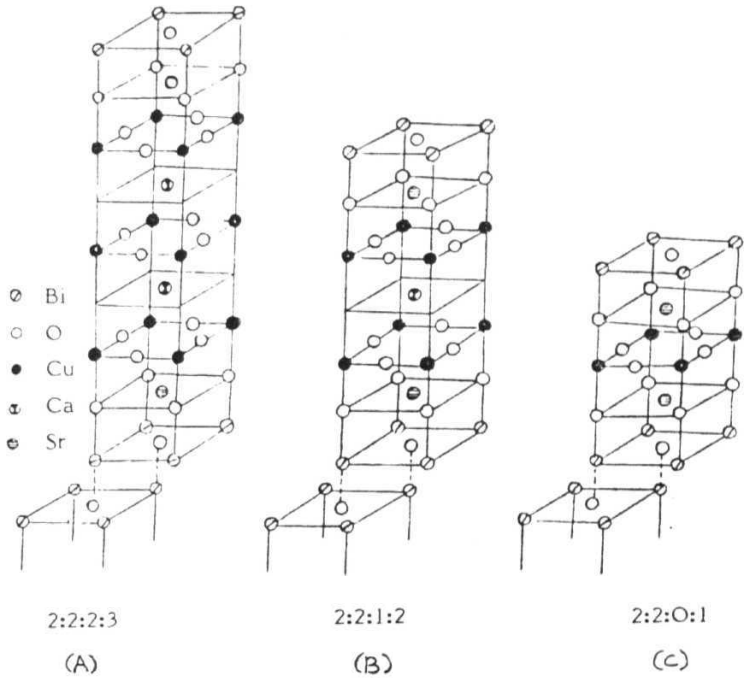


**Fig-1.1 Crystal substructure of the three superconducting phases of Bi-Sr-Ca-Cu-0 superconductors.**

## 1.4 Bi-Sr-Ca-Cu-O glass-ceramic superconductors and the motivation for the present work:

The most commonly used methods for the synthesis of high $T_c$ superconductors are the solid state sintering method and the sol-gel method. Another method of preparation is the 'glass ceramic route' which gained popularity due to its promising application values. The conventional solid state reaction method of preparation of these superconductors give poorly sintered materials with low density [71].

Glass-ceramics are crystalline materials formed through the controlled devitrification of glasses. Glasses are melted, fabricated to shape and then converted to a ceramic by a specific heat treatment. This process of obtaining crystalline material is called the 'glass-ceramic route'. The glass ceramic route offers advantages such as possible improvement in the gross homogeneity, reduced phase segregation and extended solid solubility. With the appropriate choice of starting composition, this method needs a relatively shorter preparation duration to give dense and pore free superconductors with preferred orientation of superconducting crystallites. This method is also important in view of the practical applications as the samples could be moulded into specific shapes such as films [72], fibres [73-77], rods [78-81], whiskers [82], hollow cylinders [83] etc.

The glass forming ability of the Bi-Sr-Ca-Cu-O system was first reported by Komatsu et al [84] in 1988 and the glass forming region of the system (fig-1.2) was reported by Komatsu [85] and Tohge [86]. Bi-Sr-Ca-Cu-O (BSCCO) or Bi-Pb-Sr-Ca-Cu-O (Pb-BSCCO) glasses of various compositions were sucessfully prepared by various groups and some of these glasses were converted to glass-ceramic superconductors through controlled

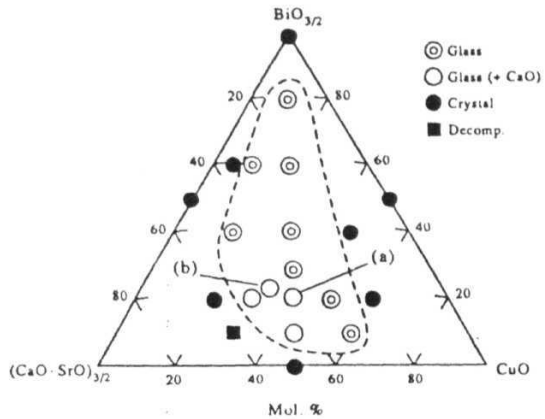


**Fig-1.2 Glass- forming region of the pse u do ternary system $BiO_{3/2}$-$(CaO.SrO)_{3/2}$-CuO samples (a) and (b) correspond to $BiCaSrCu_2O_x$ and $Bi_2Ca_2Sr_2Cu_3O_x$ respectively.**

devitrification [87-95]. The term 'high $T_c$ superconducting glass-ceramics' was coined by Komatsu et al [84] to describe superconducting materials obtained by this technique.

A number of fabrication techniques have been attempted to obtain glasses and glass ceramics of different forms. Thin tubes and coils of Bi-Sr-Ca-Cu-0 glasses have been synthesised by Abe et al [78] by the melt casting technique. This is achieved by sucking the melt into cold silica glass tubes by vaccuum techniques. Very fine glass rods could be obtained by the addition of $Al(OH)_3$ or $Al_2O_3$ to the melt. Abe et al [83] also successfully prepared superconducting pipes using this technique. These find applications in microwave cavities, magnetic shielding and electrical current transportation. Addition of $Al_2O_3$ lowers the melting temperature, increases the viscosity of the melt making it easier to form glass and also enhances the phase seperation of the 2212 phase which is formed directly as a primary crystalline phase during cooling [96,97].

It is also reported that the addition of $Al^{+3}$ ions play an important role in the formation of whiskers of 2212 superconductors [81,98]. Wang et al [82] prepared superconducting whiskers by heating glassy metal quenched plates in a stream of oxygen gas.

Komatsu et al [74] reported the drawing of BSCCO glass fibres from BSCCO glass plates softened in an electric furnace and subsequently heat treating them to give glass-ceramic fibres. Gas jet fibrization was also found to be applicable to the preparation of fibtres by LeBeau et al [76]. This technique involves the use of a gas stream to force a liquid drop into a nozzle where it is shaped and frozen by the flowing gas. Zheng et al have reported the continous drawing of fibre from $V_2O_5$ doped $Bi_4Sr_3Ca_3Cu_4O_y$ glass [77].

Yoshimura et al [72] utilized the rapid **quenching after rapid melting (RQRM)** technique for preparing films. In this technique **a sample is prepared in the form of a rod** by **cold** isostatic pressing. The bottom of this rod is **then melted in a $X_e$-arc imaging furnace.** The molten droplet is dropped into a rapidly rotating **stainless steel twin roller** which produces the amorphous films.

Thick films of 2212 superconductors were prepared by the deposition of 4334 glass material on a silver substrate and subsequently exposing it to quick devitrification to obtain aligned superconducting crystallites [99].

Various methods have been attempted to improve the stability of the glasses and the superconducting properties of the glass-ceramics. The addition of boron and silica was found to increase the stability of the glasses [100 ]. But higher boron content deterred the formation of the 2212 phase. Addition of Sb effectively improved the formation of 2223 phase and resulted in increased connectivity between the superconducting grains [101-102].

Randomly oriented growth of 2223 superconducting grains gave rise to the problem of decreased density of the glass ceramics and therefore lower current density. Miller et al [103] showed that hot pressing of quenched glass flakes at **temperatures close** to glass transition temperature helped in obtaining dense and pore free superconducting ceramics. Texturing experiments by Abe et al [78] by the heat treatment of glasses **in thermal** gradients helped in the greater directional growth of the **2223 phase.**

**Kim** et al [104] could obtain larger crystals of 2223 at a **relatively** shorter **time by** the seeding technique i. e., by adding $Bi_{1.8}Pb_{.33}Sr_{1.87}Ca_2O_x$ seeds **to both polycrystalline**

and glassy Bi-Pb-Sr-Ca-Cu-O materials.

Substantial attention has been focused on seeking optimised starting compositions, processing conditions and material properties in order to maximise the applications of the materials prepared by this technique. There is however a lot of difference in the conclusions arrived at by different groups and there are still problems associated with the materials synthesised by this technique which may affect commercial applications. There have been many reports concerning the effect of heat treatment on the superconducting properties of BSCCO and Pb-BSCCO glass-ceramics in order to understand the correlation between the superconducting properties and the normal state resistivity or magnetic susceptibility (83, 84, 92, 100, 105-119]. Several groups have reported the detailed crystallization and phase formation studies on both BSCCO [113, 120-126] and Pb-BSCCO [109-112, 128-135] glasses. Kinetic studies of the crystallization of the BSCCO [120-122, 124, 125] and Pb-BSCCO [109, 110, 128] glasses have also been reported. Tatasumisago et al [120] reported the kinetic studies of crystallization of the glasses of composition $Bi_xSr_2CaCu_2O_w$ (x=1.5, 2.7) using DSC technique. They reported crystallization energy of about 400 kJ/mol. and concluded that crystallization starts from the surface. Komatsu et al [121] reported crystallization kinetics of $Bi_2SrCaCu_2O_x$ glasses. DTA and X-ray diffraction were used by Mathias et al [136] and Sato et al [124] to understand the kinetics of crystallization of $Bi_2Sr_2CaCu_2O_y$ glasses. Zheng et al [122, 127] reported the effect of $Cu^{+1}/Cu_{total}$ on the thermal stability and the initial crystallization behaviour of $Bi_4Sr_3Ca_3Cu_4O_y$ glasses using DSC and X-ray diffraction techniques. They concluded that the initial cryatal growth is 3-dimensional. They however did not clarify the formation mechanism of the 85 K superconducting phase. The kinetic studies of crystallization have been reported by Bansal [128] on $Bi_{1.5}Pb_{0.5}Sr_2Ca_2Cu_3O_x$ and by Wong-Ng et al [109,

110] on $Bi_{1.84}Pb_{0.34}Sr_{1.91}Ca_{2.03}Cu_{3.06}O_y$ and $Bi_{1.5}Pb_{0.5}Sr_{1.25}Ca_{1.75}Cu_2O_y$ glasses using X ray diffraction, DTA and resistivity measurements.

Understanding the properties of the glasses which are precursors of high $T_c$ glass-ceramic superconductors might be helpful in optimising the glass ceramic process. The Bi-Sr-Ca-Cu-O glasses are a relatively new family of TMO glasses which do not contain any of the conventional glass formers like $TeO_2$, $P_2O_5$, $B_2O_3$, $GeO_2$ etc. It would therefore be of interest even to study the properties of these glasses as such and campare them with other TMO glasses reported in the literature. In this connection the detailed study of DC electrical conductivity in these glasses may be useful to ascertain the nature of the conduction mechanism and analyse the experimental data in view of various theoretical models reported in the literature.

When a second transition metal ion is introduced in a TM containing glass matrix, it brings about effects like oxidation-reduction reaction between the two types of TM ions, phase separation, additional distortion of the glass matrix [137-139] etc. $Bi_4Sr_3Ca_3Cu_4O_x$ glasses partially substituted with 3d dopants like Fe, Cr and Mn at Cu-site were synthesised to study the effect of a second TM doping on the properties of these glasses.

Substitutional studies in high $T_c$ superconductors have been found to be of prime interest both from theoretical as well as experimental point of view [140]. All the major high $T_c$ superconductors have their genesis in substitution at one or more cationic sites in the parent materials.

Of all the cationic sites, CuO network is of prime importance for the occurance of

superconductivity in these materials [141, 142]. Hence a systematic creation of point defects in the $CuO_2$ planes by replacing the Cu atoms by other 3d elements is a useful tool for probing parameters essential for superconductivity. The change in normal electronic properties when point defects are introduced into the $CuO_2$ planes can give information regarding the interaction of charge carriers with impurity.

Substitutional effects at Cu site in Y-123 has been extensively studied [26-31]. Cu in Y-123 has two sites- the chain site and the plane site [17-20] and the influence of substitution at the chain site and at the plane site on superconductivity are very much different. Though detailed X-ray and neutron diffraction work have been devoted to the problem of site preference for a specific dopant, the site preference is still controversial especially for low concentrations of dopants [143-145].

Substitutional studies at Cu site on BSCCO superconductors would be more informative since the Cu in this family of superconductors has only one site– the CuO plane. There are however few reports on the 3d TM substitution in the Bi-superconductors. This is because unlike the Y-123 system, the Bi system has three related superconducting phases and it is difficult to prepare a single phase superconductor with a consistent $T_c$.

There have been some reports on the effect of of 3d TM dopants like Fe, Co, Ni and Zn on the superconducting properties of 2212 superconductors synthesised by the conventional solid state reaction method [146-150]. There is no good agreement between the results reported by different groups presumably because of the different preparation conditions used by different groups. However there has been no report on the synthesis of 3d TM doped superconductors by the glass ceramic route. It is also noticed that partial substitution of Mn and Cr has not been attempted in the superconducting Bi-samples.

Substitutional studies on BSCCO superconductors synthesised by the glass route would be more meaningful as a thorough mixing of the dopants can be ensured while synthesising the glasses, thereby reducing the possibility of formation of precipitates of the dopants.

In view of the above, the present studies were undertaken with the following objectives. The first objective has been to synthesise BSCCO glasses of various compositions (varying CuO content) and to study various properties of these glasses especially the DC electrical conductivity in order to ascertain the nature of conduction mechanism in these glasses and to analyse the data in view of various theoretical models available in the literature.

Secondly, detailed systematic studies were carried out on the $Bi_4Sr_3Ca_3Cu_4O_z$ glasses in order to understand the superconducting phase formation and mechanisms of crystal* lization. The parallel studies of electrical resistivity and X-ray diffraction on $Bi_4Sr_3Ca_3Cu_4O_z$ glasses as a function of heat treatment temperature and duration was carried out to understand the phase formation and its effect on the electrical conduction.

Thirdly, the effect of CuO content on the structure and properties of the BSCCO glasses and the corresponding glass-ceramics was undertaken. This study is to ascertain whether there is any correlation between the properties of the glass and the corresponding glass-ceramic.

Fe, Cr and Mn doped BSCCO glasses were synthesised to study the effect of 3d TM dopants on the properties of these glasses. The 3d TM doped glass-ceramics were synthesised from the glass precursors in order to understand the influence of 3d TM dopants

on the structure and the superconducting properties of these ceramics. Since the present studies show that $Bi_4Sr_3Ca_3Cu_4O_x$ glass gives the best superconducting properties among all the compositions studied, all the doping studies were carried out on this composition.

Chapter II of the thesis deals with the description of various experimental techniques used in the course of this study. DSC, DC conductivity, RT magnetic susceptibility, ESR and FT/IR are the studies carried out on the glasses while XRD, electrical resistivity, AC susceptibility and SEM studies were conducted on the Bi-glass ceramic superconductors.

In chapter III, the results of various studies on the undoped and the 3d TM doped Bi-Sr-Ca-Cu-O glasses have been discussed and analysed. The detailed analysis of the DC conductivity data has been undertaken in view of various theoretical models available in the literature.

Chapter IV contains the results of the crystallization studies on Bi-Sr-Ca-Cu-O glasses to obtain glass-ceramic superconductors. The results and analysis of studies on undoped and 3d TM doped glass ceramic superconductors have also been discussed.

At the end, the summary of the present studies and conclusions are included.

# Chapter 2

# EXPERIMENTAL TECHNIQUES

This chapter deals with the description of various experimental techniques used in the course of this study. The techniques include X-Ray Diffraction (XRD), Differential Scanning Calorimetry (DSC), Magnetic Susceptibility, Infra-Red (IR) spectroscopy, density measurements, Electron Spin Resonance (ESR), DC Resistivity (4-probe method), AC Susceptibility (Meissner studies) and Scanning Electron Microscopy (SEM). A brief description of each technique and its utilization in the present study is given in the following pages.

## 2.1 X-Ray Diffraction:

X-ray is the portion of the electromagnetic spectrum between 1-200 $A$. Only a small part of the total X-ray spectrum (0.2-20 $A$) is used by conventional X-ray spectrometer. The X-rays reflected from a lattice plane follow the Bragg's equation

$$nX = 2d_{hkl}sin\theta \tag{2.1}$$

where n is an integer (order of reflection)

A is the wave length of the X-rays used

$d_{hkl}$, the **interplanar** spacing between planes having miller indices $h, k, l$

**and** $\theta$ **the angle** at which the X-ray beams are incident on the plane.

In a poly crystalline material or the powder of a crystalline material, the crystals are randomly oriented. If such a sample is struck by an X-ray beam, there may be many planes which are oriented in such a way that Bragg's law is satisfied and we obtain a resultant diffraction pattern with peaks corresponding to all such planes. In order that more number of planes are exposed, the sample is rotated by an angle *9* on its own axis during exposure. The diffracted beams are collected by a scintillating counter which acts as a detector. This is rotated by *20.* This output is fed to a recorder which records the output (which is proportional to the intensity of the diffracted beam) versus *26.*

In order to obtain a powder XRD spectra, the fine powder of the material under study was mounted on a perspex plate using vacuum grease as a binder. Bulk XRD spectras were obtained by using bulk samples.

From a careful study of the XRD spectra, a flood of information on the structural aspects of the sample can be obtained. The XRD pattern is unique for every sample. The position of the peak helps in the determination of the cell parameters, the d values and the shape of the unit cell or about the arrangement of lattice points in the unit cell. The lattice parameters can be calculated by indexing the sharp peaks (assigning $h, k, l$ values) and then using the relationship

$$(h^2/a^2 + k^2/b^2 + l^2/c^2)d_{hkl}^2 = 1 \qquad (2.2)$$

From the positions, the relative intensities of the peaks or from the area under its profile, the position of the atoms in a unit cell can be determined. The orientation of the crystallites can also be determined from the relative intensities. The shape of the peak provides information regarding the crystallite size and lattice imperfections including strains.

The XRD studies at room temperature were carried out using a SIEFERT X-RAY diffractometer, the schematic diagram of which is given in fig-2.1. $Cuk_{\alpha}$ radiation (A = 1.5418 *X)* was used. The machine was operated with a beam current of 30 mA and power of 40 kV. For phase identification, the patterns were compared against standard patterns reported in the literature. In order to obtain the cell parameters accurately, the data *(20* and *hkl* values) were fed to a programme assuming a pseudo tetragonal symmetry and the cell parameters obtained with an accuracy of 2 decimal places. The error in the estimation of cell parameters could be due to small error in reading the *20* values which is ±0.1°.

## 2.2 Differential Scanning Calorimetry:

DSC is a technique in which the temperature of the sample studied ($T_s$) is compared to that of an inert reference material ($T_r$) during a programmed change in temperature. The two do not register any difference in temperature until some thermal event such as structural relaxation, melting, decomposing or change in the crystal structure of the sample occurs. If the sample temperature lags behind the reference, then the event is endothermic and is exothermic if the sample temperature is greater. This difference in temperature AT is calorimetric in DSC. The DSC plot is obtained by recording this change in enthalpy as a function of scanning temperature. The horizontal baseline corresponds to AT = 0.

The schematic diagram of the DSC instrument is given in fig-2.2. A constantan disc acts as a primary means of transferring heat to the sample and reference positions. It is also one of the elements of the temperature measuring thermoelectric junctions. The sample and the reference are placed in pans which sit on raised platforms on the constantan disc. The differential heat flow to the sample and reference is monitored by

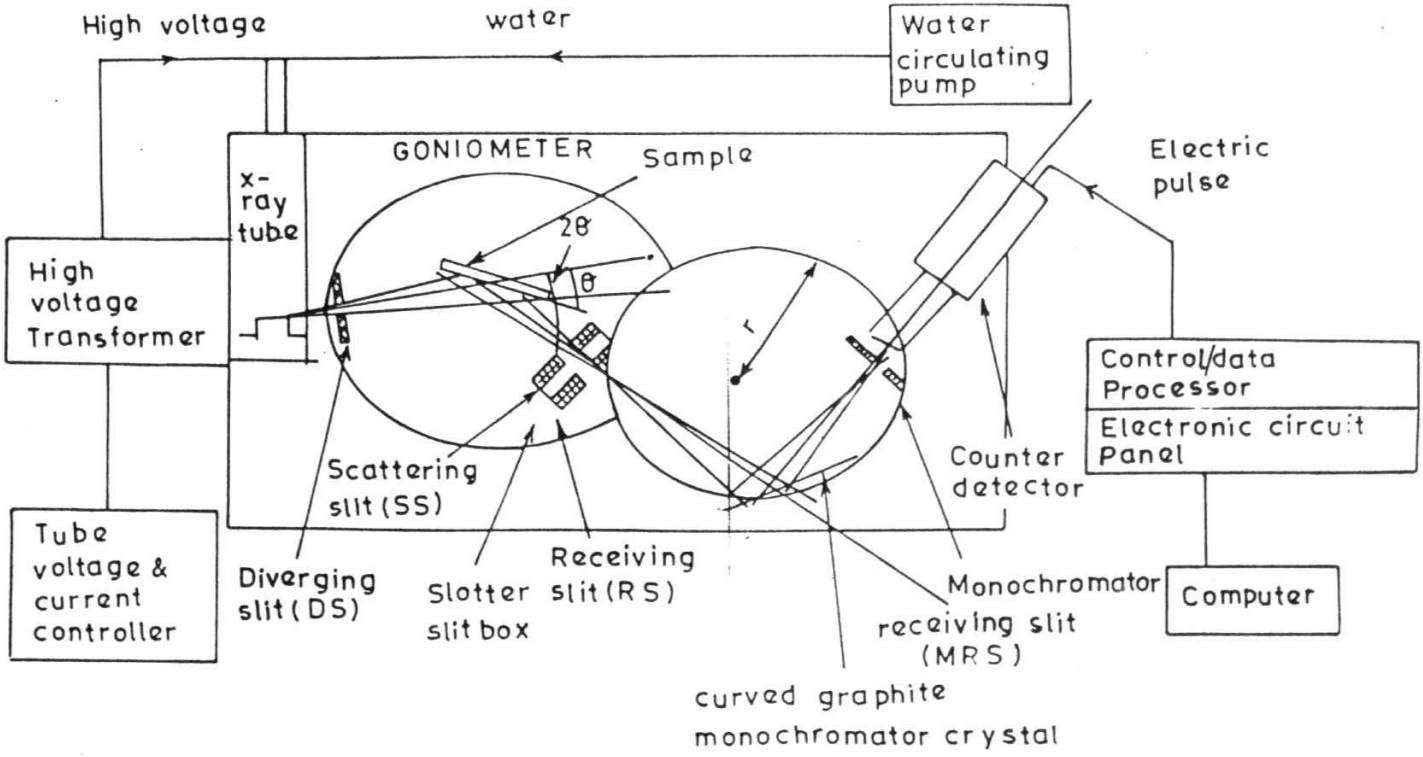


Fig-2.1 Schematic diagram of an X-Ray Diffractometer.

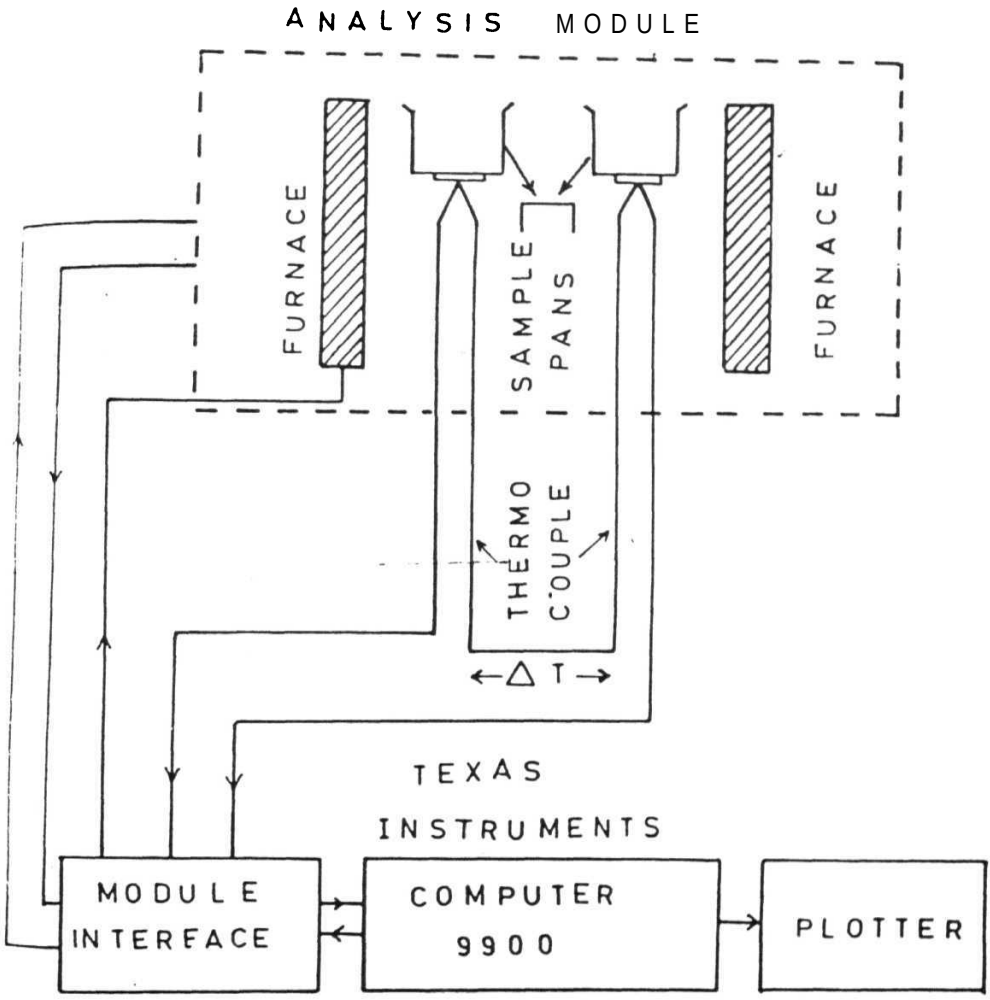


**Fig-2.2 Schematic diagram describing a Differential Scanning Calorimeter.**

chromel-constantan area thermocouples formed by the junction of the constantan disc and chromel wafer which center the bottom to each platform. Chromel and alumel wires are connected to the under side of the chromel wafers and the resultant chromel-alumel thermocouple is used to directly monitor the sample and reference temperatures. The difference AT between sample and reference is given by

$$\Delta T = T_s - T_r + R(C_s - C_r)dT_p/dt \qquad (2.3)$$

where C is the total heat capacity of the sample (or reference) plus crucible, R is the thermal resistance and $dT_p/dt$, the rate at which the programmed temperature changes. The enthalpy can be obtained from the area under the peak by comparing against a reference material with known enthalpy changes.

DSC studies were carried out on amorphous Bi-Sr-Ca-Cu-O system to obtain parameters like the crystallization onset temperature ($T_o$), the glass transition temperature ($T_g$) and the crystallization temperature ($T_x$) using commercial Perkin-Elmer DSC-4 instrument equipped with a data processing system. The crystallization activation energy and Avarami constant for the present glasses were also estimated.

## 2.3 Electron Spin Resonance:

A highly uniform and stable static magnetic field H is applied to a paramagnetic material placed in a microwave resonant cavity. The microwave magnetic component perpendicular to the direction of H, causes magnetic dipole transitions when microwave energy $h\nu$ (where $\nu$ is the frequency of the microwave) is equal to the Zeeman energy splitting $g\beta H$ of the two spin states (M = 1/2 and M = -1/2) of the paramagnetic species i.e. $h\nu = g\beta H$, where g is the spectroscopic splitting factor representing the nature of unpaired

electrons and $\beta$ is the Bohr magneton *(0* = eh/2me = 9.274 $\times 10^{-24}$ J/T). Resonance transitions are obtained by sweeping the magnetic field, rather than sweeping the microwave frequency. The type of unpaired electron, the nature of electron spins (s,p,d type) and their microscopic environments can be derived from ESR parameters.

The present studies were carried out using a JEOL FE 3X X-band ESR spectrometer. The spectrometer consists of a Gunn oscillator as a microwave source whose frequency and power can be varied to the desired level. The cavity resonator is in TE(Oll) cylindrical mode with a goniometer which facilitates the sample to be at a point where the magnetic field is most homogenous and uniform. The detection and modulation system monitors, amplifies and records the signal. The magnet system provides a highly stable, linearly variable and homogenous magnetic field. The variable temperature setup which is attached to the spectrometer is controlled by a digital temperature controller in the low and high temperature ranges to an accuracy of ±0.1°. The schematic diagram of the set up is given in the fig-2.3. All the samples were scanned using a modulation frequency of 100 KHz, modulation width of 6.3 G and microwave power of 5 mW.

## 2.4 DC conductivity studies on amorphous materials:

The two methods used in the resistivity measurements are the constant voltage and the constant current methods. Low current measurement techniques are often used to determine the value of high resistances. For this, a constant voltage is impressed across the resistance to be measured and the resulting current is read from an ammeter.

The errors in low current measurements arise from generated currents in the various circuit elements. Some of the commonly generated currents are the thermoelectric

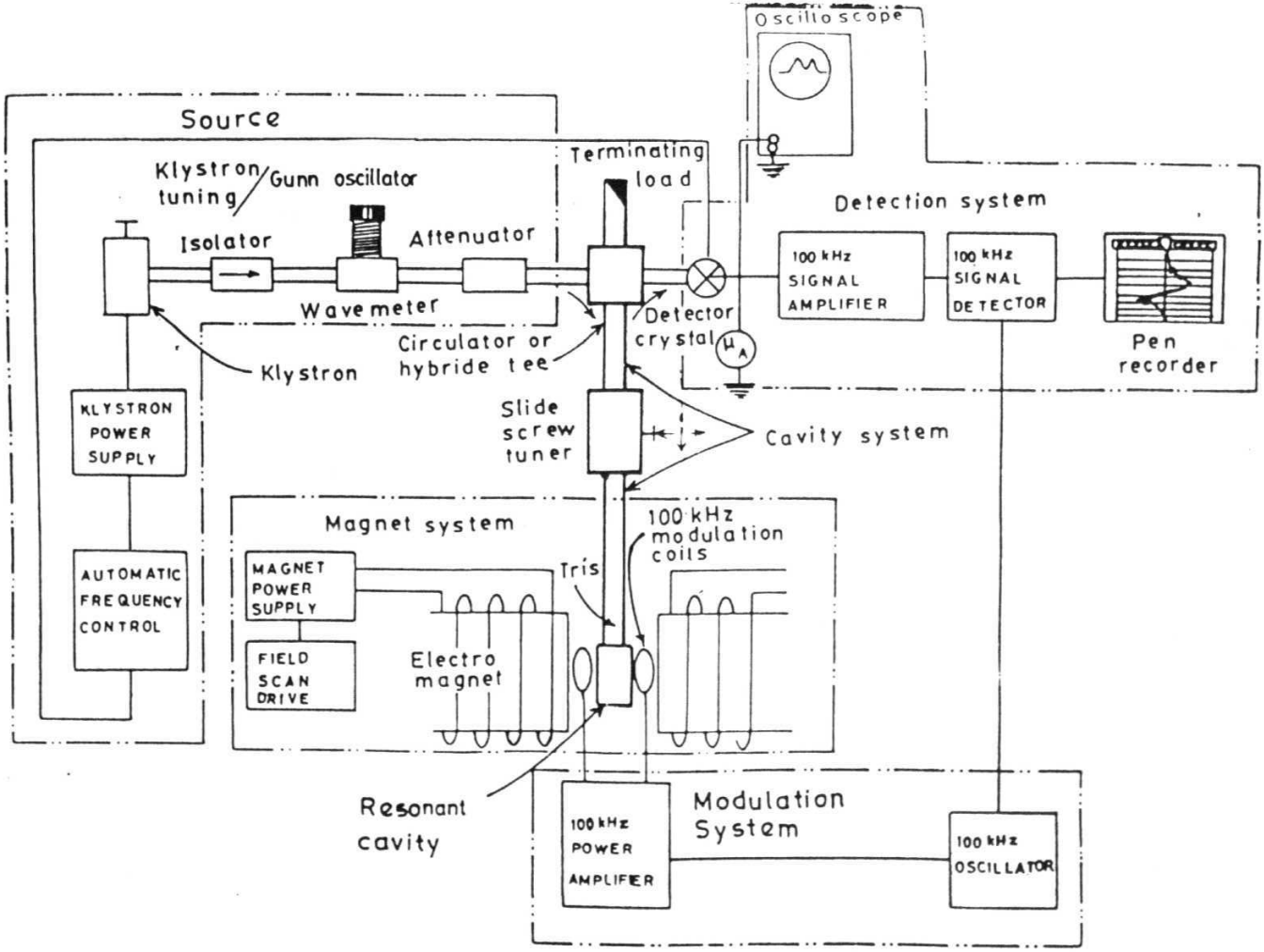


Fig-2.3 Schematic diagram of an Electron Spin Resonance spectrometer.

currents generated due to the friction within a coaxial cable, the piezoelectric currents generated due to mechanical stress and the noise currents from electrochemical effects. Another source of error is due to the ground loops formed by the ground leads which can induce sufficient disturbance voltage. This can be prevented by grounding the set up at only one point. The high impedance level of electrometers prevent the fast decay of electrostatic effects. This effect can be minimised by keeping the set up away from power lines and other sources and by proper shielding. The effects of leakage resistance can be minimised by the use of good quality triaxial cable and the use of guarded input connections. Capacitance effects can be countered by minimising the capacitance in the circuit, by use of short and low capacitance cables.

The measurements were carried out on the glasses by the standard 2-probe method as a function of temperature. Two different experimental set ups were used · one for the temperature range below RT and another for temperatures above RT. The low temperature cryostat was immersed in a liquid nitrogen dewar to obtain low temperatures, while the high temperature set up was placed in a closed chamber with a heater to raise the temperature. A schematic representation of the experimental set up is described in fig-2.4. The cryostat is connected to a Kiethley 617 programmable electrometer with built in constant voltage source and coupled with a Lakeshore temperature controller equipped with a Si-sensor. A temperature accuracy of ±0.2 K could be obtained. The parallel faces of the samples were coated with silver paint. In order to relieve the samples of any mechanical stress and to stabilise the silver electrodes on the faces of the samples, the glasses were annealed at a temperature $\approx 100^{o}C$ below the glass transition temperature of these glasses. Ohmic behaviour was ascertained and all the necessary precautions to minimise errors in the measurement of current were taken. The DC conductivity data as a function of temperature from $480^{o}C$ down to the lowest temperature where the current

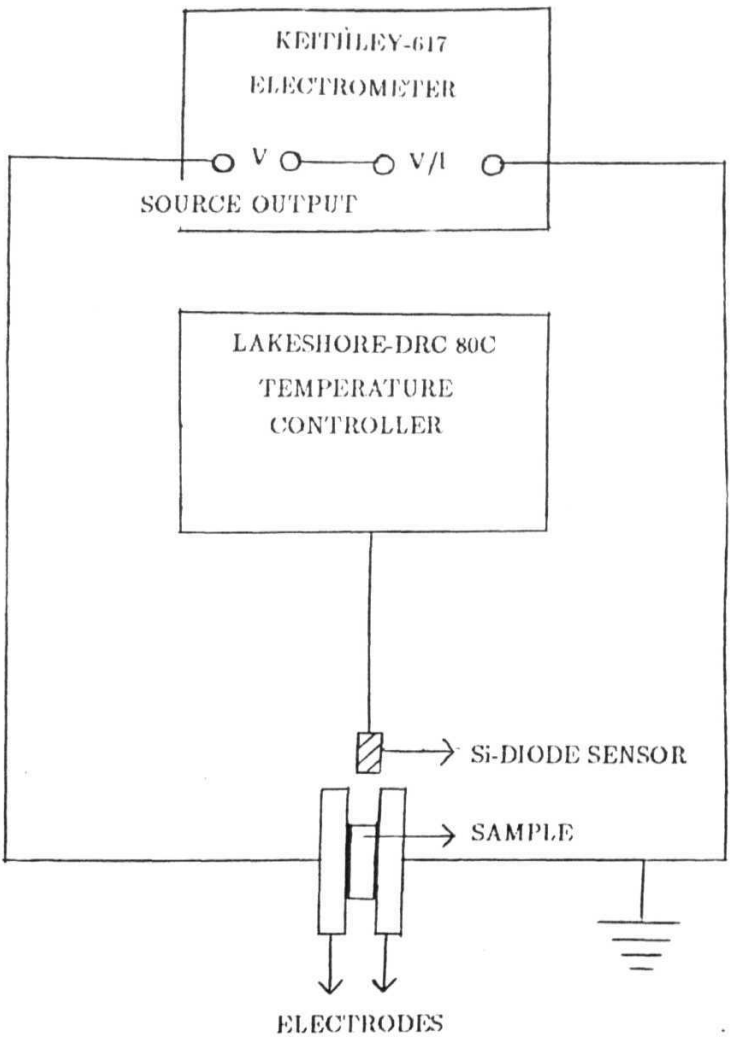


**Fig-2.4 Schematic representation of the experimental set up for measurement of DC conductivity as a function of temperature.**

across the sample was ≈ $10^{-14}$ A (limitation of the electrometer) was recorded.

The conductivity at a given temperature is obtained from the relationship

$$v(T) = (1(T)/V).(l/A) \quad (2.4)$$

where $V$ is the constant voltage applied,
$I(T)$ is the current at a temperature T,
$l$ is the thickness of the sample
and $A$ the area of cross section of the sample.

## 2.5 FT Infra-Red studies:

Infra-Red region is that portion of the electromagnetic spectrum which lies between 3600 $cm^{-1}$ to around 300 $cm^{-1}$ and the far IR region covers approximately 300 $cm^{-1}$ to 20 $cm^{-1}$ wavenumbers. The essential component of an IR spectrometer are the source of IR radiation, a detector and a recorder. When the energy of the radiation transmitted by a reference and the sample is the same, the detector does not produce any signal. When the sample absorbs radiation and results in an inequality in the transmitted beams, a resultant pulsating signal is produced with frequency equal to the frequency of the IR radiation. The recorder records such signals as the whole spectrum is scanned.

JASCO FT IR-5300 spectrometer has been used for the present study as the fourier transform method enables a large sampling and a better resolution. This is a transmission spectrometer and scans the IR region between 4600 to 400 $cm^{-1}$.

## 2.6 RT Magnetic susceptibility studies:

**The three** methods by which the magnetic susceptibility can be **obtained are the Guoy, the Faraday and** the NMR method. Room temperature magnetic **susceptibility studies were carried out using the** Faraday's method on a CAHN **1000** system. **In this technique a small** volume of sample is subjected to a region of strong magnetic **field** so **that the** product **H.(dH/dx)** is constant over the volume of the sample. Sensitive **weighing techniques** (quartz fibre torsion balance) are used to detect the forces acting on the samples and the whole set up is enclosed in a glass enclosure to avoid external disturbances. The force acting on the sample in the absence and in the presence of the magnetic field is measured. The resultant force on the sample is an indirect measure of the susceptibility. This is compared against reference samples of known susceptibility in order to obtain the susceptibility of the sample. $CuSO_4.5H_2O$ and $HgCo(CNS)_4$ were used as **the** references in the present study. The system is calibrated to measure the forces in units of weight. The susceptibility $\chi_{sample}$ of the sample is given by the equation

$$\chi_{sample} = XrcJ.(w_{ref}/\Delta w_{ref}).(\Delta w_{sample}/w_{sample}) \quad (2.5)$$

where $\chi_{ref}$ is the susceptibility of the reference,

$w_{ref}$ and $w_{sample}$ are the weights of the reference and the sample in the absence of magnetic field,

$\Delta w_{ref}$ and $\Delta w_{sample}$ are the weight changes of the reference material **and** the sample after **the field** is applied.

**The balance has a sensitivity of $1\mu g$ and susceptibility values with an error of $\pm 0.1 \times 10^{-6}$ $gm^{-1}$ can be obtained.**

## 2.7 Density measurement:

The density of irregular shaped solids can be determined by the Archimedes method. The density of our samples were obtained using a **programmable Sartorius micro balance** using 2121 density programme. The error in the density measurement **was ±0.01** gm/cm$^3$.

The density is obtained from the relation

$$\rho = W_a.\rho_f/(W_a - W_f) \qquad \textbf{(2.6)}$$

where $p$ is the density of the sample,
$W_a$ is the weight of the sample in air,
$W_f$ is the weight of the sample in fluid,
and $\rho_f$ is the density of the fluid used.

Double distilled water and $CCl_4$ were the fluids used for the density measurements of our samples.

## 2.8 DC electrical resistivity studies:

The two probe method is used to measure resistances greater than 10Ω. But when this method is used to measure low resistances, the leads which carry the test current causes **a** significant voltage drop and hence the lead resistance are significant and introduce considerable errors in the measurement. Therefore, the four probe **method is generally preferred for** the measurement of low resistances. Although some **small current may flow through the** sense leads, the current is small (pA or less) **and hence the voltage drop** across **the lead** is negligible and the voltage measured by the meter is **same** as that **across**

the sample. In order to minimise the effects of voltage drop across test leads in the measurement, the voltage sensing leads are connected as close as possible to the resistor. The effects of thermo EMF in the measurement of low voltages are eliminated by the current reversal method or the offset compensated Ohm method. The error can be minimised by a proper design of the cryostat to decrease thermal gradient changes.

The resistivity measurements on the superconducting samples were carried out by the four probe method in the temperature range 10-300 K using a closed cycle He refrigerator (APD Cryogenics) coupled to a Lakeshorc 330 auto tuning temperature controller equipped with a Si-diode sensor (DT-470-SD-12). We could obtain a temperature accuracy of ±0.1 K. The rectangular shaped samples were mounted on the cold head of the refrigerator using General Electric adhesive. Fine copper wires used as current and voltage leads are fixed to the sample using (Elteks) silver paint. Kiethley 224 programmable constant current source was used and the voltage measured by a Kiethley 181 nanovoltmeter taking the necessary precautions to minimise errors in the measurement of voltage. A schematic diagram of the resistivity set up is given in fig-2.5. The resistance at a given temperature is obtained using Ohm's law.

The resistivity at a given temperature is calculated by the relationship

$$p(T) = R(T).(A/l) \qquad (2.7)$$

where $R$ is the resistance at a temperature T,

$A$ is the area of cross section of the sample,

and / is the distance between the voltage leads,

The small error in the resistivity measurement is introduced because of errors in the measurement of $A$ and /.

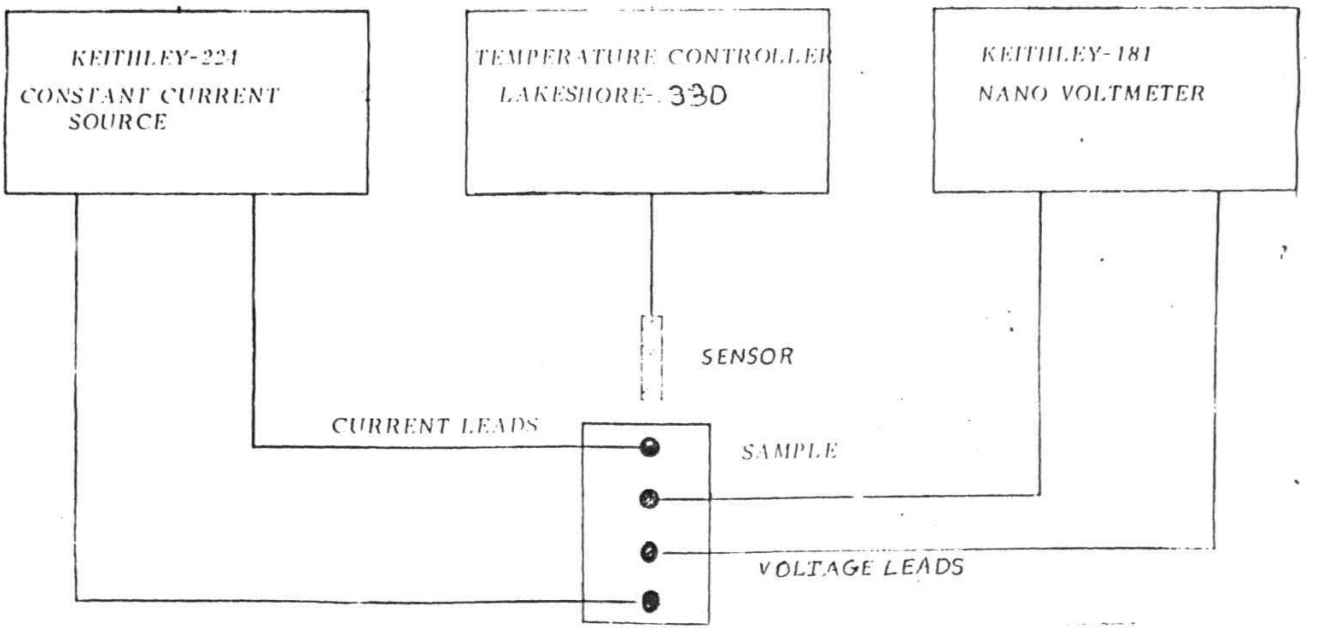


Fig-2.5 Diagram of the experimental set up used for the study of DC resistivity as a function of temperature by the 4-probe method.

## 2.9 Scanning Electron Microscopy:

A microscope is an instrument designed to render visible objects which are too small to be seen by the naked eye. Light microscope is adequate for particles which are bigger than few tenths of a millimeter in diameter but fails for objects whose sizes are smaller than the wave-length of visible light. Electron Microscopes are used for such objects. The electron microscopes use electron lenses instead of ordinary lens. An electrostatic or magnetic field (locally strong axial field) in the direction of electron beam acts like a converging lens and the envelope of the electron beam is exactly analogous to the light beam passing through the converging lens. When the primary beam hits the surface of the sample secondary electrons are generated which are detected and processed to get an image on the CRT. The sample to be studied is gold coated using an ion sputtering unit.

The present samples were studied using a JEOL JSM-35 model Scanning Electron Microscope. A maximum magnification of 180000x and a minimum of 20x could be achieved using this microscope. The image obtained on the CRT is photographed using a camera attached to the set up and subsequently processed to obtain SEM micrographs.

## 2.10 AC susceptibility studies:

AC susceptibility studies on polycrystalline high $T_c$ materials facilitate an unambiguous determination of the macroscopic parameters like the $T_{c(onset)}$ of different phases present in the material, determining the critical current density, the nature of coupling between the grains etc. The real part of the susceptibility data as a function of temperature

shows a sharp drop below $T_c$ as a result of diamagnetic shielding of grains and saturates depending on the temperature and the field amplitude. The imaginary part of susceptibility in polycrystalline materials, peak below $T_c$ as a result of losses incurred due to flux motions in the grains and grain boundaries.

The AC susceptibility measurements were carried out by the mutual inductance bridge method. The schematic representation of the experimental set up (fig-2.6) shows that the system consists of a primary coil and two coaxially wound secondary coils - one of which holds the sample to be studied and the other acts as reference. The current is driven through the primary using an oscillator. Jn the absence of sample, the net voltage induced across the secondary as a result of this current is zero. When the sample is present, the resultant induced voltage is proportional to the susceptibility of the sample . In practice, a small resultant voltage is seen even in the absence oi the sample due to small non-uniformities in the two secondary coils. This is compensated by subtracting the background voltage, by conducting measurements with and without samples. The primary coil is wound on a wooden frame and has a resistance of *35ft.* Additional turns are provided at both the ends of the coil for field uniformity through out the length of the primary. The primary coil is placed outside the cryostat. The secondary coils are of length 2.54 cm, having 3250 windings each and are wound using insulated 38 gauge copper wire and placed inside the cryostat. The sample is placed at the center of one of the secondaries. An APD helium closed cycle refrigerator is used to achieve low temperatures. The temperature is monitored to an accuracy of ±0.1 K with a Si-diode sensor placed close to the samples. The leads from the primary coil are connected through a $1.2k\Omega$ resistor to the signal output of the oscillator in a EG&G PAR 5210 lock-in-amplifier. A sine signal of 33 Hz frequency is used in energising the primary. The induced voltage across the secondary is measured by the lock-in-amplifier in the differential input mode

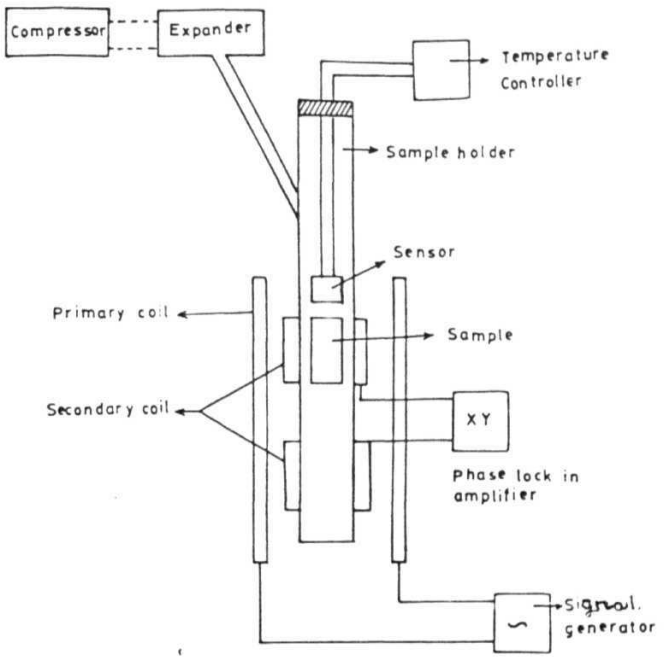


**Fig-2.6** **Schematic diagram of the AC susceptibility experimental set up.**

in order to get a better signal to noise ratio. The sample is cooled to the lowest temperature in zero field. The temperature is raised in steps and stabilised before taking the reading. Since the susceptibility $\chi'$ is proportional to the induced voltage, the induced voltage was plotted against temperature in order to obtain the bulk $T_c$ of the samples for a small field of 0.1 Oe.

# Chapter 3

## STUDIES ON Bi-Sr-Ca-Cu-O GLASSES

This chapter deals with the preparation and characterisation of undoped and 3d TM doped Bi-Sr-Ca-Cu-0 glasses of various compositions. DSC and FT/IR studies have been carried out on both the doped and undoped glasses. The glasses have been characterised by XRD studies and density measurements. The $Cu^{+2}$ ion concentration in the undoped glasses was estimated from the room temperature magnetic susceptibility of the glasses. The detailed DC conductivity studies on these glasses have been described and analysed in view of various theoretical models of electrical conduction in Transition Metal (TM) containing oxide glasses. This chapter also contains the results of ESR studies carried out on the doped and undoped Bi-Sr-Ca-Cu-O glasses.

### 3.1 Introduction on glasses:

Crystalline solids are characterised by periodic lattice in which the atoms are regularly arranged. Disordered solids are the solids showing departure from this ordered state. Glasses do not exhibit long-range periodicity of atomic arrangements and are 'amorphous' having liquid like atomic structure. The correlations between the positions of the atoms are completely lost over distances more than five atomic spacings. Glasses have been defined as 'super cooled liquids'.

Glasses are generally realised by heating certain crystalline substances like $SiO_2$ or

mixtures like $V_2O_5$-$TeO_2$ to the molten state and quenching them quickly enough to preclude crystallization i.e. the components are unable to rearrange themselves and will therefore attain a randomly arranged disordered array [151].

The basic criterion for the preparation of glasses is that the cooling rate is fast enough that crystallization is by passed. This is best illustrated by the Time-Temperature-Transformation (TTT) diagram as shown in fig-3.1. The time for the onset of crystallization in an under cooled melt (i.e. a melt at a temperature below the equilibrium melting point $T_m$) is plotted against temperature. As the temperature is lowered below the equilibrium melting temperature ($T_m$), the free energy difference between the liquid and the crystalline phases increase and consequently the time for crystallization decreases. At the glass transition temperature ($T_g$), the crystal growth becomes impossible and the liquid remains frozen to give glass. By using sufficiently large cooling rates, the crystal growth and nucleation can be eliminated. Depending on the cooling rates required for a system to give amorphous materials, different techniques are used in the preparation of glasses like the single and double roller quenching method and the plate quenching method.

Glasses can be classified into oxide, semiconducting and metallic glasses. Their differences lie in the relative strength of their chemical bonds. Turnbel [152] proposed a kinetic theory of glass formation in which the limiting rates for the process of nucleation and crystal growth in liquids are established in order to obtain glasses. Prediction of glass formation in a new system requires a knowledge of the phase diagram of the system and the viscosities of the melt. According to Rawson [153], the smaller the value of the ratio of melting temperature to bond strength, the greater the tendency to form glasses.

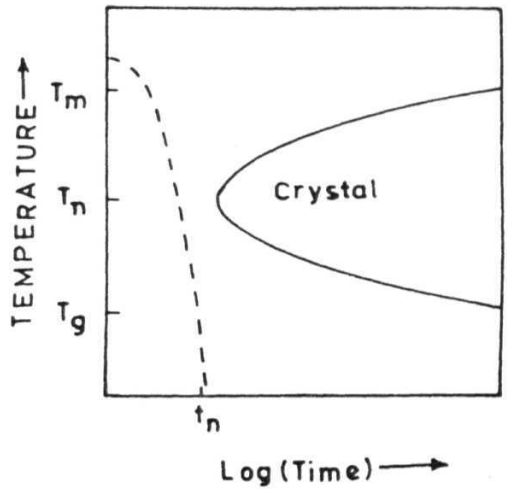


Fig-3.1 Time-Temperature-Transformation (TTT) diagram for a typical gla system.

The chemical composition of oxide glasses are expressed in the form $A_mB_nO$ where **m and n** are the number of atoms of A and B per oxygen atom. The cation A (generally alkali ions) are bound less tightly to the surrounding atoms than the cation B. Zachariason [154] suggested 4 rules for the formation of oxide glasses, based on the structural and energy considerations. They are

(1) each oxygen atom should be linked to not more than two cations.

(2) the coordination number of oxygen ions about the central cation must be small.

(3) at least three corners of each polyhedron should be shared.

(4) oxygen polyhedra should share corners and not edges or faces.

The glass must contain appreciable amounts of cations which form vitreous oxides on other cations which are able to replace any of the former, isomorphously. These cations are responsible for the glass forming ability.

Transition metal oxide glasses have transition metal oxides as the major constituents besides a glass former. Some common examples of glass formers are $TeO_2$, $GeO_2$, $P_2O_5$, $SeO_2$ and $SiO_2$. To increase the ability to go into a glassy state easily a modifier like $Fe_2O_3$, MgO, CaO, SrO and BaO is also included in the composition.

The electrical properties of various TMO glasses have been studied in depth over the last four decades. These glasses have semiconducting properties which arise due to the presence of transition metal ions in multivalent states in the glass matrix and are of great interest because of their uses such as in memory switching devices [155] and their use as cathode materials in batteries [156]. The electron-phonon interaction in these glasses is strong enough for small polarons to form and the electrical conduction process proceeds

via polaron hopping among the TM ions of different valence states [157-158]. The studies on various oxide glass systems have been reviewed by J. D. Mackenzie [159] and L. Murawski et al [160]. Extensive work has been reported on Vanadium oxide based glass systems [139, 161-170]. Information is also available on glasses containing Iron Oxide [171-173], $WO_3$ and $MoO_3$ [174-179]. Recently a number of reports on glasses containing CuO [180-183] have been published. Several theoretical models (section-3.6.1) have been proposed to understand the electrical conduction mechanism in 3d TM containing oxide glasses. Interpretation of the conduction process is difficult since the conductivity is affected by numerous factors including the nature and concentration of the TMO, the concentration of TM ions in a reduced valence state, the preparation conditions and the existence of microscopic or macroscopic structure within the glass matrix.

The initial studies on several systems presumed that the glass formers are non-interacting solvents and hence do not actively affect the conduction. Later studies indicate the effect of the glass forming oxides on the structure and properties of the glasses [160].

## 3.2 Preparation of the BSCCO and Pb-BSCCO glasses:

A number of glass fabrication techniques have been tried in order to obtain glasses and glass ceramics of various forms. The most common technique is the mixing of oxides or nitrates of bismuth, strontium, calcium, copper and lead (in the case of lead doped samples) and melting them in alumina or platinum crucibles with thorough mixing to ensure homogeneity. The temperature at which the melt is quenched and the duration of melting is limited to reduce significant evaporation of Bi and Pb. The melt is quenched

by either metal plate quenching [87, 184], single roller quenching [90], **twin roller** quenching [86] or quenching into liquid nitrogen [105]. The various **methods adopted to** obtain films, fibers, **filaments,** wires and tubes have been described at length in **chapter-1**.

### 3.2.1 Preparation of the $Bi_4Sr_3Ca_3Cu_yO_z$ glasses:

Glasses of composition $Bi_4Sr_3Ca_3Cu_yO_z$ ($3 < y < 6$) (433y) were prepared **from** 99.99% pure $Bi_2O_3$, $SrCO_3$, $CaCO_3$ and CuO. The chemicals were weighed out in the appropriate ratio and mixed thoroughly in an agate mortar. The mixture was calcined at $800^oC$ for 24 hours in an electrical furnace. The reacted black powder was melted at $1000^oC$ in a platinum crucible and held at that temperature for 15 minutes to ensure thorough mixing. The melt was quickly poured on a clean thick copper block and rapidly pressed by another copper block. Black shining glasses of 0.5 to 1 mm thickness could thus be obtained.

### 3.2.2 Preparation of $Bi_4Sr_3Ca_3Cu_{4-x}M_xO_z$ glasses:

Glasses of composition $Bi_4Sr_3Ca_3Cu_{4-x}M_xO_z$ (M = Fe, Cr and Mn) were prepared using 99.99% pure $Bi_2O_3$, $SrCO_3$, $CaCO_3$, CuO and oxides of the 3d TM. The method of preparation was identical to the method employed for the synthesis of the 433y glasses. Amorphous materials could be obtained up to a dopant content of x = 0.2 **for** M = Cr and Mn and up to x = 0.3 for Fe.

## 3.3 Characterisation studies :

### 3.3.1 Characterisation of the 433y glasses:

Room temperature XRD spectra of 433y glasses did not show any reflection peaks. The amorphous nature of the glasses were thus ascertained. Density measurements were carried out by the Archimedes principle described in chapter-2. It was found that the density of the glass system shows an increase with increase in CuO content. The total number of Cu ions per unit volume of the glasses ($Cu_{total}$ = N) was obtained from the glass composition and the density studies. The N value was found to increase with increase in Cu content of the glass. The room temperature magnetic susceptibility of the glasses was measured by Faraday method. Since the magnetic susceptibility is proportional to the paramagnetic ion concentration, the $Cu^{+2}$ ion concentration was obtained by comparing against a known standard sample of $CuSO_4.5H_2O$. The $Cu^{+1}$ concentration is obtained from N and $Cu^{+2}$ concentration values on the assumption that the total copper in the glass is constituted of $Cu^{+1}$ and $Cu^{+2}$ ions. The susceptibility and $Cu^{+2}$ concentration decreases with increase in CuO content up to y = 5 followed by an increase for y = 6 sample. The value of c (= $Cu^{+1}/Cu_{total}$)increases by about 20% as CuO content increases from y = 3 to y = 5. Further increase in CuO content leads to a decrease in c value. The density, susceptibility, N values, the $Cu^{+1}$ concentration and the c values of the glasses are given in table-3.1.

### 3.3.2 Characterisation of the 3d TMO doped glasses:

The glassy nature of the 3d TM doped BSCCO glasses was ascertained from the **XRD** studies. Density measurements were carried out on these glasses by Archimedes method. The density does not vary significantly with doping (Table-3.2). However, all the doped

Table-3.1

Various physical parameters of $Bi_4Sr_3Ca_3Cu_yO_z$ glasses.

| Composition | Density ($g\ cm^{-3}$) | N ($10^{21} cm^{-3}$) | $X$ ($10^{-6}\ g^{-1}$) | $Cu^+$ ($10^{21} cm^{-3}$) | $c = Cu^+/N$ | $R = N^{-1/3}$ (Å) |
|---|---|---|---|---|---|---|
| 4333 | 5.74 | 6.27 | 1.38 | 3.12 | **0.50** | 5.41 |
| 4334 | 5.89 | 8.38 | 1.16 | 5.64 | **0.67** | 4.92 |
| 4335 | 6.02 | 10.2 | 1.03 | 7.70 | 0.76 | 4.61 |
| 4336 | 6.11 | 11.7 | 1.32 | 8.75 | 0.73 | 4.37 |

Table-3.2
DSC parameters and density of the 3d doped 4334 glasses.

| sample | (°C) | (°C) | enthalpy (cal/gdeg) | density ($g/cm^3$) |
|---|---|---|---|---|
| Fe doped | | | | |
| x = 0 | 471 | 470 | 2.01 | 5.89 |
| x=0.025 | 449 | 455 | 1.45 | 5.89 |
| x=0.05 | 471 | 478 | 1.63 | 5.84 |
| x=0.1 | 456 | 402 | 1.98 | 5.86 |
| x = 0.2 | 469 | 475 | 2.08 | 5.84 |
| x=0.3 | 450 | 458 | 1.55 | 5.83 |
| Cr doped | | | | |
| x=0.025 | 449 | 453 | 2.02 | 5.87 |
| x=0.05 | 448 | 454 | 1.91 | 5.88 |
| x=0.1 | 446 | 448 | 1.95 | 5.86 |
| x=0.2 | 449 | 454 | 1.97 | 5.84 |
| Mn doped | | | | |
| x=0.025 | 453 | 458 | 1.88 | 5.87 |
| x=0.05 | 460 | 463 | 2.19 | 5.87 |
| x=0.1 | 404 | 470 | 2.19 | 5.84 |
| x=0.2 | 453 | 457 | 1.91 | 5.83 |

glasses have slightly lower density in comparison to the base glass.

## 3.4 Differential Scanning Calorimetry studies:

### 3.4.1 DSC studies on 433y glasses:

From the DSC studies at a scan rate of 10°C/minute, the values of the crystallization onset temperature ($T_o$), the glass transition temperature ($T_g$), the crystallization temperature ($T_x$) and the enthalpy of the glasses were obtained (Table-3.3). Fig-3.2 shows a typical DSC plot for the 433y glass. The $T_o$ and the $T_g$ values do not vary appreciably with composition. The $T_x$ value is found to be highest for the 4334 glass. AT = $T_x$- $T_g$ is a measure of the thermal stability of the glass. AT is found to be highest for the 4334 glass indicating it to be the most stable glass among the present compositions. The enthalpy is found to increase with increase in CuO content. Zheng et al [127] reported that as the $Cu^{+1}/Cu_{total}$ ratio and the total Cu oxide content increase, the glass transition and the crystallization temperature decrease. Sato et al [124] also reported the effect of $Cu^{+1}/Cu_{total}$ ratio on the thermal stability of 2212 glasses. We do not find any definite correlation between $Cu^{+1}/Cu_{total}$ ratio and the thermal parameters of the present glasses.

### 3.4.2 DSC studies on 3d TM doped glasses:

DSC studies were conducted on the 3d doped BSCCO glasses at a scan rate of 10°C/minute and the onset temperature, the crystallization temperature and the enthalpy obtained (Table-3.2). The glass transition temperature is not clearly marked as it is not sharply defined and lies between 355 to 370°C for all the compositions. The $T_o$ and the $T_x$ do not show any systematic variation with the dopant content for any of the three series of

Table-3.3

Transition temperatures obtained from the DSC studies on the 433y glasses.

| sample | $T_g$ (°C) | $T_o$ **TO** | $T_x$ (°C) | $\Delta T = (T_o - T_g)$ | enthalpy (cal/gdeg) |
|---|---|---|---|---|---|
| 4333 | 367 | 450 | 457 | 83 | 1.54 |
| 4334 | 358 | 471 | 476 | 113 | 2.01 |
| 4335 | 360 | 444 | 450 | 84 | 2.17 |
| 4336 | 360 | 449 | 452 | 89 | 3.75 |

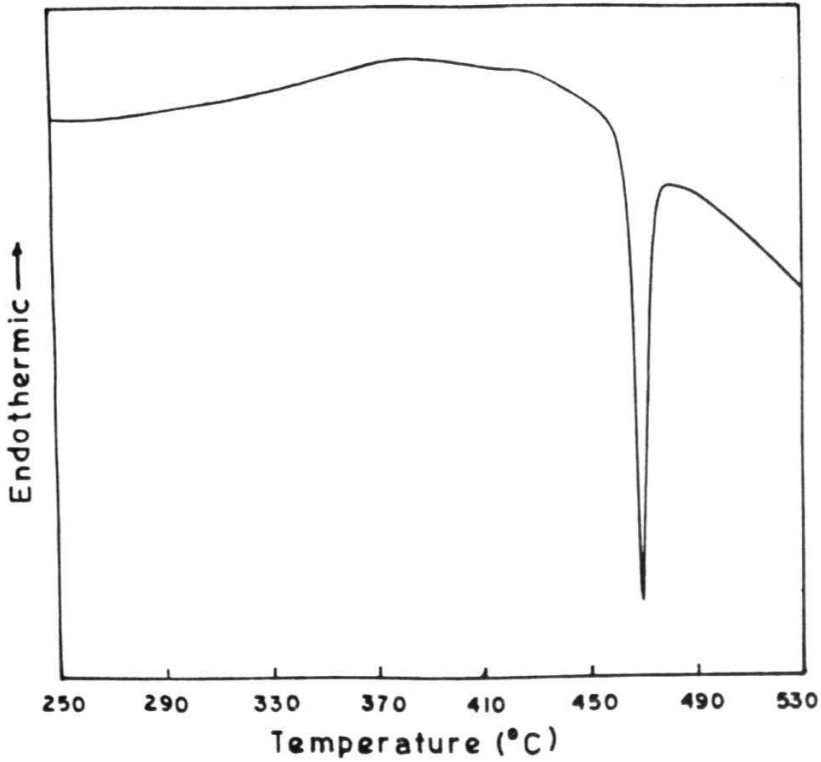


Fig-3.2 A representative DSC spectra for the 433y glasses.

samples studied. The doped glasses however have $T_o$ and $T_x$ values smaller than that of the 4334 glass.

## 3.5 FT/IR studies on glasses:

Fig-3.3 shows the FT/IR spectra for $Bi_2O_3$, $SrCO_3$, $CaCO_3$ and CuO, the starting chemicals for the synthesis of the glass and a typical spectra for the amorphous 433y glass system. A broad absorption band at 500 $cm^{-1}$ and a peak at around 860 $cm^{-1}$ are present in all the glass samples (fig-3.4). The peak at 860 $cm^{-1}$ do not correspond to any of the absorption peaks in the IR spectra of the starting materials. A representative FT/IR spectra for the Fe doped glasses is given in fig-3.5 and it is seen that 3d TM doping does not give rise to any variations in the FT/IR spectra.

The absorption band at around 500 $cm^{-1}$ which corresponds to the phonon frequency of the glasses does not alter appreciably with variation in composition or as a result of doping. This is further confirmed from the results of DC conductivity studies on these glasses. Bishay and Maghrabi [185] observed absorption peak at 860 $cm^{-1}$ in IR spectra of fused $Bi_2O_3$ and assigned it to a totally symmetric stretching vibration mode of $BiO_3$ pyramidal point group $C_{3v}$ . Zheng et al [186] reported the absorption peak at 840 $cm^{-1}$ in the Infrared spectra of Bi-Sr-Ca-Cu-0 glasses and assigned it to $BiO_3$ pyramidal units. Miyaji et al [187] reported absorption peak in the Infrared spectra of Bi-Sr-Ca-Cu-0 and Bi-Sr-Cu-0 glasses but not in Bi-Ca-Cu-0 glass. They found that this peak is not present in SrO free glasses and its intensity increases with increasing SrO content. Miyaji et al have argued that the three-coordinated Bi has not been found in any crystal and the formation of $BiO_3$ pyramidal units in these glasses is therefore doubtful. Distorted $BiO_6$ octahedra generally forms in most oxide crystals such as $\alpha$-$Bi_2O_3$ [188] and $Bi_4Si_3O_{12}$

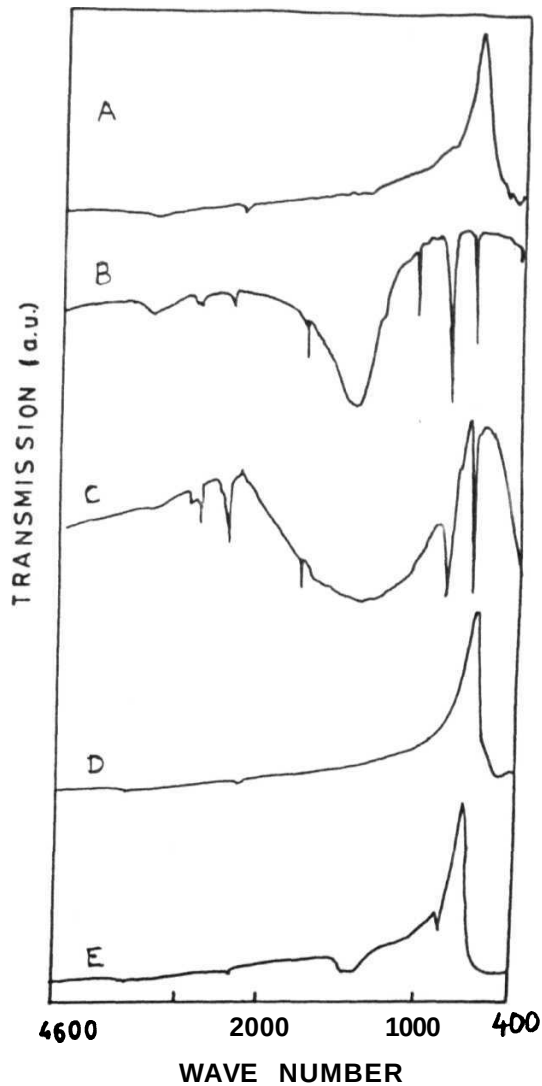


**Fig-3.3 Typical FT/IR spectra of a BSCCO glass and the components constituting the glass (A) $Bi_2O_3$; (B) $SrCO_3$; (C) $CaCO_3$; (D) CuO and (E) Bi-Sr-Ca-Cu-O glass.**

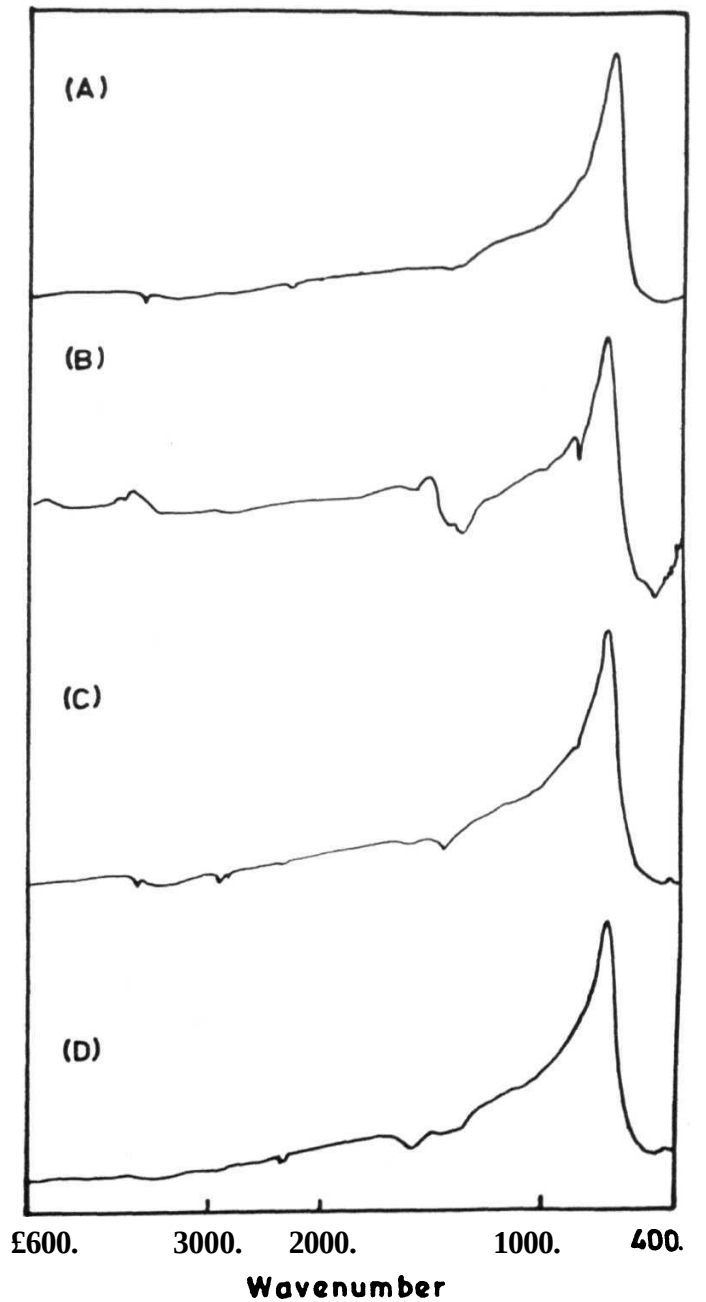


**Fig-3.4 FT/IR** spectra for the 433y **glasses** (A) y =3; (B) y = 4; (C) y = 5 and (D) y = 6.

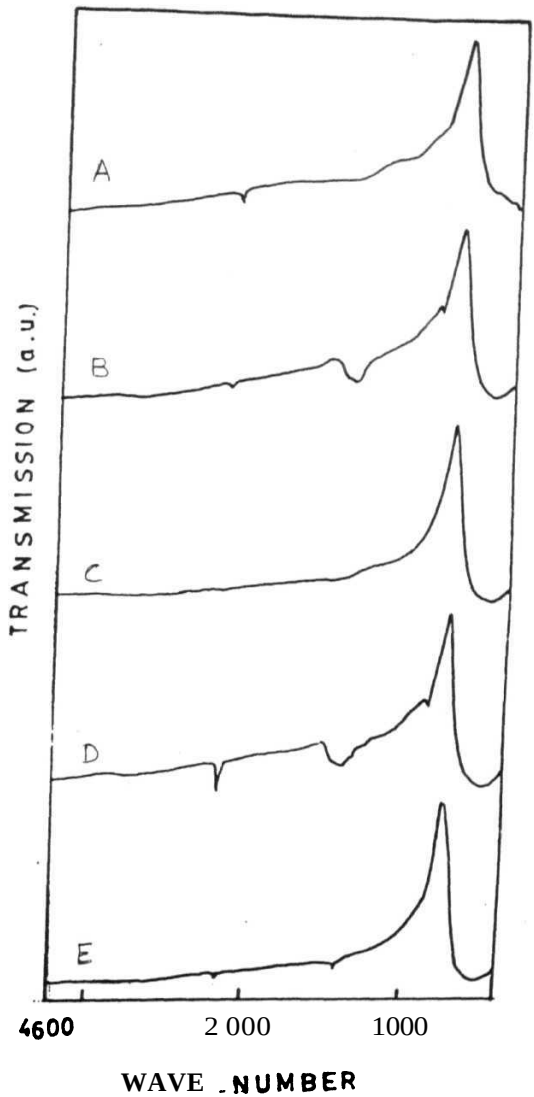


Fig-3.5 A representative FT/IR spectra for the $Bi_4Sr_3Ca_3Cu_{4-x}Fe_xO_z$ glasses (A) x = 0.025; (B) x = 0.05; (C) x = 0.1; (D) x = 0.2 and (E) x = 0.3.

[189]. The six Bi–O bonds in $BiO_6$ octahedron are classified into two groups of short Bi-0 (2.0–2.2 $A$) and long ones (2.5-2.8 $A$) on the basis of Bi-0 interatomic distances. It is assumed that the distorted $BiO_6$ octahedron involves a $BiO_3$ species, when three Bi-0 distances in the $BiO_6$ are nearly equal. Based on these considerations they argued that in the SrO containing glasses there are $BiO_6$ octahedra which have three shorter Bi-0 distances, giving the peak at 860 $cm^{-1}$ due to $C_{3v}$ symmetry.

Since the first phase formed on crystallization of these glasses (chapter-4) is indicating that Sr is located adjacent to Bi-0 planes, the assignment of 860 $cm^{-1}$ peak to $BiO_6$ octahedra with three Bi–O distances nearly equal leads to the conclusion that Sr preferentially occupies the site near BiOe octahedra in the present glasses causing a strong interaction between Sr and BiOe octahedra.

## 3.6 DC conductivity studies:

### 3.6.1 Theoretical background :

The theoretical models used in the analysis of the experimental data are briefly described below.

The formation of small polarons in 3d TM containing glasses is the basis for various theoretical models discussed in this section.

Consider an electron momentarily fixed at some point of the crystal. As a result of electron lattice interaction, the surrounding lattice particles will be displaced to new equilibrium positions; the induced displacements will be such as to provide a potential

'well' for the electron. If the well is sufficiently deep, the electron will occupy a bound state, unable to move unless accompanied by the well. The unit consisting of the electron, together with its induced lattice deformation, is called 'polaron'.

The electrical conduction in the TM ion containing glasses is discussed by Mott [157] in terms of the small polaron hopping between localised sites. The important feature of small polaron conduction is the transition behaviour between the conduction in a polaron baud, characterised by exact conservation of the lattice energy and conduction by hopping which is characterised by an alteration in the phonon occupation numbers. In the high temperature range i.e. T> $\theta_D/2$,($\theta_D \approx h\nu_o/k$ is the Debye temperature and $\nu_o$ the phonon frequency of the material), the DC conductivity is due to small polaron hopping among the nearest neighbours and the conductivity in the non-adiabatic regime is given by

$$a = \frac{\nu_o N e^2 R^2}{kT} c(1 - c)exp(-2\alpha R)exp(-W/kT) \tag{3.1}$$

where $a$ is the conductivity at temperature T, $\nu_o$ is the phonon frequency, c is the ratio of concentration of TM ions in the low valence state to the total number of transition metal ions N, $R = 1/N^{1/3}$ is the average hopping distance, $\alpha$ is the electron wave function decay constant of the 3d electron wave function and W is the activation energy for conduction. Assuming a strong electron-lattice interaction, Austin and Mott [158] have shown that

$$\begin{aligned} W &= W_H + {}^{1}\text{-}W_D \quad \text{for } T > \theta_D/2 \\ W &= W_D \qquad\qquad\quad \text{for } T < \theta_D/2 \end{aligned} \tag{3.2}$$

where $W_H$ is the poloron hopping energy and $W_D$ is the disorder energy arising from

energy difference of the neighbouring sites. The tunneling term $\exp(-2\alpha R)$ in equation-3.1 reduces to unity if the polaron hopping is in the adiabatic regime and the conduction is mainly controlled by the activation energy W. The conductivity equation reduces to

$$\sigma = \frac{\nu_o N e^2 R^2}{kT} c(1-c) exp(-W/kT) \tag{3.3}$$

The Mott's model predicts an appreciable departure from linearity in the $\log\sigma$ versus $1/T$ plot below a temperature $T = \theta_D/2$ indicating a decrease in the activation energy with decrease in temperature. According to this model, the activation energy at the lowest temperature is entirely due to $W_D$. Thus by the Mott's theory, conductivity at high temperature is due to small polaron hopping between the nearest neighbours and the dominant conduction mechanism is thermally activated hopping in which electron site change is accompanied by the emission and absorption of many phonons and hence a change in the phonon occupation numbers. At low temperature, when the polaron binding energy is small and the disorder energy of the glass plays a dominant role in the conduction, it is suggested [190] that the carrier may also hop beyond the nearest neighbour distance to a site at lower energy. In this temperature range, the conduction is in polaron band characterised by site transfers in which phonon occupation numbers are unchanged. The conductivity expression given by Mott [191] for this variable range hopping (VRH) conduction mechanism is

$$\sigma = Aexp(-B/T^{1/4}) \tag{3.4}$$

$$\text{where } A = e^2 N(E_f) R^2 \nu_o$$

$$\text{and } B = 2.1\left[\frac{\alpha^3}{kN(E_f)}\right]^{1/4} = 2.4\left[\frac{W_D(\alpha R)^3}{k}\right]^{1/4}$$

and $N(E_f)$ is the density of states at the fermi level. The Mott's conductivity equation

has the form of Arrhenius equation

$$\sigma = \sigma_o exp(-W/kT) \tag{3.5}$$

If conduction is in the adiabatic mode, $\sigma_o$ is almost independent of composition or $\exp(-2\alpha R)$ is constant for all the glasses and changes in $\sigma$ as a result of composition variation is entirely due to variation in W. Hence it has been suggested by Sayer & Mansingh [166] and Murawski [160] that the nature of hopping can be ascertained from the plot of $\log\sigma$ versus W at a fixed temperature T. The hopping will be in the adiabatic regime, if the temperature $T_e$ estimated from the slope of such a plot is close to T and non-adiabatic if they are widely different.

A generalised phonon hopping model has been proposed by Holstein [192], Emin and Holstein [193] and Friedman and Holstein [194] on the basis of molecular crystal model considering $W_D = 0$. The DC conductivity according to this model is expressed as

$$\sigma = \frac{8\pi\nu_o N e^2 R^2}{3kT} exp\left[-\frac{(W_H - J)}{kT}\right] \tag{3.6}$$

for the adiabatic polaron hopping regime and for the non-adiabatic regime it is given by

$$\sigma = \frac{3Ne^2R^2J^2}{2kTh}\left(\frac{\pi}{kTW_H}\right)^{1/2} exp\left(\frac{-W_H}{kT}\right) \tag{3.7}$$

where J is the polaron bandwidth related to electron wave function overlap on adjacent sites. They have shown that J should satisfy the condition $J < W_H/3$ for the formation of small polarons and the nature of the hopping can be ascertained from the inequality

$$J \gtrless \left[2kT\frac{W_H}{\pi}\right]^{1/4}\left(\frac{h\nu_o}{\pi}\right)^{1/2} \tag{3.8}$$

(>) for hopping in the adiabatic regime and (<) for hopping in the non-adiabatic regime.

A detailed theoretical model of the temperature dependence of activation energy is given by Schnakenberg [190]. According to this model, the conduction at high temperature is due to optical multiphonon processes. With decrease in temperature, the multiphonon processes are replaced by a single optical phonon process. At the lowest temperature, the polaron hops with one or more acoustic phonons making up the energy difference between sites. The conductivity expression in this model is given by

$$\sigma \sim \beta\tau(\beta)exp[-\beta U(\beta)]exp[-\beta\Delta W) \tag{3.9}$$

for $T > \Theta_D/4$ and

$$\sigma \sim exp(-\beta\Delta W) \tag{3.10}$$

for $T < \Theta_D/4$

where $\beta = 1/kT$, $\tau(\beta)$ is the temperature dependent relaxation time, $U(\beta)$ is the temperature dependent activation energy and is related to $W_H$ in the Mott's model by the equation

$$\frac{W}{W'} = \frac{\tanh(h\nu_o/4kT)}{h\nu_o/4kT} \tag{3.11}$$

where $W'$ is the high-temperature activation energy and can be taken as $\approx W_H$ and W, the activation energy at lower temperatures. AW is the activation energy at the lowest temperature and can be equated to $W_D$ in the Mott's model.

Extracting the temperature dependent terms, the Schnakenberg's conductivity expression can be written as

$$\sigma \sim \frac{1}{T}\left[\sinh\left(\frac{h\nu_o}{2kT}\right)\right]^{1/2} exp\left[-\left(\frac{4W_H}{h\nu_o}\right)\tanh\left(\frac{h\nu_o}{4kT}\right)\right] exp\left(\frac{-W_D}{kT}\right) \qquad (3.12)$$

**A simple** model **for** conductivity has been **proposed by Greaves [195] in which the excitations by optical** and acoustic phonons are considered to **make independent contributions to** the jump frequency. The conductivity expression

$$\sigma T^{1/2} = A exp\left(\frac{-B}{T^{1/4}}\right) \qquad \textbf{(3.13)}$$

is found to fit the intermediate temperature range where neither the $1/T$ nor the $1/T^{1/4}$ fitting of Mott's theory holds.

Triberis and Friedman [196-198], based on the Microscopic Generalised Molecular Crystal Model, applicable to the small polaron hopping motion in a disordered system, used percolation theory to evaluate the DC conductivity of a disordered material at high and low temperatures.

For the high temperature ($h\nu_o \ll$ kT) small polaron hopping regime, the hops are characterised by the absorption and emission of many phonons. Taking correlations into account the conductivity in this temperature range varies as

$$exp\left[-\left(\frac{T_o}{T}\right)^{1/4}\right] \quad \text{and} \quad T_o = \frac{17.8\alpha^3}{N_o k} \qquad \textbf{(3.14)}$$

**and** the conductance in the low temperature ($h\nu_o >$ kT) small polaron hopping regime varies as

$$exp\left[-\left(\frac{T_o^*}{T^*}\right)^{1/4}\right] \quad \text{and} \quad T_o^* = \frac{12.5\alpha^3}{N_o k}$$

where $N_o$ is the density of states and $a^{-1}$ is the spatial extent of **the electronic wave** function localized at **a** single site.

Thus the theory predicts a low to high temperature slope **ratio of 1.09** in the $\ln\sigma$ versus $T^{-1/4}$ plots between the low and high temperature regime.

### 3.6.2 Experiment and Results:

The DC electrical COL ductivity measurements were carried out as a function of temperature on several glass samples with $Bi_4Sr_3Ca_3Cu_yO_z$ ($3 < y < 6$) and $Bi_4Sr_3Ca_3Cu_{3.8}M_{0.2}O_z$ (M = Fe, Cr and Mn) composition. The conductivity of the samples of the same composition taken from different batches prepared under identical conditions, showed agreement within 5% in their room temperature conductivity. The conductivity on the same sample in different runs agreed within 2%. The lower limit of the temperature range utilised was decided by the experimental difficulty in measuring currents less that $10^{-14}$A with the equipment available. The electrical conduction in the present glass is electronic in nature as indicated by the invariance of the current in the sample with time after a **fixed** voltage is applied.

#### (a) $Bi_4Sr_3Ca_3Cu_yO_z$ glasses:

Fig-3.6 shows the variation of logarithm of electrical conductivity as a function of **the** inverse of temperature for various glass compositions. It is observed **that the plot is** linear above 260 K and follows Arrhenius equation and shows an almost temperature independent activation energy above 260 K. The solid lines in fig-3.6 **are the linear least**

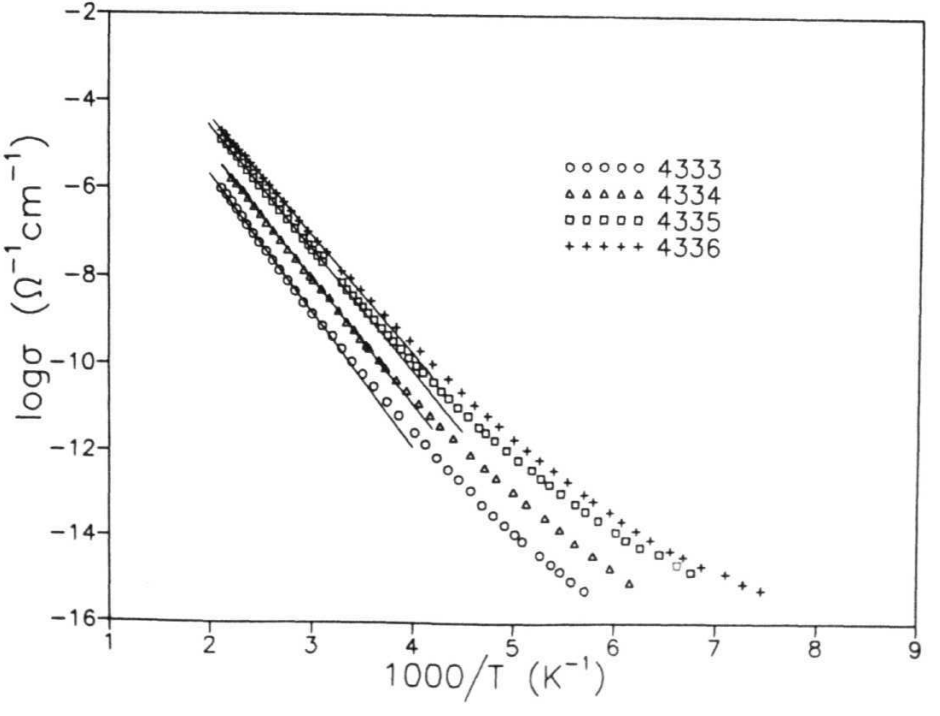


Fig-3.6 Plot of log$\sigma$ versus $10^3/T$ for $Bi_4Sr_3Ca_3Cu_yO_z$ glasses (○) y = 3; (△) y = 4; (□) y = 5; (+) y = 6. The solid lines are the linear best fits as per Mott's model.

square fits used to obtain the activation energy W. At any given temperature, the conductivity increases and the activation energy decreases with increase in CuO content (Table-3.4). These results are similar to what is reported for **Vanadium glasses [166,** 168]. **The** conductivity of these glasses is about 3-4 orders of **magnitude higher than that** of copper phosphate containing glasses with similar amount of copper [180]. **It therefore** appears that the other constituents of the glass play an important role in the conduction process. Below 260 K, the activation energy is found to decrease smoothly **with** decreasing temperature. This is most apparent in the glasses having higher conductivity at **low** temperatures. This kind of variation in the $\log\sigma$ versus $1/T$ is characteristic of small polaron hopping mechanism in TMO containing glasses.

In order to consider the effect of $T^{-1}$ in the pre-exponential part in equation-3.1, $\log(\sigma T)$ is plotted against $10^3/T$ in the temperature range studied (fig-3.7). These plots are similar to fig-3.6 but the activation energy estimated from the $\log(\sigma T)$ versus $10^3/T$ plots is slightly higher than the values obtained from the $\log\sigma$ versus $10^3/T$ plots.

The polaron radius $r_p$ can be estimated from the equation given by **Bogolomov et al [199] for** non-dispersive system as

$$r_p = \frac{1}{2}\left(\frac{\pi}{6N}\right)^{1/3} \tag{3.16}$$

**Using the N values from table-3.i, $r_p$ is calculated and listed in** table-3.4. **The $r_p$ value is small and comparable to the reported values for other glass systems. This shows the presence of** strong electron-phonon interaction **and** the **formation of small polarons in the present** glasses.

Table-3.4
Parameters estimated from electrical conductivity of $Bi_4Sr_3Ca_3Cu_yO_z$ glasses.

| Composition | $\sigma_{423}$ $(10^{-7}\Omega^{-1}cm^{-1})$ | $W_{423}$ (eV) | $\alpha$ $(\AA^{-1})$ | $r_p$ $(\AA)$ | $(10^{11}Hz)$ | $(10^{13}Hz)$ |
|---|---|---|---|---|---|---|
| 4333 | 3.55 | 0.63(5) | .34 | 2.18 | 2.45 | .20 |
| 4334 | 5.89 | 0.60 | .40 | 1.98 | 2.00 | .57 |
| 4335 | 24.5 | 0.56 | .35 | 1.86 | 4.14 | 2.81 |
| 4336 | 43.7 | 0.54(5) | .37 | 1.76 | 3.84 | 1.93 |

† from Mott's eqn.3.3
‡ replacing c(1-c) by $c(1-c)^4$ in eqn.3.3

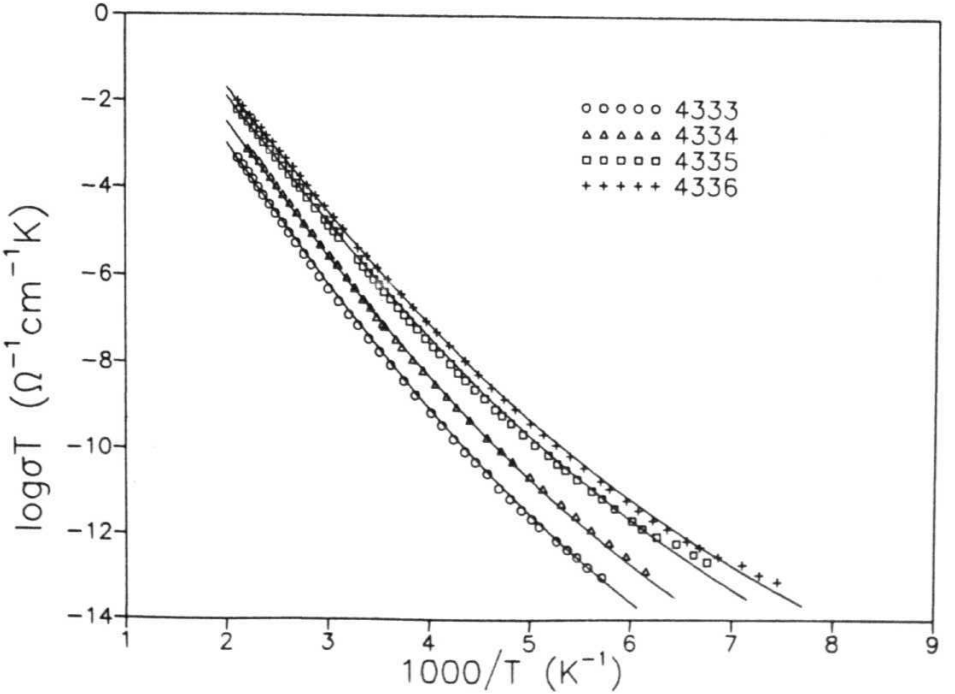


**Fig-3.7** Plot of $\log(\sigma T)$ versus $10^3/T$ for $Bi_4Sr_3Ca_3Cu_yO_z$ glasses (○) y = 3; (△) y = 4; (□) y = 5; (+) y = 6. The solid curves are the theoretical best fits to Schnakenberg's model.

According to Mott's model, an appreciable departure from linearity in the $\log\sigma$ vs. $1/T$ plot occurs at a temperature $T = \theta_D/2$, which is about 260 K from fig-3.6. Thus the Debye temperature, $\theta_D$ for the present glass system is $\approx$520 K and the $\nu_o$ value obtained from the relation $\theta_D \approx h\nu_o/k$ is 1.15 x $10^{13}$ Hz. The $\nu_o$ value is almost independent of composition. This shows that the structure of these glasses does not change with composition. This hypothesis that the structural arrangements of all the samples are similar, is supported by IR studies on these glasses. IR studies show an absorption band around 500 $cm^{-1}$ which gives a phonon frequency of $\approx$ 1.53 x $10^{13}$ Hz for the whole range of compositions studied.

In order to study the nature of the conduction mechanism i.e. if equation-3.1 or 3.3 is valid for the present glass system, $\log\sigma$ is plotted against W at a fixed temperature (say 423 K) for the compositions studied. Fig-3.8 shows such a plot to be a straight line with slope corresponding to an estimated temperature $T_c$ of 404 K. The temperature estimated from the slope of the plot is close to the fixed experimental temperature. This implies that the hopping in these glasses occur in the adiabatic regime with the thermal activation energy dominating the conduction process. The tunneling term $\exp(-2\alpha R)$ in equation-3.1 can therefore be ignored and equation-3.3 is more appropriate to describe conduction in these glasses.

The nature of hopping conduction can be ascertained by the Holstein's condition, considering equation-3.8. Assuming that $W \approx W_H$ in the high temperature range, the RHS of equation-3.6 at 423 K for $\nu_o = 10^{13}$ Hz is found to be 0.038-0.04 eV for the present glasses. An estimation of J can be obtained by assuming that the entire concentration dependence of the activation energy is due to the variation in J. The change in activation energy is from 0.54 to 0.64 eV, and so a possible variation in J of $\sim$0.1 eV. Since W is

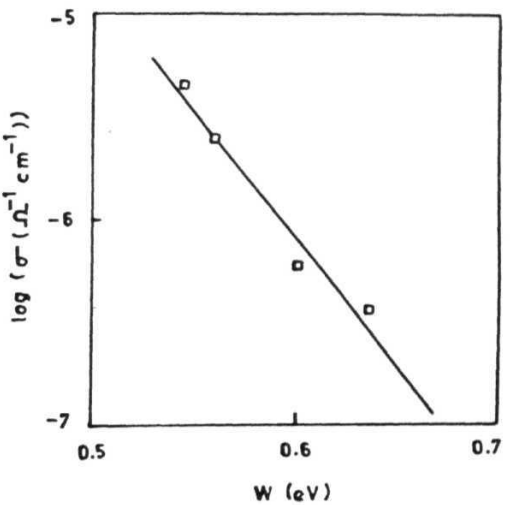


**Fig-3.8** Plot of log$\sigma$ versus activation energy W for the 433y glasses at 423 K. The solid line is the least square fit of the experimental data.

likely to change with composition, the true variation in J may be smaller than 0.1 eV. However the change in W is large enough for the adiabatic hopping theory to be most appropriate to describe the polaron conduction in the present glass system. From an estimation of the limiting value of J, the condition for the small polaron formation i.e. J < $W_H/3$ is also satisfied.

The $\nu_o$(adiabatic) and the a values for the various glasses estimated from equation-3.3, in the adiabatic regime using the physical parameters in table-3.1, are listed in table-3.4. The $\nu_o$(adiabatic)is about two orders of magnitude smaller than the phonon frequency estimated from log$\sigma$ versus $10^3/T$ plots and the IR studies. This discrepancy can be explained by taking into account the effect of interaction between the polarons i.e. the correlation effects [166]. This would imply that the factor c(1-c) in equation-3.3, should be replaced by $c(1-c)^{n+1}$. The existence of such an effect is quite likely because of large c value of these glasses. The $\nu_o$(adiabatic) estimated with n = 3 is of the same order of magnitude as obtained from $\theta_D$ and IR studies (table-3.4).

The theoretical fit of equation-3.11 for $\nu_o=10^{13}$ Hz, along with the experimental points is plotted in fig-3.9. It gives a reasonable fit to the data points above 350 K but deviates at lower temperatures. This shows that the decrease in activation energy with decrease in temperature alone cannot account for the temperature dependence of conductivity. The temperature dependence of the pre-exponential factor is also to be considered for comparison with the experimental data.

The temperature dependence of conductivity according to Schnakenberg's model is given by equation-3.12. Fig-3.7 shows the experimental data and the theoretical curves (solid lines) obtained from equation-3.12. The values of $\nu_o$, $W_H$ and $W_D$ obtained from

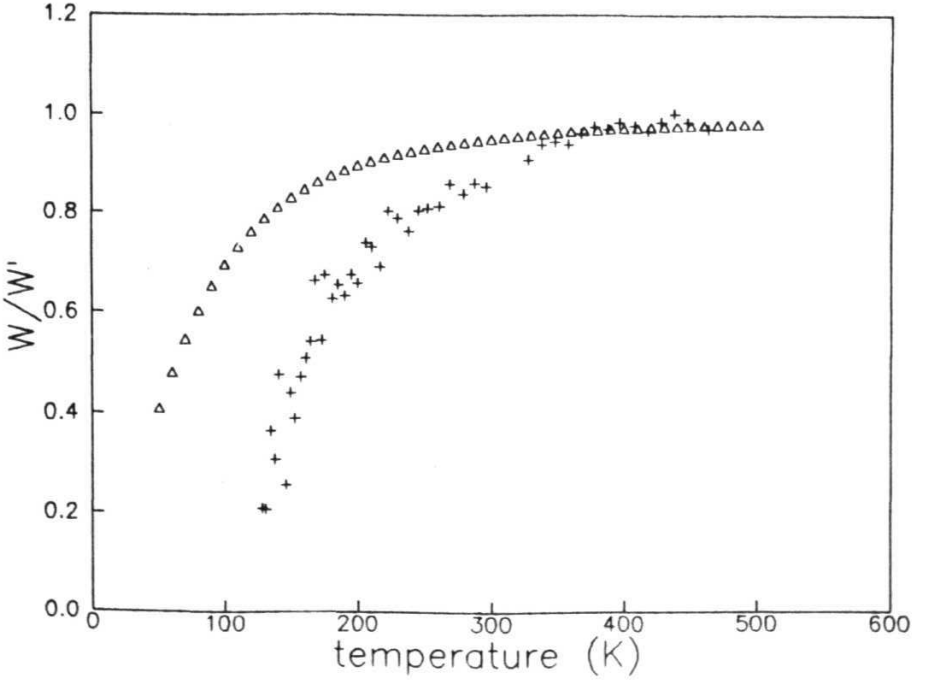


**Fig-3.9** Plot of $W/W^1$ versus temperature for the 4336 glass sample. (△) is the theoretical curve obtained from equation-3.11 using $\nu_o = 10^{13}$Hz.

the best fits of the theoretical curves to the experimental data are given in table-3.5. The hopping energy $W_H$ increases with the increase in CuO content and is close to the values obtained from the experimental data. The $\nu_o$ value is close to the value obtained from Mott's model and IR studies. The disorder energy $W_D$ is close to the predictions of Miller-Abraham's theory [200]. Using $\nu_o$ and $W_H$ values, the value of small-polaron coupling constant $\gamma = W_H / h\nu_o$ is estimated. The calculated values of 7 are listed in table-3.5 and range between 9.78 and 12.84. The value of 7 > 4 usually indicates strong electron-phonon interaction in solids [158]. The calculated value of 7 gives effective polaron mass $m_p$ [158, 160] about $10^5$ times the mass of an electron. The numerical value of $m_p$ and 7 confirms the presence of strong electron-phonon interaction and the formation of small polarons in the present glasses [158, 201].

The low temperature data is also analysed in view of Mott's Variable Range Hopping mechanism [191] and Greave's theory [195]. Since the experimental data for the 4333 and 4334 glasses could not be obtained in the temperature range below 160 K due to their high resistivities, $\log\sigma$ against $1/T^{1/4}$ could be plotted only for 4335 and 4336 glasses (fig-3.10). A linear fit was obtained as per equation-3.4. The $N(E_f)$ values estimated from equation-3.4, using a values from high temperature data is $\sim 10^{20}$ $eV^{-1}cm^{-3}$ and is a reasonable value for the localised states [191]. The $W_D$ values obtained from the same equation are found to be unacceptably large. This shows that tunneling term may be negligible in the high temperature range but perhaps cannot be ignored in the low temperature range. Unrealistically high values of $W_D$ were obtained from the variable-range hopping analysis for vanadate [168] and some other copper oxide glasses [181] also. The Mott's Variable-Range-Hopping analysis may not explain the conductivity behaviour in the low temperature region considered. According to the Greave's model, the Variable-Range-Hopping may take place in the intermediate temperature range and

Table-3.5

Parameters estimated from the best fits of Schnakenberg's model to the experimental data.

| Composition (433y) | $\nu_o$ ($10^{13}$ Hz) | $W_H$ (eV) | $W_D$ (eV) | $7 = W_H/h\nu_o$ |
|---|---|---|---|---|
| 4333 | 1.25 | 0.68 | 0.07 | 13.15 |
| 4334 | 1.27 | 0.63 | 0.09 | 11.99 |
| 4335 | 1.29 | 0.56 | 0.12 | 10.49 |
| 4336 | 1.37 | 0.55 | 0.125 | 9.78 |

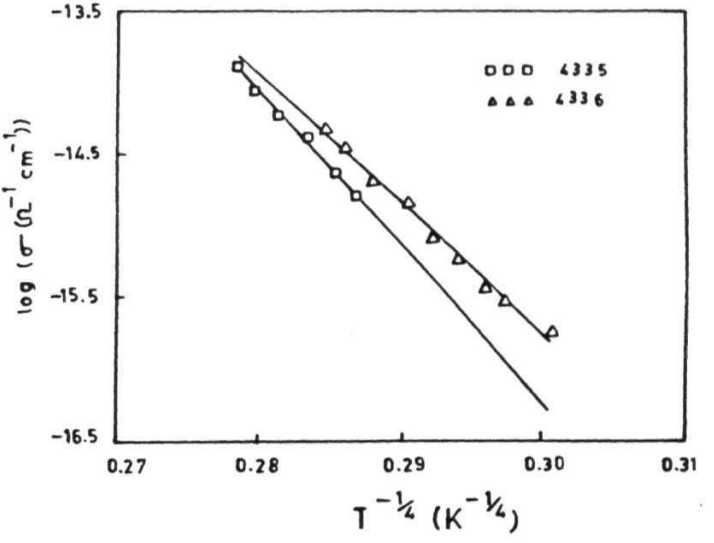


**Fig-3.10 Plot of $\log\sigma$ versus $T^{-1/4}$ for $Bi_4Sr_3Ca_3Cu_yO_z$ glasses (□) $y = 5$ and (△) $y = 6$.**

**the** conductivity expression according to this model is

$$\sigma T^{1/2} = A exp(-B/T^{1/4}) \quad \textbf{(3.17)}$$

where A and B are given by the equations described in equation-3.4. **We, however do** not find a linear variation of $\log(\sigma T^{1/2})$ as a function of $T^{-1/4}$ **in the intermediate** temperature range. We also find that the Triberis model is not applicable **to the present data.**

**(b) 3d TMO doped glasses:**

The electrical conductivity measurements on the $Bi_4Sr_3Ca_3Cu_{3.8}M_{0.2}O_x$ glasses show that the conductivity behaviour of the 3d TM doped glasses is similar to that of the undoped glasses. Fig-3.11 shows the variation of logarithm of conductivity as a function of inverse of temperature. The conductivity at room temperature does not vary (table-3.6) substantially with the 3d TM dopants. The variation in conductivity as a function of temperature is similar to that of the 4334 glass.

Fig-3.12 shows the variation of $\log(\sigma T)$ versus $1/T$. The solid curves **are** the best fits **obtained from** Schnakenberg's equation-3.12. The experimental **data is consistent with the** predictions of Schnakenberg's model. The values of $\nu_o$, $W_H$, $W_D$ **and** 7 **obtained from** the best fits of equation-3.12 to the experimental data are **given in table-3.6. The** $W_H$ values are close to that of the 4334 glass while $W_D$ decreases **marginally as** a **consequence of doping.** The $\nu_o$ values show little change with doping **which is consistent with the** results **of** the IR studies. The $\gamma$ values also show very little change **with doping.**

**From the above results** we **conclude that the conduction mechanism in the BSCCO glasses does not change** as a result **of doping at** Cu **site** even **for a 5% dopant concentration. The conduction parameters also do** not vary **appreciably. Hence, the conductivity**

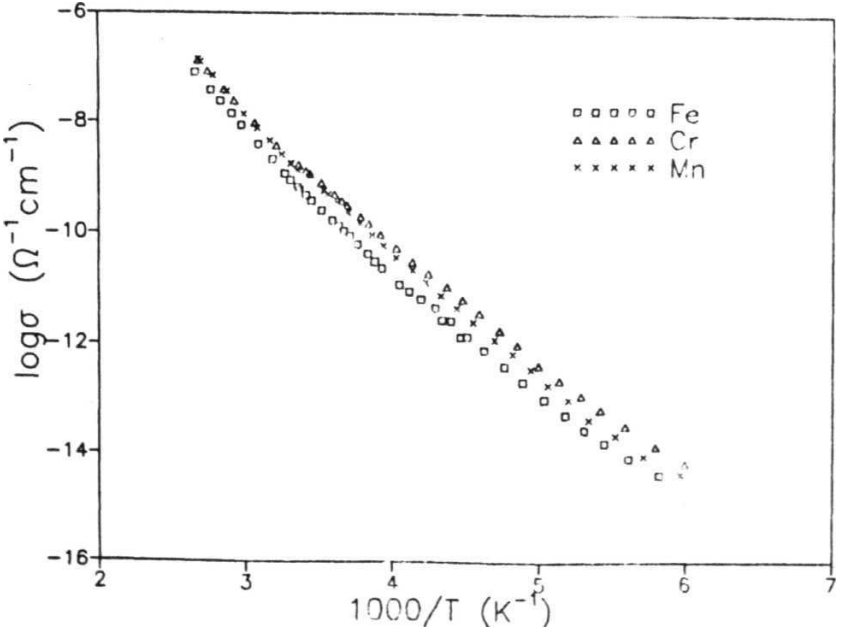


**Fig-3.11** Plot of logσ versus $10^3/T$ for the $Bi_1Sr_3Ca_3Cu_{3.8}V_{0.2}O_x$ (M = Fe, Cr and Mn) glasses.

Table-3.6

Room temperature conductivity and the conductivity parameters estimated from the best fits of Schnakenberg's model to the experimental data of $Bi_4Sr_3Ca_3Cu_{3.8}M_{0.2}O_z$ doped glasses.

| Sample M | $\sigma_{298}$ ($10^{-9}$ $\Omega^{-1}$ $cm^{-1}$) | ($10^{13}$ Hz) | $W_H$ (eV) | $W_D$ (eV) | $\gamma = W_H/h\nu_o$ |
|---|---|---|---|---|---|
| **M=Fe** | 0.665 | 1.27 | 0.635 | 0.07 | 12.08 |
| M=Cr | 1.657 | 1.28 | 0.62 | 0.07 | **11.70** |
| **M=Mn** | 1.319 | 1.26 | 0.64 | 0.06 | 12.27 |

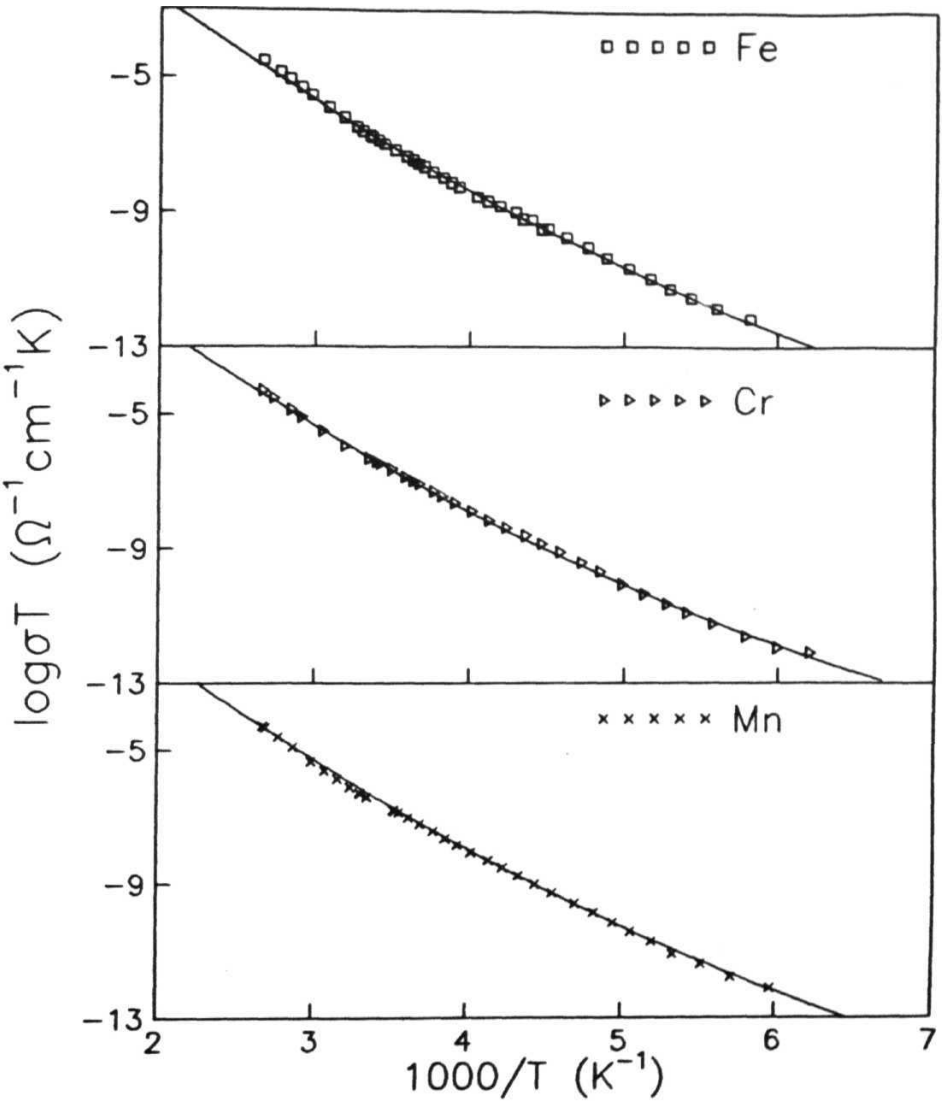


**Fig-3.12** Plot of $\log\sigma T$ versus $10^3/T$ for the $Bi_4Sr_3Ca_3Cu_{3.8}M_{0.2}O_x$ (M = Fe, Cr and MD) glasses. The solid curves are the theoretical best fits to Schnakenberg's equation.

**studies** for the doped samples were restricted to these **three glass compositions.**

## 3.7 ESR studies on glasses:

### 3.7.1 Theoretical background:

**All forms** of spectroscopy are based on the determination of energy **levels of molecules,** atoms and nuclei. These energy levels arc created by interactions which **can take place** between matter and radiation. ESR is restricted to the study of magnetic dipoles of electronic origin and is usually studied at microwave frequencies ($10^9$ to $10^{11}$ Hz). ESR **essentially** consists of observing transitions between the Zeeman levels **of the unpaired electron** in an external magnetic field H. Observing the magnetic field **at which resonance** occurs may allow one to determine the magnetic dipole moment, the **local environment** of paramagnetic species and any other non magnetic splitting (like zero **field splitting).**

The spinning electron has orbital motion around the nucleus. This electron **which** is acting as a small magnetic dipole will experience a torque tending **to turn it into** alignment with the field, but this can not take place as the electron **spin has the orbital** angular momentum about the nucleus. The axis of the spinning **electron will then precess around the** magnetic field axis. The frequency of procession is the **Larmour precession frequency** $\omega$, **and is related to** the **applied magnetic field by** the **equation** $\omega = \gamma H$ **where** 7 is **the** magnetogyric ratio of the electron. **It** is the **ratio of magnetic moment to mechanical moment of inertia, which is equal to** $7 = \frac{g\beta}{h/2\pi}$ **The basic energy equation** $h\nu = g\beta H$ **where** $\beta$ **is the magnetic moment of the electron, the Bohr magneton and g is the spectroscopic splitting factor and is a measure of the contribution of the spin and orbital motion of the electron and to its total angular momentum.**

**Spin Hamiltonian** is a particular part of **total Hamiltonian (which represents the total energy of the system),** which plays the main role in **interpreting ESR spectrum. If we restrict ourselves** to magnetic fields, electron spin and nuclear **spin of the nucleus at the symmetry,** the spin Hamiltonian (H) can be written as

$$\mathcal{H} = \beta H.g.S + I.A.S + S.D.S \qquad (3.18)$$

Where the first term is the zeeman interaction, the second term is the **hyperfine** interaction and the third term is the second order fine structure (or crystal **field interaction).** Here $\beta$ is the Bohr magneton, H is the applied magnetic field, S and I are the **electronic** and nuclear spin vectors respectively and g and A are the matrices expressing the energies of coupling between the magnetic fields associated with the vector quantities. Excluded from equation-3.17 are the nuclear zeeman, quadrapole and higher order crystal **field** terms because of the general inability to measure their effects in glasses.

For axial symmetry, the spin Hamiltonian can be written as

$$\mathcal{H} = g_{\|}\beta H_z S_z + g_{\perp}\beta(H_x S_x + H_y S_y) + hA_{\|}S_z I_z + hA_{\perp}(S_x I_x + S_y I_y) \qquad (3.19)$$

where the value g for H || to z will be called $g_{\|}$, g factor for **H** in the **XY plane** i.e., **H** ± **z will have** constant value $g_{\perp}$. $A_{\|}$ and $A_{\perp}$ are also defined **in the same way.Here** $g_x = g_y = g_{\|}$ **and** $g_z = g_{\perp}$ where as in the case of rhombic symmetry $g_x \neq g_y \neq g_z$ and $A_x \neq A_y \neq A_z$.

**Relating the experimental** spectra to **equation-3.18 requires that the spin Hamiltonian** be **diagnolized to** yield the so called **'resonance condition',** $H_{res}$ **- an expression for the magnetic field at which** resonance occurs as **a function of** the **principal-axis values of the**

**matrix quantities, the microwave frequency** $\nu$ and **the nuclear magnetic quantum number m/. In an actual experiment,** $m_I$ **takes on values I,** I-1,....., **I with equal probability, leading to** $2I+1$ equally intense lines. Of course, $H_{res}$, being a vector **quantity is specified both its** magnitude and its orientation with respect to **the principal axis coordinate** systems **of** the interaction matrices.

It is occasionally useful, particularly when dealing **with glass spectra, to define an 'effective' g value** corresponding to some particular value of $H_{res}$ according to the relation $g_{eff}\beta H_{res} = h\nu$, where h is plank's constant. These effective values of g should not **be** confused with the principal axis components of the matrix g in equation-3.18.

## ESR of Cu, Fe, Cr and Mn Ions

*Cu ions:* Cu ion can exist in three valence states $Cu^{+1}$, $Cu^{+2}$ and $Cu^{+3}$. $Cu^{+1}$ ion **has** S = 0 and hence can not give any ESR. $Cu^{+3}$ ion has S = **1 and is observable at very** low temperatures only. But $Cu^{+2}$ is very common and ESR is observable even at high temperatures. $Cu^{+2}$ has spin (S) equal to 1/2 and nuclear spin (I) equal to 3/2 **for both** isotopes $^{63}Cu$ and $^{65}Cu$. The number of lines observable is equal to $(2I+1)$ four. So, the ESR spectrum of $Cu^{+2}$ in most oxide glasses is distinctive and easily recognized on **the** basis of the principal **'g'** values ($g_{\|} \approx 2.3$, $g_{\perp} \approx 2.06$) and **a four line hyperfine splitting due** $^{63}Cu$ **and** $^{65}Cu$ [202].

***Fe ions***: Fe ions **normally** exist **in** three states $Fe^{+1}$, $Fe^{+2}$, $Fe^{+3}$. **Among** these **ions** $Fe^{+3}$ **is the most** stable ion **and the other two** ions **are unstable and their spectrum is observable at very low temperatures only.** $Fe^{+3}$ **has spin equal to 5/2 and the nuclear spin equal to 5/2, so the number of lines expected are six though it is not observed.** $Fe^{+3}$

ion is easily recognized with $g_{eff} = 6$ or $g_{eff} = 4.3$ and $g_{eff} = 2.0$ [203].

*Cr ions*: Cr exists in six different states viz. as $Cr^{+1}$, $Cr^{+2}$, $Cr^{+3}$, $Cr^{+4}$, $Cr^{45}$, $Cr^{+6}$. The principal valence states of chromium in solids are the +3 and +6. **But most** of the Cr doped glasses show signal due to $Cr^{+3}$ only. $Cr^{+3}$ has electron spin 3/2 and nuclear spin equal to 3/2. So, the number of lines observed in the ESR spectrum are four. For this $3d^3$ ion 'g factor does not fall below $\approx$ 1.95. ESR studies on chromium doped glasses shows the presence of signals at g = 5 and g = 1.97 due to $Cr^{+3}$. The g = 5 is due to zero field splitting of the $Cr^{+3}$ ion energy levels by the ligand electric field [204].

*Mn ions:* Mn ion exists in three different states viz $Mn^{+2}$, $Mn^{+3}$, $Mn^{+4}$. But among these $Mn^{+2}$ ion is the most stable and its spectrum is observable even at the high temperatures.

$Mn^{+2}$ shares the same $3d^5 6s_{5/2}$ electronic structure as $Fe^{+3}$, but its ESR spectra are distinctly different due to the addition of hyperfine structure and the occurrence of the fine structure splittings which are typically an order of magnitude smaller than those of $Fe^{+3}$ ions.

$Mn^{+2}$ ion has spin equal to 5/2 and nuclear spin equal to 5/2. The number of lines observable for $Mn^{+2}$ ion are six. This intense hyperfine sextet centered on g = 2.0 has long been recognized as the principal signature of $Mn^{+2}$ in glasses [205].

### 3.7.2 Experiment and results:

ESR studies were carried out on the doped and undoped BSCCO glasses in the temperature range 150-300 K as described in chapter-2 of the thesis.

#### (a) ESR of $Bi_4Sr_3Ca_3Cu_yO_z$ glasses:

Fig-3.13 show the ESR spectra for the 433y glasses at room temperature. The signal is broad and centered at g = 2.23 and with peak to peak line width of 425 G. On the basis of the g value and the comparison with the ESR spectra of $Cu^{+2}$ in other glass systems, the observed ESR signal could be assigned to $Cu^{+2}$ in an octahedral environment [206]. The absence of resolved hyperfine structure leads to the conclusion that there is a broad distribution of spin hamiltonian parameters. Fig-3.14 shows the ESR spectra of 433y glasses at 150 K. The hyperfine structure is still not fully resolved to estimate the hyperfine parameters. Due to the experimental limitation it was not possible to go to still lower temperatures.

The $Cu^{+2}$ concentration was estimated by double integration method of the RT spectra of these glasses and comparing against a standard sample of $CuSO_4.5H_2O$. The $Cu^{+2}$ concentration obtained is about 2 orders of magnitude less than that obtained from room temperature magnetic susceptibility data and does not vary systematically with increase in CuO content. Thus it is seen that only a small fraction of $Cu^{+2}$ ions are ESR active in these glasses. This situation is similar to that of CuO which is ESR silent and yet paramagnetic.

The absence of ESR has been reported by many groups in high $T_c$ superconductors [207-209]. The $Cu^{+2}$ in all these materials exist in either square planar $CuO_2$ planes as

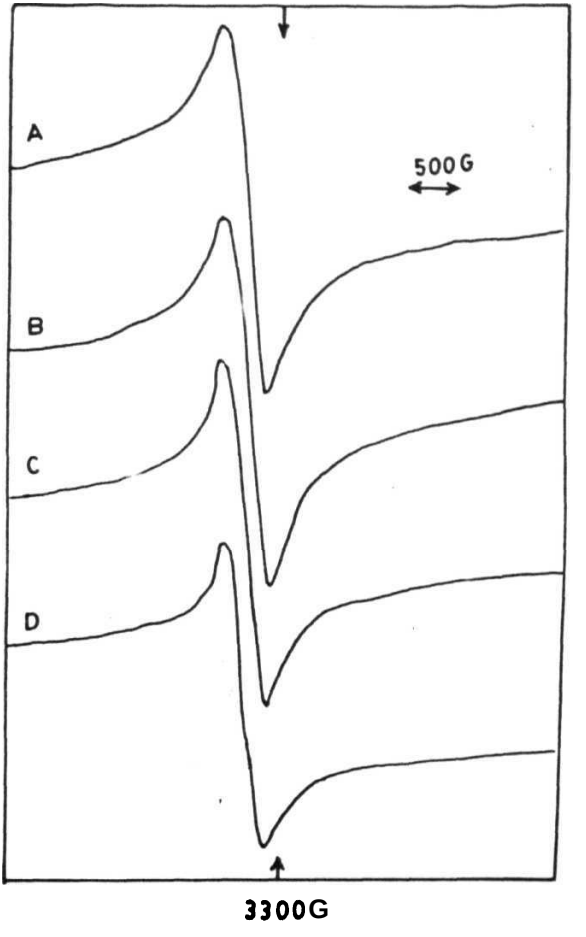


**Fig-3.13** Room temperature ESR spectra for the 433y glasses. (A) y = 3; (B) y = 4; (C) y = 5 and (D) y = 6.

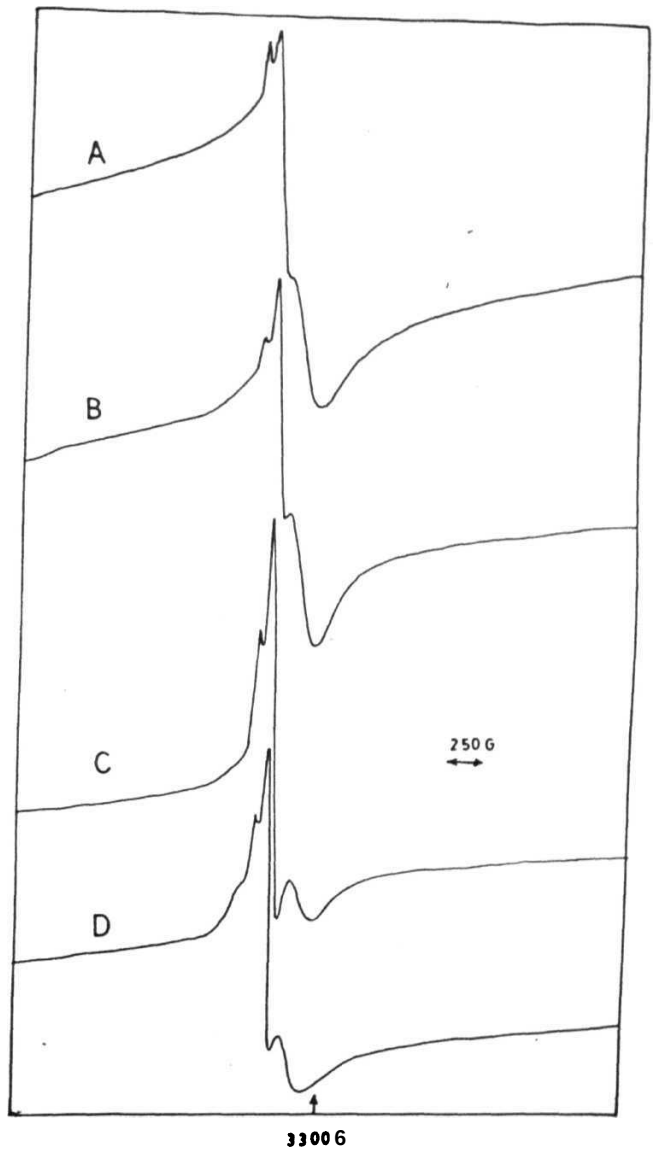


**Fig-3.14** ESR spectra for the 433y glasses at 150 K. (A) y = 3; (B) y = 4; (C) y = 5 and (D) y = 6.

in BSCCO systems or in one diamensional 180° Cu-O-Cu chains.

The small value of $Cu^{+2}$ concentration obtained for the present glass system can be explained by assuming that there exists a short range ordering in these glasses at the atomic level. Most of the Cu ions in this material could be present in square planar Cu-0 units which do not contribute to ESR signal. The formation of 2201 phase (having a single $CuO_2$ plane) as a first product of crystallization of these glasses also strengthens this contention.

(b) ESR of 3d TM doped glasses:

Fig-3.15 and fig-3.16 show the ESR spectra for the Fe doped BSCCO glasses at RT and 150 K respectively. The spectra is similar to the spectra obtained for undoped BSCCO glasses. The presence of Fe as $Fe^{+3}$ in these glasses is confirmed from the presence of two signals-one at g=4.3 and another around g=2.0 superimposed on the Cu spectra. The intensity of both these signals are found to increase with increase in dopant concentration. The g=4.3 signal can be attributed to $Fe^{+3}$ both in four fold and six fold coordination [210] while the g=2.0 signal is due to Fe ion in six fold coordination [211].

The ESR spectra for the Mn doped glasses at RT and 150 K are shown in fig-3.17 and 3.18. The spectra shows a sextet centered at g=2.0 superimposed on the Cu spectra. This is a signature of the presence of Mn as $Mn^{+2}$ in these glasses [204]. This is however insufficient to obtain any information regarding the environment of $Mn^{+2}$ in these glasses.

Fig-3.19 and 3.20 show the ESR spectra for Cr doped glasses at RT and 150 K respectively. The existence of Cr as $Cr^{+3}$ is not seen because of the overlap of Cu and $Cr^{+3}$

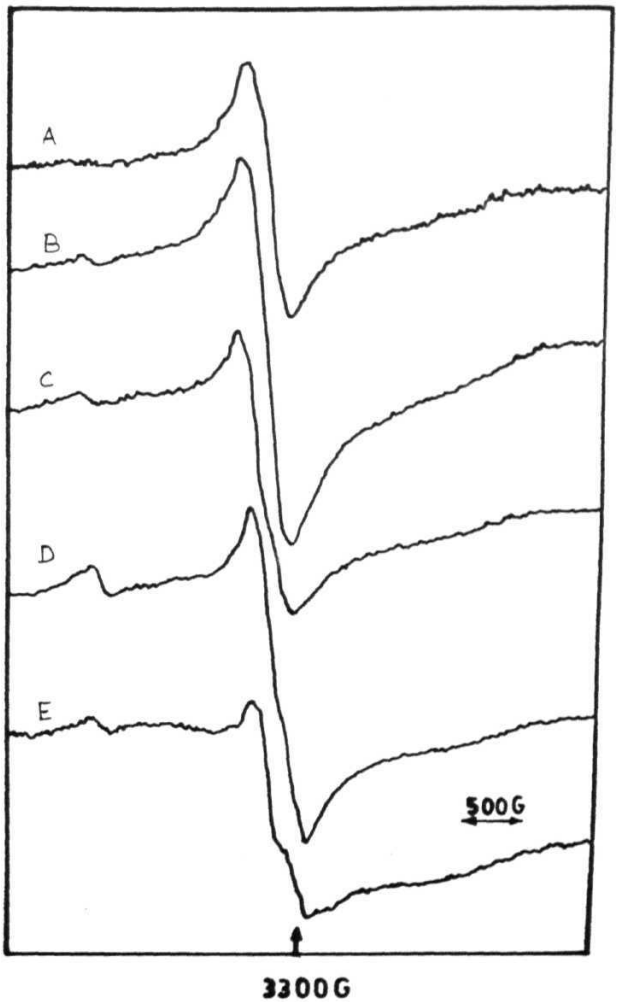


**Fig-3.15** Room temperature ESR spectra for the $Bi_4Sr_3Ca_3Cu_{4-x}Fe_xO_y$ glasses (A) x = 0.025; (B) x = 0.05; (C) x = 0.1; (D) x = 0.2 and (E) x = 0.3.

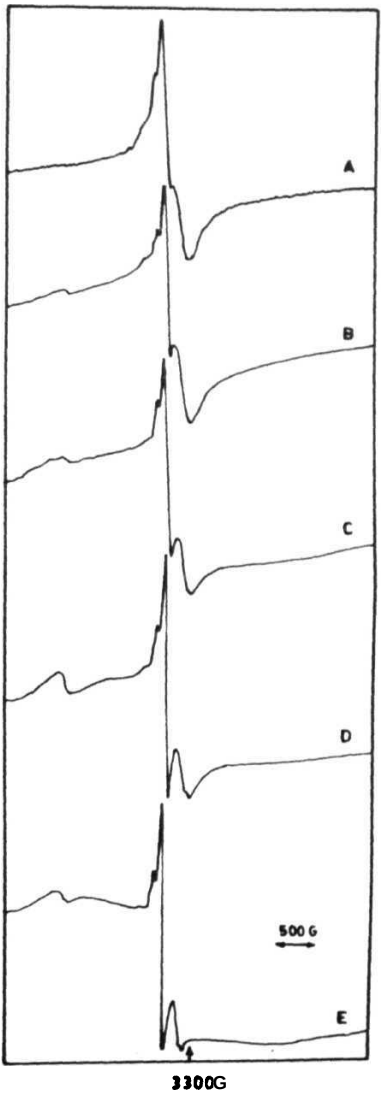


**Fig-3.16 ESR spectra for the $Bi_4Sr_3Ca_3Cu_{4-x}Fe_xO_z$ glasses at 150 K. (A) $x$ = 0.025; (B) $x = 0.05$; (C) $x = 0.1$; (D) $x$ = 0.2 and (E) $x = 0.3$.**

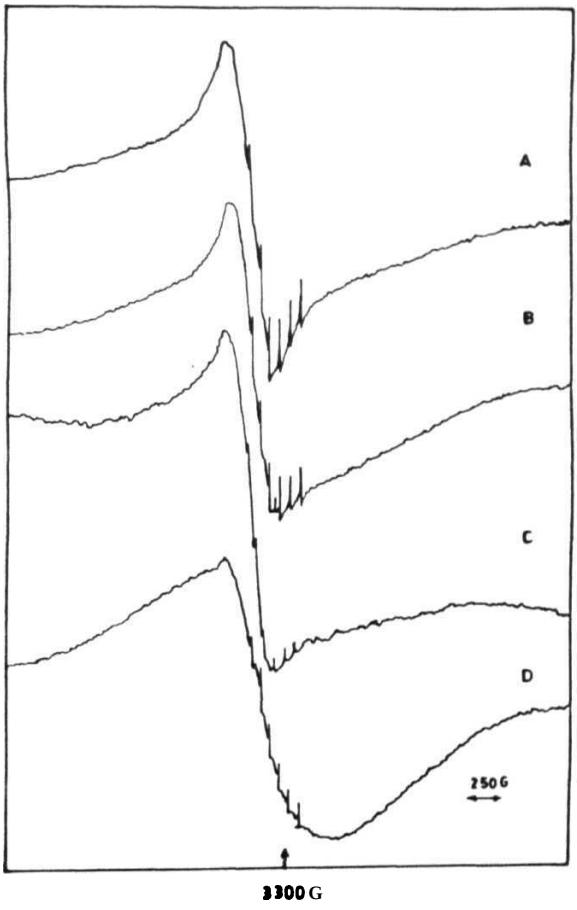


**Fig-3.17 Room** temperature ESR spectra for the $Bi_4Sr_3Ca_3Cu_{4-x}Mn_xO_y$ **glasses.** **(A) x =** 0.025; (B) x = 0.05; (C) *x* = 0.1; (D) % = 0.2.

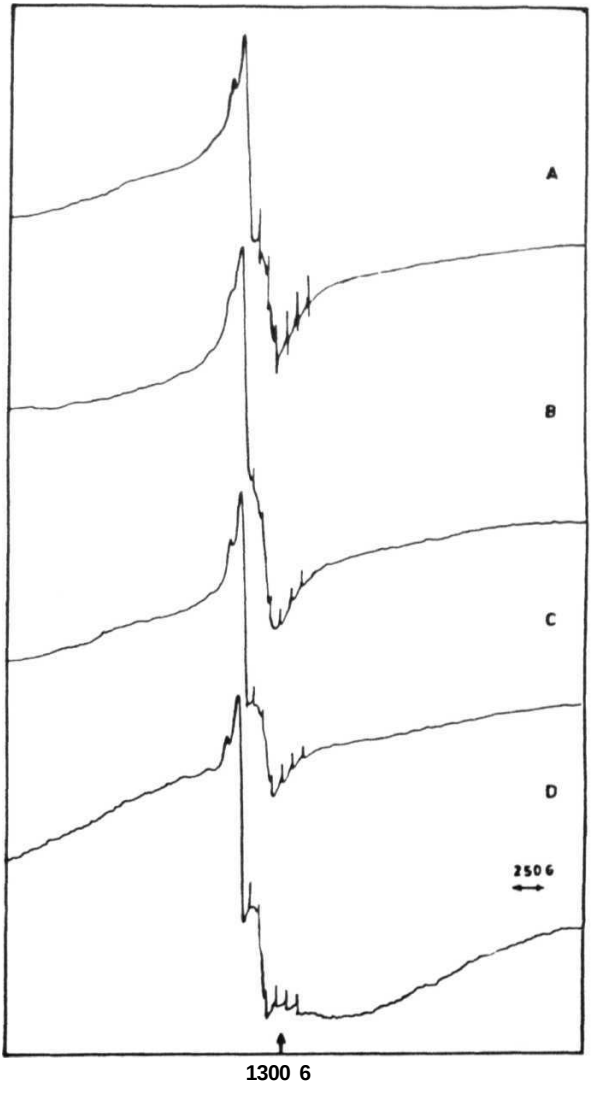


**Fig-3.** ESR spectra for the $Bi_4Sr_3Ca_3Cu_{4-x}Mn_xO_z$ glasses at 150 K. (A) x = 0.025; (B) x = 0.05; (C) x = 0.1; (D) x = 0.2.

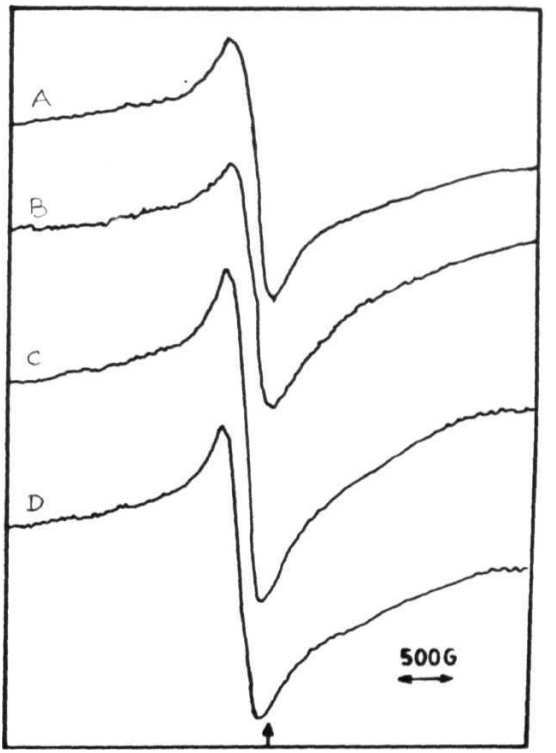


**Fig-3.19 Room temperatuie £SR spectra for the $Bi_4Sr_3Ca_3Cu_{4-x}Cr_xO_z$ glasses. (A) x = 0.025; (B) x = 0.05; (C) x = 0.1; (D) x = 0.2.**

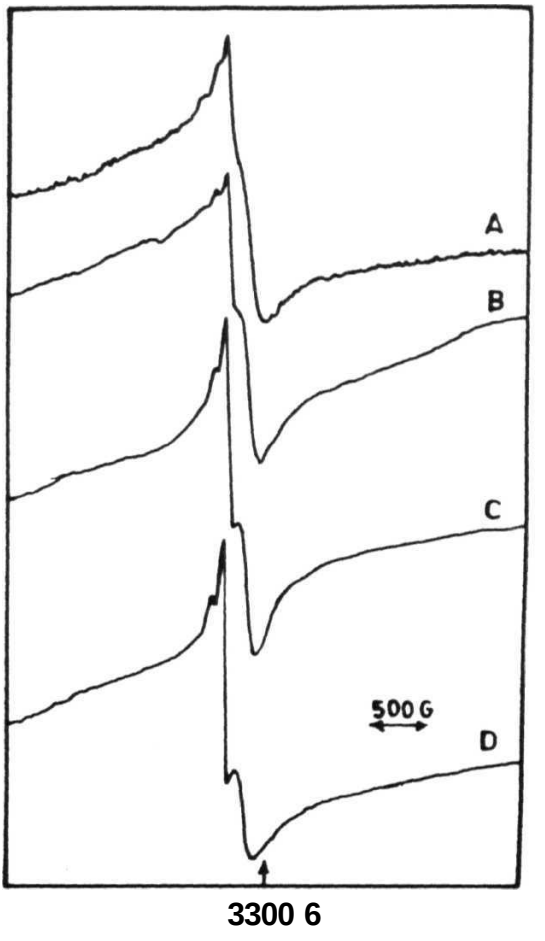


**Fig-3.20** ESR spectra for the $Bi_4Sr_3Ca_3Cu_{4-x}Cr_xO_z$ glasses at 150 K. (I) x = 0.025; (B) $x$ = 0.05; (C) x = 0.1; (D) $x$ = 0.2.

signals. The presence of $Cr^{+3}$ is however confirmed from the change in the line shape of the spectra as in the case of 3d doped glasses and the undoped glasses with higher CuO content.

# Chapter 4

## STUDIES ON Bi-Sr-Ca-Cu-O SUPERCONDUCTING GLASS CERAMICS

This chapter deals with the crystallization and phase formation studied on $Bi_4Sr_3Ca_3Cu_4O_x$ glasses. The parallel studies of XRD and electrical resistivity were carried out on the samples as a function of heat treatment temperature and duration, in order to understand the phase formation and its effect on the electrical conduction. The systematic studies of the effect of CuO content and the 3d TM dopants (Fe, Cr and Mn) on the structural and superconducting properties of the superconducting glass ceramics are also presented.

### 4.1 Crystallization studies on $Bi_4Sr_3Ca_3Cu_4O_x$ glasses:

#### 4.1.1 Thermal analysis of $Bi_4Sr_3Ca_3Cu_4O_x$ glasses:

Differential scanning calorimetery technique was used for thermal analysis of the sample. The variable heating rate DSC method was employed to evaluate the kinetics of crystallization. Bulk glasses were used instead of powder in order to avoid the effect of particle size distribution. It is known that the crystallization peak shifts to higher temperature with increase in the heating rate. The DSC scans at 5, 10, 15 and 20°C/min were recorded. Table-4.1 shows the change in crystallization peak temperature with scanning rate. The DSC crystallization peak temperature $T_x$ and the heating rate are related and different equations have been derived correlating these parameters. One of the equation

Table-4.1
Change in Crystallization peak temperature as a function of DSC **scan rate**

| scan rate ($\Phi$) °/minute | $T_p$ (C) |
|---|---|
| 5 | 468 |
| 10 | 476 |
| 15 | 482 |
| 20 | 486 |

Table-4.2
Electrical parameters of the 4334 samples heat treated at 820°C for various durations

| heat treatment duration | $\rho_{300}$ (m$\Omega$ cm) | $T_{c(zero)}$ (K) | *Po* (m$\Omega$ cm) | $\alpha'$ ($\mu\Omega$ cm $K^{-1}$) | TCR |
|---|---|---|---|---|---|
| 1 hr. | 149.6 | <8 | - | - | -ve |
| 2 hrs. | 102.3 | <8 | - | - | -ve |
| 6 hrs. | 22.83 | 16 | | - | -ve |
| 12 hrs. | 11.47 | 56 | | ~ | -ve |
| 24 hrs. | 6.03 | 60 | 3.92 | 7.08 | +ve |
| 48 hrs. | 4.40 | 64 | 2.45 | 6.56 | +ve |
| 96 hrs. | 4.19 | 74 | 1.49 | 8.98 | +ve |

which has been successfully applied to study crystallization [212] has the form

$$ln\frac{\Phi}{(T_p - T_s)} = \frac{-E_a}{RT_p} + ln\nu \tag{4.1}$$

**and** relates the the activation energy $E_a$ to the exotherm peak **temperature** $T_p$ **and** the heating rate $\Phi$ of the DSC scan. $\nu$ is the frequency factor and along with $E_a$ is related to the reaction rate constant (k) by

$$k = \nu \exp\frac{E_a}{RT_p} \tag{4.2}$$

The plot of $\ln\frac{\Phi}{(T_p - T_s)}$ versus $1/T_p$ (fig-4.1) is found to be a straight line verifying the applicability of equation-4.1 to the present glass. The crystallization activation energy $E_a$ calculated by the least square fitting of the data is 388 kJ/mole. Higher values of $E_a$ ranging from 400 to 432 kJ/mole are reported for Bi-Sr-Ca-Cu-O glasses by other groups [120, 122, 125]. The Avrami value n calculated from equation

$$n = \frac{2.5}{\Delta T}\frac{RT_p^2}{E_a} \tag{4.3}$$

for this sample is 3.69 which indicates a bulk crystallization process.

### 4.1.2 Crystallization and high $T_c$ phase formation:

Three separate samples of 4334 glass were heat treated in an electrical furnace in air. The temperature was scanned from room temperature to 500°C for sample 1, to 650°C **for** sample 2 and 820°C for sample 3 at a rate of 15°/min. On reaching the maximum temperature the samples were quenched to room temperature in air. Parallel XRD and DC resistivity studies were carried out on the heat treated samples in order to understand the phase formation. The interior morphology of the samples was studied by carrying out XRD studies after acid-etching the surface of the samples. Change in weight of the

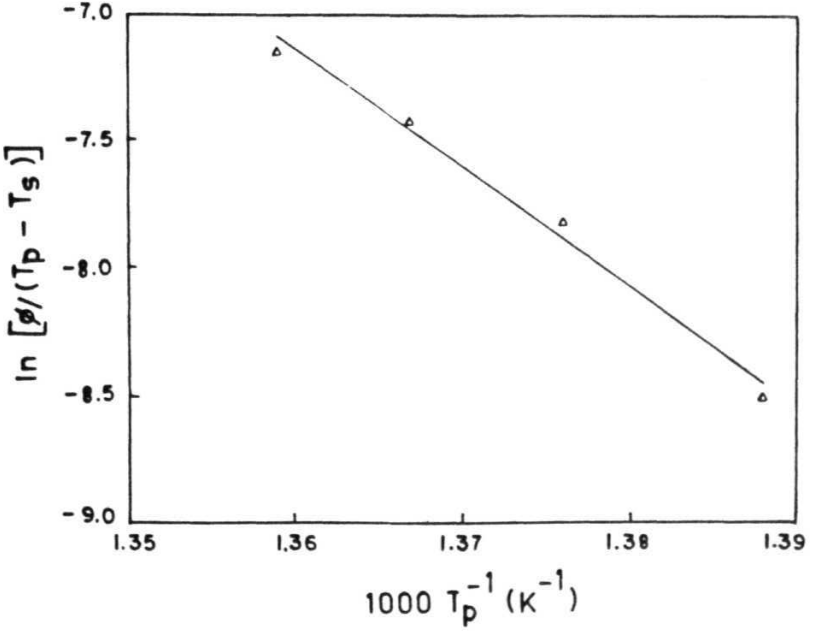


Fig-4.1 $\ln[\Phi/(T_p-T_s)]$ versus $1/T_p$ for 4334 glass.

samples as a result of heat treatment were recorded using a microbalance. The samples were heat treated at 820°C for different durations to study the growth of high $T_c$ superconducting phase.

**Electrical and** superconducting properties:

Fig-4.2(A,B,C) show resistivity *(p)* versus temperature (T) plot for samples scanned from RT to 500, 650 and 820°C respectively at a scanning rate of 15°C/min. The samples heat treated up to 500 and 650°C showed semiconducting behaviour in the whole temperature range of 8-300 K. The sample heat treated up to 820°C showed semiconducting behaviour in the temperature range 100-300 K. Below 100 K, resistivity drops at around 90 and 30 K indicative of superconducting transitions were observed. The sample did not however show $T_{c(zero)}$ down to the lowest temperature of 8 K. The room temperature resistivity of the samples was found to decrease with the increase in maximum temperature scanned.

A comparison with the RT resistivity of the 4334 glass sample show that the sample scanned up to 500°C showed a drop in RT resistivity of about 2 orders of magnitude (from 7.3 x $10^8$ to 1.84 x $10^7$ Ω-cm) while the sample scanned up to 650°C, showed a drop of about 8 orders of magnitude (to 7.3 Ω-cm). The room temperature resistivity is found to have dropped to 0.428 Ω-cm for the sample scanned up to 820°C. These results indicate that the rate of devitrification reaction is maximum in the 500-650°C temperature range. It was also found that no change in weight of the sample took place on crystallization. However, as the temperature was raised to 650°C, an increase in weight of the sample was observed.

Fig-4.3 shows *p* versus T plot for 4334 glass ceramic samples heat **treated** at **a** fixed

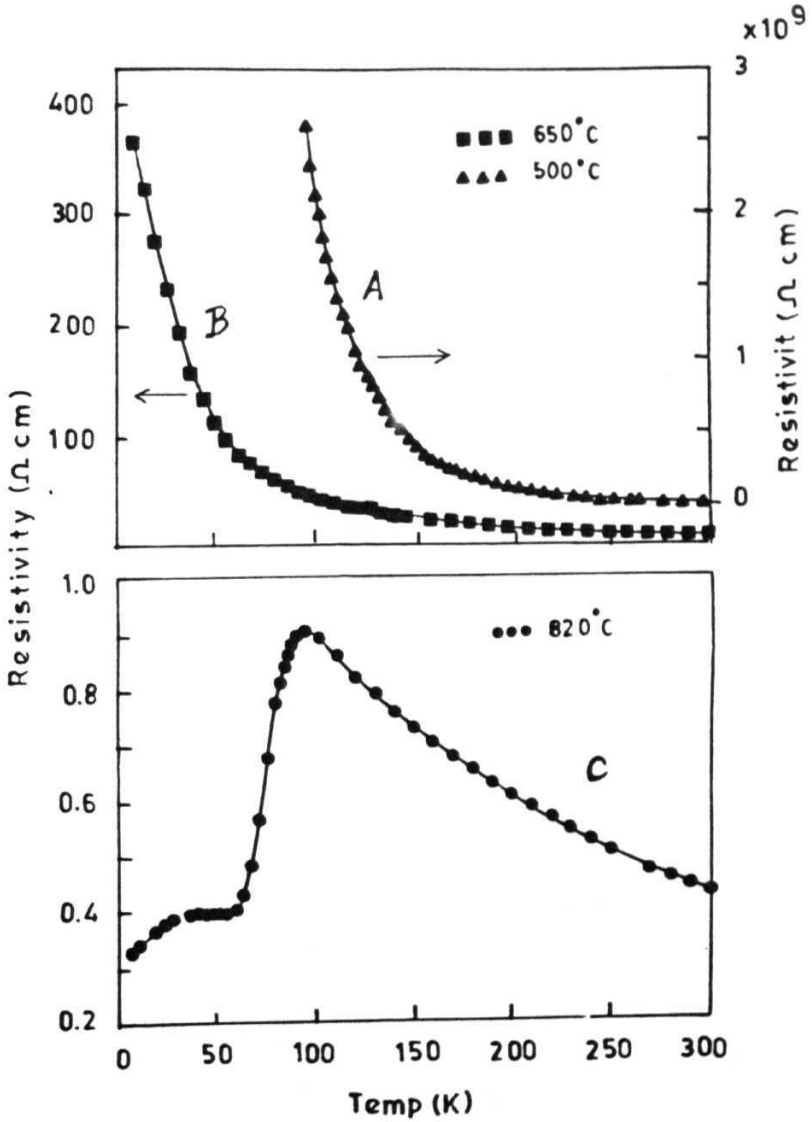


Fig-4 2 Resistivity versus temperature plots for 4334 glass samples heat treated by scanning the temperature from RT to (A) 500; (B) 650 and (C) 820°C.

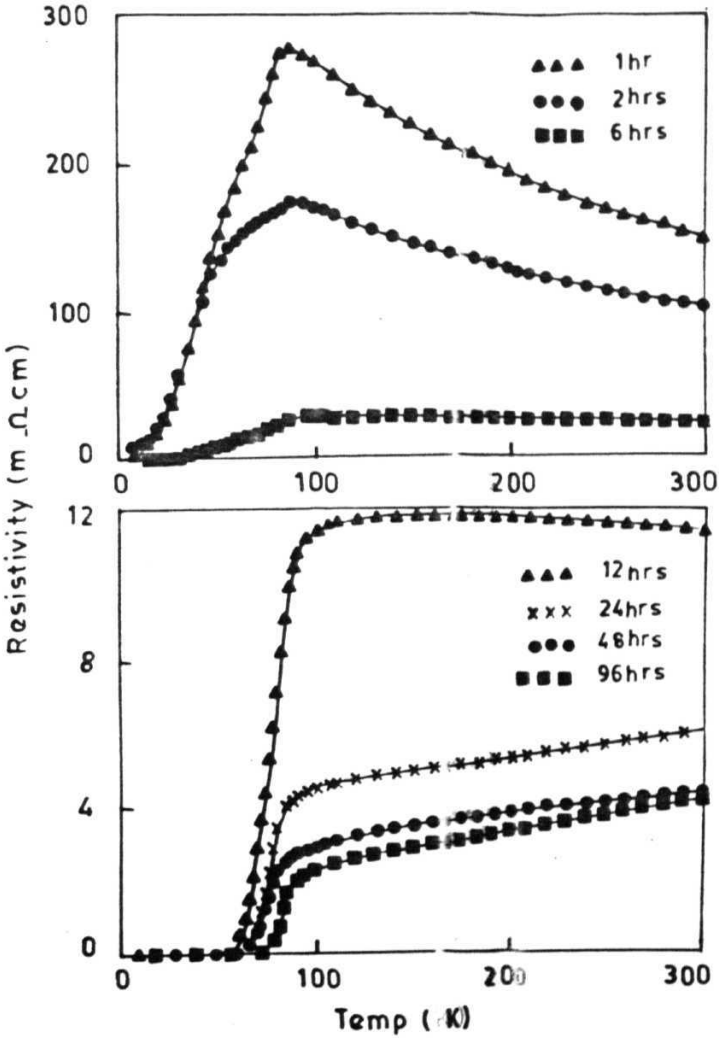


Fig-4.3 Resistivity versus temperature plots fo; r433 gl sceramic samples beat treated at a fixed temperature of 820° C fa va ous durations.

temperature of 820°C for various durations followed by furnace cooling. The samples reached the superconducting state at a temperature dependent on heat **treatment** duration (table-4.2). The *p* versus T plots for the sample heat treated for less than 12 hours showed semiconducting behaviour in the normal state region i.e. 100-300 K temperature range. The normal state resistivity decreases with increase in heat treatment duration. The Insulator-Metal transition i.e. the change in sign of the temperature coefficient of resistivity is observed when the sample is heat treated for 12 hours and the RT resistivity $\approx 10^{-2}\ \Omega$-cm. The sample heat treated for longer durations showed metallic behaviour i.e. a positive temperature coefficient of resistivity in 100-300 K temperature range. The temperature dependence of normal state resistivity of the metallic samples is described by a linear equation of the form

$$p(T) = \rho_o + \alpha T \qquad \textbf{(4.4)}$$

where $\rho_o$ and $\alpha = (d\rho/dT)$ are the residual resistivity and the metallicity of the material respectively. The $\rho_o$ and $\alpha$ values estimated by the least square fitting of the experimental data are given in table-4.2. The metallicity is found to be increasing with heat treatment duration. On the other hand, the $\rho_{300}$ and $\rho_o$ decrease with increasing heat treatment duration. The $T_{c(zero)}$ increases and reaches a value of 74 K after a heat treatment of 96 hours. The superconductivity does not improve with further heat treatment. The $\rho$-T plot (fig-4.4) for a sample heat treated at 850°C for 24 hours shows an increase in $T_{c(onset)}$ to 110 K without significantly increasing the $T_{c(zero)}$. This indicates the formation of Bi-2223 phase at this temperature. Thus a temperature close to 820°C seems to be more favourable for the preparation of single phase Bi-2212 superconductors.

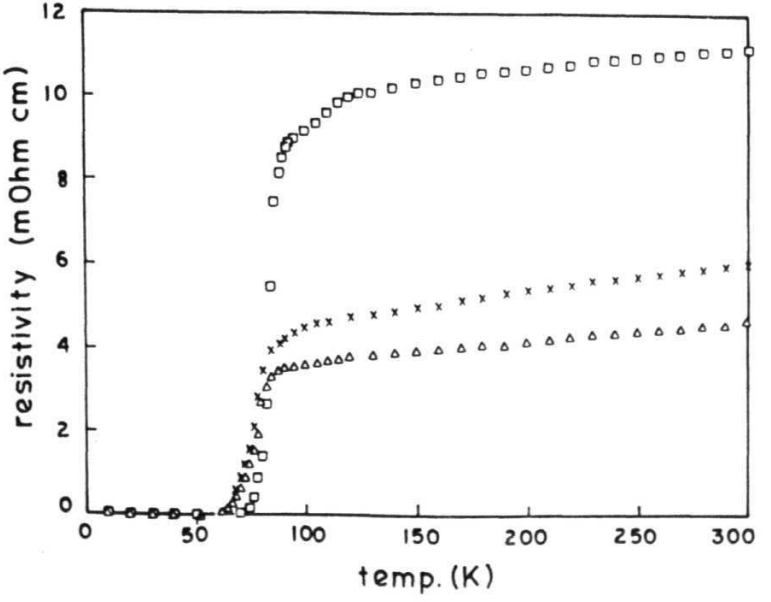


Fig-4.4 Resistivity versus temperature for 4334 glass sample heat treated at 850°C for 24 hrs (□). The plots for bulk sample and pellet heat treated at 820°C for 24 hours are also shown for comparison.

**X-ray diffraction** studies:

Fig-4.5 shows bulk XRD patterns at room temperature for the 4334 glass sample scanned to various temperatures. The XRD pattern of the bulk glass is shown in fig-4.5(A). The XRD pattern for the sample heat treated to 500°C show some weak reflections similar to the published XRD peaks of $Bi_2Sr_2CuO_z$ crystalline phase (fig-4.5(B)). Fig-4.5(C) shows the XRD pattern of the same sample after acid-etching the surface layers. The pattern remains similar implying that the formation of $Bi_2Sr_2CuO_z$ crystalline phase is a bulk process. The sample registers no change in weight as a result of this heat treatment implying that the formation of this phase does not involve the uptake of oxygen from the atmosphere. Fig-4.5(D) shows the pattern for the sample heat treated to 650°C . One can notice the emergence of weak reflection peaks which can be assigned to $Bi_2Sr_2CaCu_2O_z$ phase and $Cu_2O$. Further increase in the temperature to 820°C led to the increase in th intensity of the peaks corresponding to $Bi_2Sr_2CaCu_2O_z$ phase at the expense of the $Bi_2Sr_2CuO_z$ phase reflection peak intensity (fig-4.5(E)). The XRD pattern of this sample after etching the surface could be assigned to $Bi_2Sr_2CuO_z$ crystalline phase (fig-4.5(F)). This implies that the growth of the $Bi_2Sr_2CaCu_2O_z$ crystalline phase starts from the surface. From the increased weight of the sample it can also be inferred that the formation of this phase at the surface of the sample is accompanied by the absorption of oxygen from the atmosphere. The heat treatment at 500°C for extended duration does not increase the intensity of the peaks in the XRD pattern. However the intensity of the peaks corresponding to the Bi-2212 phase increase considerably at the expense of the Bi-2201 peaks when the heat treatment is carried out at 820°C for extended duration. Fig-4.7 shows the XRD pattern for the 4334 glass heat treated at 820°C for 96 hours. All the peaks could be assigned to Bi-2212 superconducting phase assuming a pseudo-tetragonal symmetry with lattice parameters $a=3.82\ A$ and $c=30.74\ A$ [42].

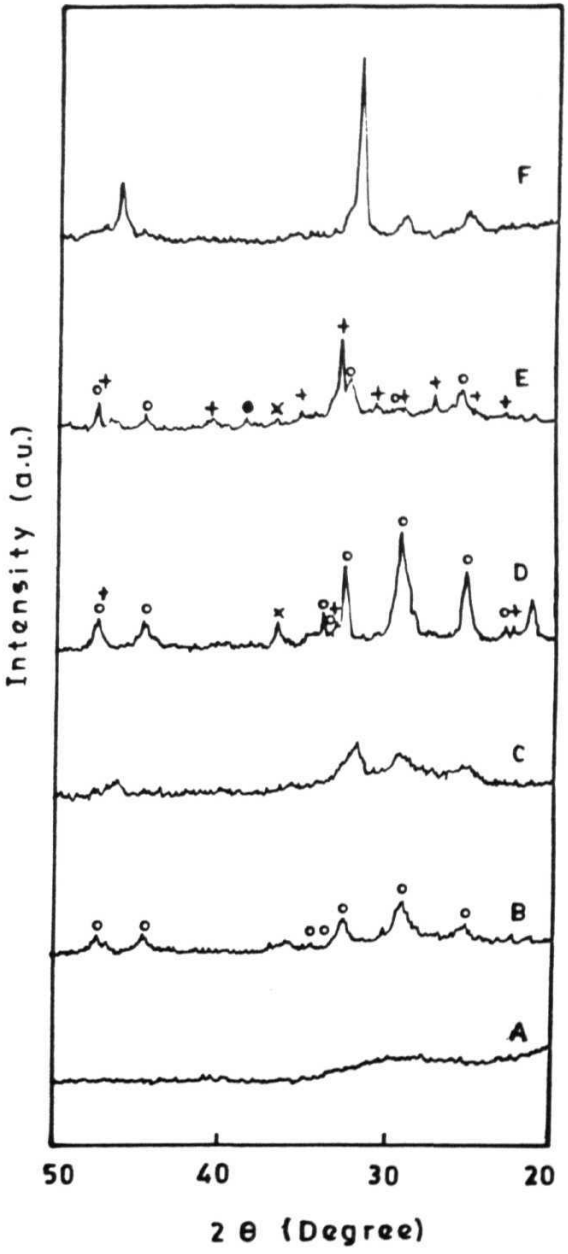


Fig-4.5 XRD powder patterns at room temperature for 4334 glass (A) and samples scanned for various temperatures (B) 500° C (C) after acid etching the surface (D) 650° C (E) 820° C (F) after acid etching the surface. (o) Bi-2201 (+) Bi-2212 (x) $Cu_2O$.

### 4.1.3 **Effect of mechanical processing on the superconducting phase formation in $Bi_4Sr_3Ca_3Cu_4O_z$** glasses:

Glasses of 4334 composition were powdered and heat treated for various durations at 820°C. **The** heat treated powder was pelletised. The pellet was **heat treated at** 820°C in air for 1 hour and then furnace cooled. Fig-4.6 shows the resistivity plots **for the mechanically** processed samples heat treated for 3 different durations at 820°C. **The** duration includes the duration of heat treatment of the pellet also. A comparison **of the** resistivity plots of the mechanically processed and the bulk sample heat treated for the same duration show that mechanical processing gives samples of metallic normal state resistivity with a $T_{c(zero)}$=40 K, for heat treatment duration of 6 hours, while heat treatment of about 24 hours duration is required to obtain metallic normal state resistivity behaviour of bulk samples. The samples also showed smaller values of normal state resistivities in comparison with that of the bulk samples. It is also seen that the $T_c(zero)$ of the processed samples were significantly higher than that of the bulk samples for lower durations of heat treatment implying that the initial oxygen absorption is significantly enhanced **by** powdering.

## 4.2 Studies on $Bi_4Sr_3Ca_3Cu_yO_z$ ($3 < y < 6$) superconducting ceramics:

### 4.2.1 **Preparation of the** samples:

Glasses of composition $Bi_4Sr_3Ca_3Cu_yO_z$ ( $3 < y < 6$ ) were **heat treated in an electric** furnace **at** 820°C for 96 hours and the samples were subsequently furnace **cooled.**

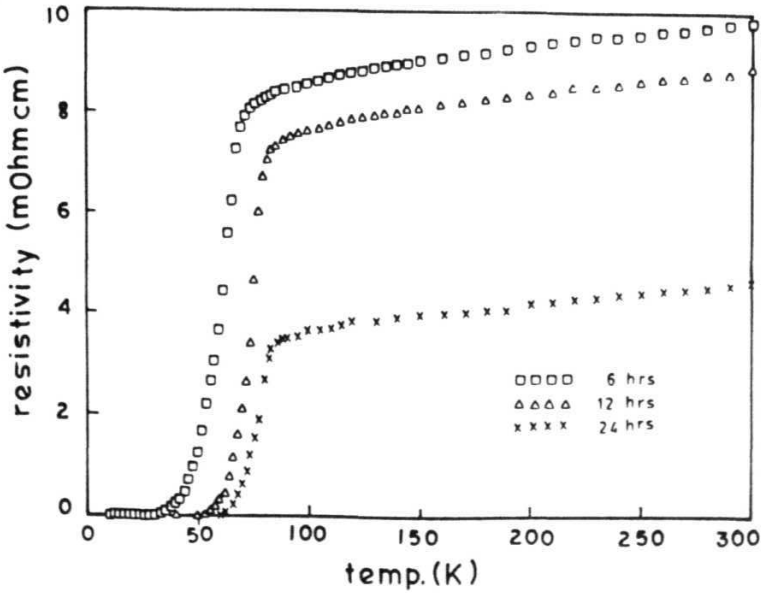


Fig-4.6 Resistivity vs. temperature plots for the mechanically processed 4334 sample heat treated at 820° C for various durations.

### 4.2.2 Structural studies:

### X-ray diffraction studies:

**The samples** were characterised by X-ray diffraction **(XRD)** studies **using** $Cuk_{\alpha}$ **radiation and the** lattice parameters obtained from the observed **reflections by the lead square fitting assuming** a pseudo tetragonal symmetry.

The **XRD** studies reveal predominantly single phase formation **for all the** samples studied. The XRD patterns (fig-4.7) show well defined reflections **all of which could be** indexed on the basis of Bi-2212 structure. The $a$ and $c$ lattice parameters **obtained** are 3.82 and 30.72 $A$ respectively and do not change with variation **in** CuO **content. The XRD patterns** of the 4334 and 4335 samples showed highly intense $[0, 0, l]$ **reflections, indicating** orientation of superconducting crystallites in a plane **perpendicular to the c-axis.** Such an indication of grain alignment is not found in the **4333 and 4336 samples. Traces of** $Cu_2O$ impurity phase were detected in the case **of ceramics containing higher CuO content.** The $Cu_2O$ impurity peak intensity was found **to** increase **with increase in CuO** content. Such traces of $Cu_2O$ impurity are also seen in the **XRD pattern of the** $Bi_2Sr_2CaCu_2O_z$ superconducting glass ceramics synthesised by **R.Sato** et **al [124].**

**Scanning Electron Microscopy (SEM) studies:**

**The scanning Electron Micrographs of** the **433y superconducting glass ceramics (fig-4.8) show that all the** samples **have** plate **like morphology, typical of superconductors in this system. The 4334 samples shows better inter-grain connectivity. The crystallite growth in the case of 4336 glass ceramics is however more uniform in comparison with the glass ceramics containing lower CuO content. This may be due to the excess CuO acting as a**

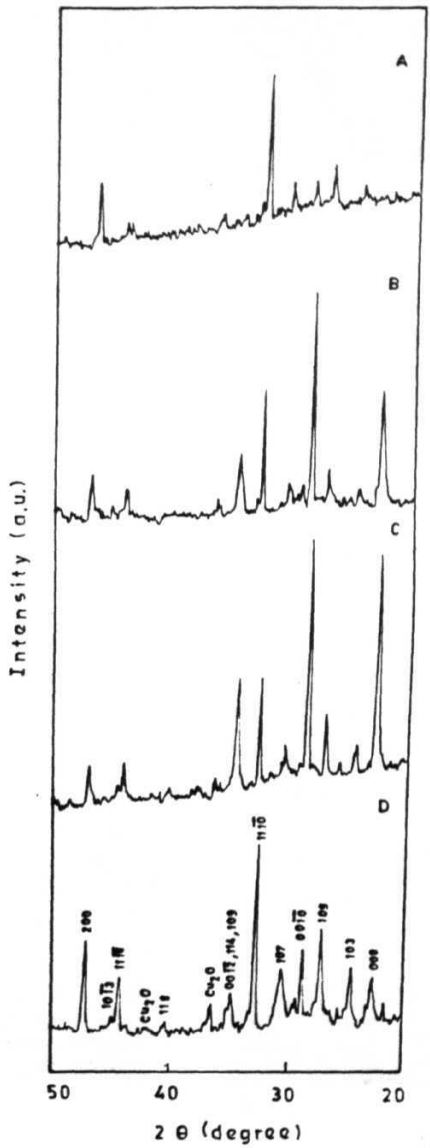


Fig-4.7 XRD patterns for 433y glass ceramics heat treated for 96 hours at 820°C. (A) 4333; (B) 4334; (C) 4335; (D) 4336.


(a)

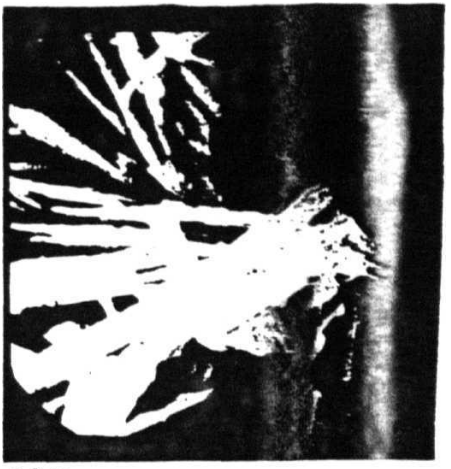


(b)

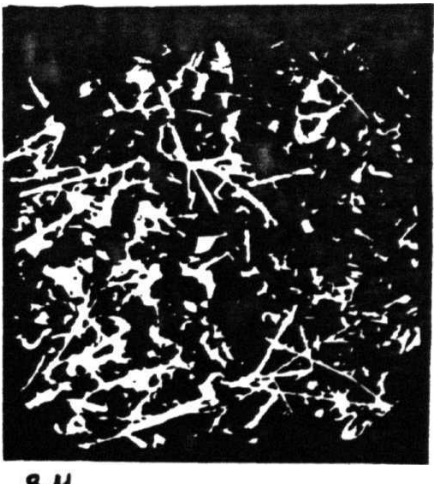


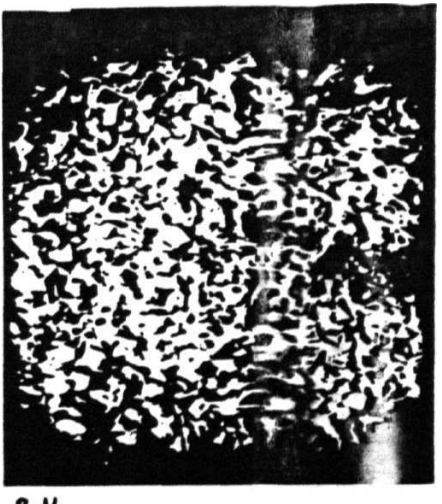


(d)

**Fig-4.8 Surface SEM micrographs of (a) 4333 (b) 4334 (c) 4335 and (d) 4336 raperconducton.**

flux and aiding the growth of superconducting crystallites.

### 4.2.3 Electrical and superconducting properties:

Meissner studies:

AC susceptibility studies were carried out on the 433y superconducting glass ceramics as a function of temperature in the temperature range 15-300 K in a low AC field of 0.1 Oe using the set up described in chapter-2. All the samples showed diamagnetic behaviour below $T_c$ = 74 K. The $T_c$ was found to be independent of the CuO content.

Electrical resistivity:

Electrical resistivity measurements were carried out by the standard four probe method as a function of temperature in the temperature range 10-300 K using the set up described in chapter-2.

The resistivity *(p)* for the $Bi_4Sr_3Ca_3Cu_yO_z$ glass ceramics as a function of temperature (T) is shown in fig-4.9. All the samples were found to be superconducting with well defined metallic behaviour down to 100 K and superconducting $T_{c(zero)}$ in the temperature range 70-74 K. The samples show a $T_{c(onset)}$ of 90 K which does not vary with CuO content. The resistivity in the normal state is a linear function of temperature and follows equation-4.4. The values of the resistivity at RT ($\rho_{300}$), the residual resistivity ($\rho_o$), the metallicity (a) and $T_{c(zero)}$ for the 433y superconducting glass ceramics are given in the table-4.3. All the 433y glass ceramic samples showed small values of $\rho_{300}$ and $\rho_o$. $\rho_{300}$ and $\rho_o$ do not show any systematic variation as a function of CuO content. The metallicity a is maximum for the 4334 glass ceramic . The $T_{c(zero)}$ is found to be lower

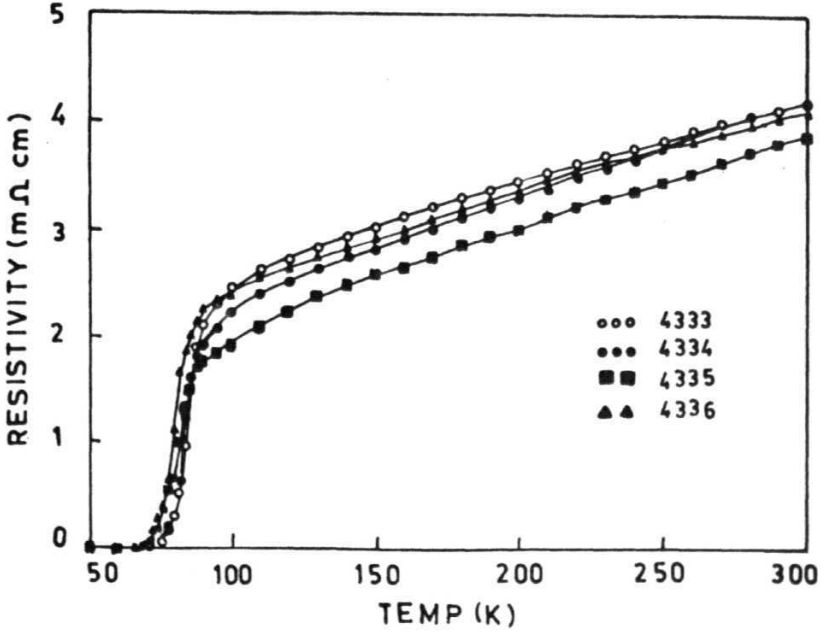


Fig-4.9 Resistivity versus temperature plots for 433y glass ceramics heat treated at 820°C for 96 hours. (○) y=3; (●) y=4; (■) y=5; (▲) y=6.

Table-4.3

**Physical and transport parameters of the 433y system**

| sample | $\rho_{300}$ (mΩ cm) | $\rho_o$ (mΩ cm) | a' ($\mu\Omega$ cm $K^{-1}$) | resistivity $T_{c(zero)}$ (K) | (in the glasses) |
|---|---|---|---|---|---|
| 4333 | 4.18 | 1.9 | 7.67 | 74 | 0.50 |
| 4334 | 4.19 | 1.5 | 8.98 | 74 | 0.67 |
| 4335 | 3.90 | 1.3 | 8.61 | 72 | 0.76 |
| 4336 | 4.11 | 1.8 | 7.92 | 70 | 0.73 |

**for the 4335** and **4336** samples. The larger transition width in the case of these samples may be due to the presence of $Cu_2O$ impurity phase and the changes in microstructure as shown in the SEM micrographs. The higher metallicity and lower superconducting transition width for the 4334 sample in comparison to the other samples may be due to better grain connectivity and alignment as seen from the SEM and XRD studies. Thus we see that a starting stochiometry of 4334 which gives superconducting ceramics with higher metallicity and $T_{c(zero)}$ and crystallites with preferential orientation is the ideal starting composition to obtain 85 K phase superconductors. An excess of CuO acts as a flux and helps in the growth of uniform crystallites. These results are in conformity with the results on 4334 and 4336 superconductors synthesised by the solid state reaction method by Tarascon et al [213]. They find that the 4334 starting stochiometry gives 85 K single phase superconductors and the 4336 composition helps in the formation of large and uniform crystallites, but shows the emergence of CuO impurity peaks.

It is seen that large changes in the CuO content do not bring about changes in the crystal lattice. The small change in $T_{c(zero)}$ of about 4 K may be attributed to the changes in the microstructure and the $Cu_2O$ impurity phase emerging due to excess CuO content.

Considering the c values of 433y glasses and the superconducting parameters of the corresponding glass ceramics (table-4.3), we find that there is no correlation between the c value and the superconducting properties or the size and orientation of crystallites. The electrical properties of the 433y glasses also do not indicate any correlation with the superconducting properties of the corresponding glass ceramics.

## 4.3 Studies on 3d TMO doped $Bi_4Sr_3Ca_3Cu_4O_z$ superconducting ceramics:

### 4.3.1 Preparation of the samples:

Glasses of composition $Bi_4Sr_3Ca_3Cu_{4-x}M_xO_z$ ($0 < x < 0.2$ for M = Cr and Mn) and ($0 < x < 0.3$ for M = Fe) were heat treated at 820°C for 96 hours and subsequently furnace cooled to obtain superconducting glass ceramics.

### 4.3.2 Structural studies:

The samples were characterised by X-ray diffraction (XRD) using $Cuk_\alpha$ radiation and the lattice parameters determined from the observed reflections by the least square fitting assuming a pseudo tetragonal symmetry.

Fig-4.10 shows a representative XRD pattern for Fe doped BSCCO glass-ceramics. The X-ray diffraction studies reveal predominantly single phase formation up to x = 0.05 for M = Fe and Cr and upto x = 0.1 for M = Mn. The XRD pattern for higher values of x show traces of impurity and Bi-2201 phase. The analysis of the XRD patterns show that the *a*-lattice parameter is equal to 3.82 *A* and does not vary appreciably with doping. The *c*-lattice parameter shows a clear decrease with doping for all the 3 doped series of samples (table-4.4).

Mossbauer studies on Fe doped 2212 by Ruzhang et al [214] have shown that Fe enters the lattice as $Fe^{+3}$. The ionic radius of $Fe^{+3}$ ion is 0.64 *X* while that of $Cu^{+2}$ is 0.69 *X*. Hence the observed decrease in the c-lattice parameter as a result of $Fe^{+3}$ substitution is explained.

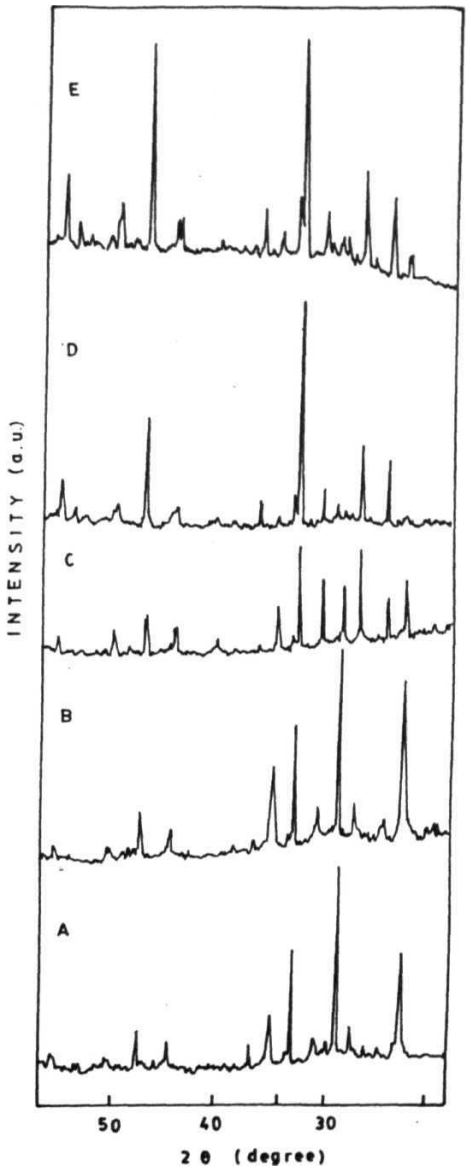


**Fig-4.10** XRD patterns for $Bi_4Sr_3Ca_3Cu_{4-x}Fe_xO_z$ superconducting glass ceramics beat treated for 96 bours at 820°C. (A) x = 0.025; (B) $x$ = 0.05; (C) x = 0.1; (D) x = 0.2 and (E) x = 0.3.

Table-4.4

Some parameters obtained from structural and transport properties **of doped** 4334 superconducting **ceramics.**

| sample | *c*-parameter *A* | P300 *(mil* cm) | *Po (mil* cm) | $\alpha'$ ($\mu\Omega$ cm $K^{-1}$) | resistivity $T_{c(zero)}$ (K) | susceptibility $T_{c(onset)}$ (K) |
|---|---|---|---|---|---|---|
| Fe doped | | | | | | |
| **x = 0** | 30.74 | 4.19 | 1.5 | 8.98 | 74 | 78 |
| x = 0.025 | 30.73 | 4.26 | 2.2 | 6.89 | 68 | 72 |
| x = 0.05 | 30.71 | 6.07 | 5.1 | 3.48 | 56 | 72 |
| x = 0.1 | 30.69 | 6.50 | 5.4 | 3.66 | 52 | 66 |
| x = 0.2 | 30.66 | 10.13 | 5.8 | 14.08 | 40 | 60 |
| x = 0.3 | 30.64 | 11.55 | 5.9 | 18.66 | 36 | 57 |
| Cr doped | | | | | | |
| x = 0 | 30.74 | 4.19 | 1.5 | 8.98 | 74 | 78 |
| x = 0.025 | 30.73 | 5.55 | 4.0 | 5.15 | 72 | 78 |
| x = 0.05 | 30.72 | 7.72 | 5.5 | 7.62 | 71 | 76 |
| x = 0.1 | 30.69 | 8.11 | 6.7 | 5.12 | 50 | 74 |
| x = 0.2 | 30.68 | 10.98 | 9.1 | 6.46 | 46 | 69 |
| Mn doped | | | | | | |
| x = 0 | 30.74 | 4.19 | 1.5 | 8.98 | 74 | 78 |
| x = 0.025 | 30.73 | 4.85 | 2.6 | 7.60 | 72 | 78 |
| x = 0.05 | 30.74 | 5.04 | 3.2 | 6.31 | 64 | 76 |
| x = 0.1 | 30.72 | 5.38 | 3.25 | 7.02 | 62 | 74 |
| x = 0.2 | 30.73 | 5.62 | 3.96 | 5.64 | 54 | 72 |

The two most stable ionic states of Cr are $Cr^{+3}$ and $Cr^{+6}$ with ionic radii 0.69 and 0.52 $A$ respectively. Cr is unlikely to exist in $Cr^{+6}$ state as the observed decrease in c-lattice parameter could have been larger than that observed as a result of $Fe^{+3}$ doping. Since $Cr^{+3}$ has an ionic radius equal to that of $Cu^{+2}$, $Cr^{+3}$ is considered to be the most probable state of Cr in this system. The small decrease in c-lattice parameter as a consequence of Cr doping can be explained by considering the different Jahn-Teller effect [215] of the 3d ions. Jahn-Teller distortion causes an elongation of the c-axis bond of the oxygen octahedron surrounding the 3d ion.

ESR studies on Mn doped Bi-Sr-Ca-Cu-0 glasses show a sextet centered at $g = 2.0$ indicating the presence of Mn as $Mn^{+2}$ in these glasses. The crystallized glass ceramics are however ESR silent. From ionic size considerations it would be improbable that $Cu^{+2}$ is substituted by Mn as $Mn^{+2}$ (ionic radii 0.80 $A$). It is also known that $Mn^{+2}$ easily oxidises into $Mn^{+3}$ and $Mn^{+4}$ with ionic radii 0.65 and 0.53 $A$ respectively. Thus the possibility of $Mn^{+2}$ being the ionic state of Mn in this system is excluded. Thus $Mn^{+3}$ having an ionic size closer to $Cu^{+2}$ is considered the most probable state of Mn in these ceramics. Since the ionic size of $Mn^{+3}$ is closer to the ionic size of $Fe^{+3}$, an appreciable change in the c-lattice parameter as seen for Fe doping is expected contrary to the very small changes observed. This can be explained considering the fact that $Mn^{+3}$ [$d^4$] is a JT ion like $Cu^{+2}$ in its octahedral configuration and hence the c-lattice may not be decreasing appreciably due to the c-axis elongation.

A comparison of the c-lattice parameter change with dopant concentration (fig-4.11) for the three dopants shows that Fe doping leads to large decrease in c-axis in comparison to Cr, while Mn doping shows very small change. We also observe that the c-lattice parameter does not change appreciably beyond the solid solubility range for all the dopants.

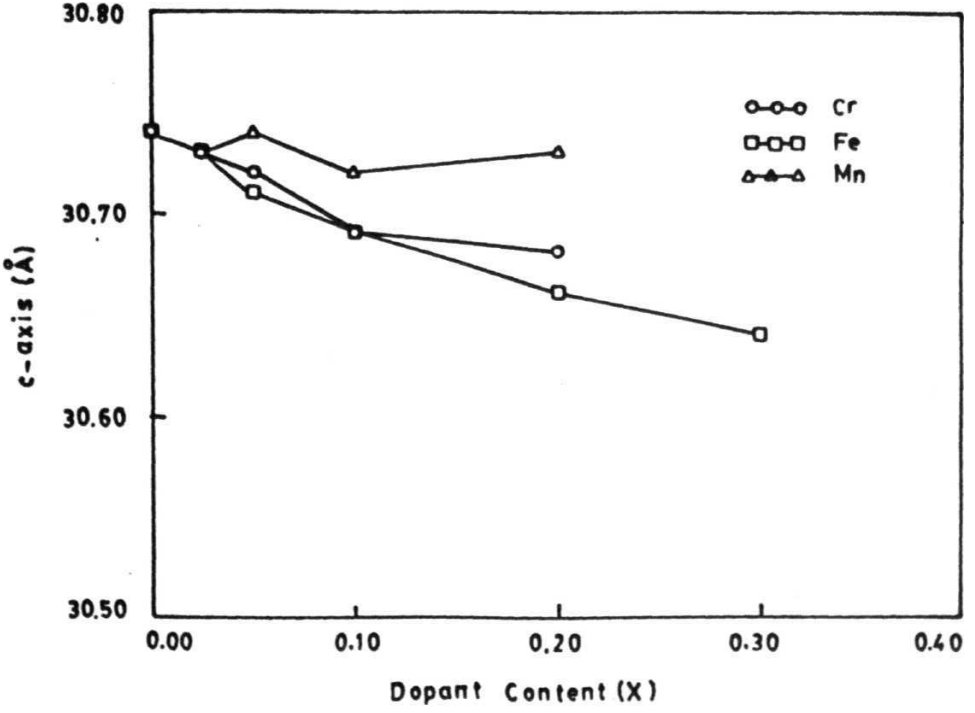


Fig-4.11 c-lattice parameter versus dopant content for the Fe, Cr and Mn doped superconductors.

From these results we conclude that within the solid solubility limit the dopant ions substitute for $Cu^{+2}$ in the CuO plane of Bi-2212 superconducting phase.

### 4.3.3 Electrical and superconducting properties:

#### Meissner studies:

AC susceptibility studies were carried out as a function of temperature in the temperature range 15-300 K applying a low AC field of 0.1 Oe in order to estimate the bulk $T_c$. All the three doped series of samples showed decreasing $T_c$ with increase in dopant concentration (fig-4.12). From a comparison of the $T_c$ drop with dopant concentration for the 3 dopants (table-4.4), we find that the drop in $T_c$ is more pronounced for the Fe doped Bi-Sr-Ca-Cu-0 superconductors while the drop is minimum in the case of Mn doped samples.

#### Resistivity studies:

Electrical resistivity studies were carried out on the $Bi_4Sr_3Ca_3Cu_{4-x}M_xO_z$ (M = Cr, Fe and Mn) superconductors by the standard four probe method in the temperature range 10-300 K.

Fig-4.13 shows the resistivity versus temperature plots for $Bi_4Sr_3Ca_3Cu_{4-x}Fe_xO_z$ system with $0 < x < 0.3$. We find that the normal state resistivity is a linear function of temperature and follows equation-4.4. The normal state resistivity at 300 K ($\rho_{300}$) and the residual resistivity ($\rho_o$) increase with increase in Fe content (table-4.4). The metallicity a decreases as x increases from 0 to 0.05. With further increase in x value, a

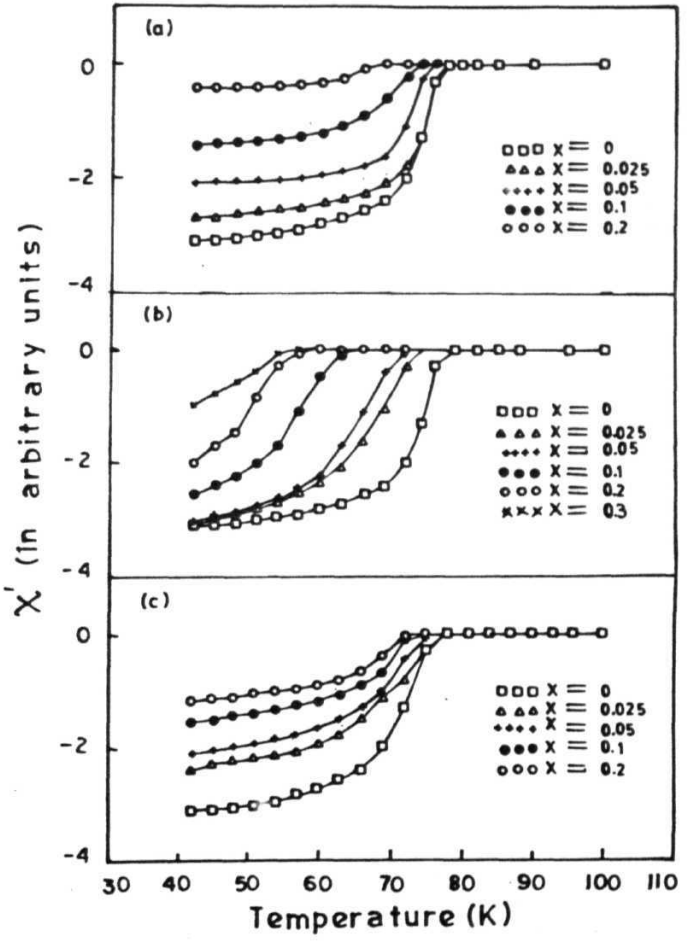


**Fig-4.12** Plot of $\chi'$ versus temperature for (a) Fe; (b) Cr; (c) Mn doped 4334 superconductors in the teroperatiïTe range 10–300 K.

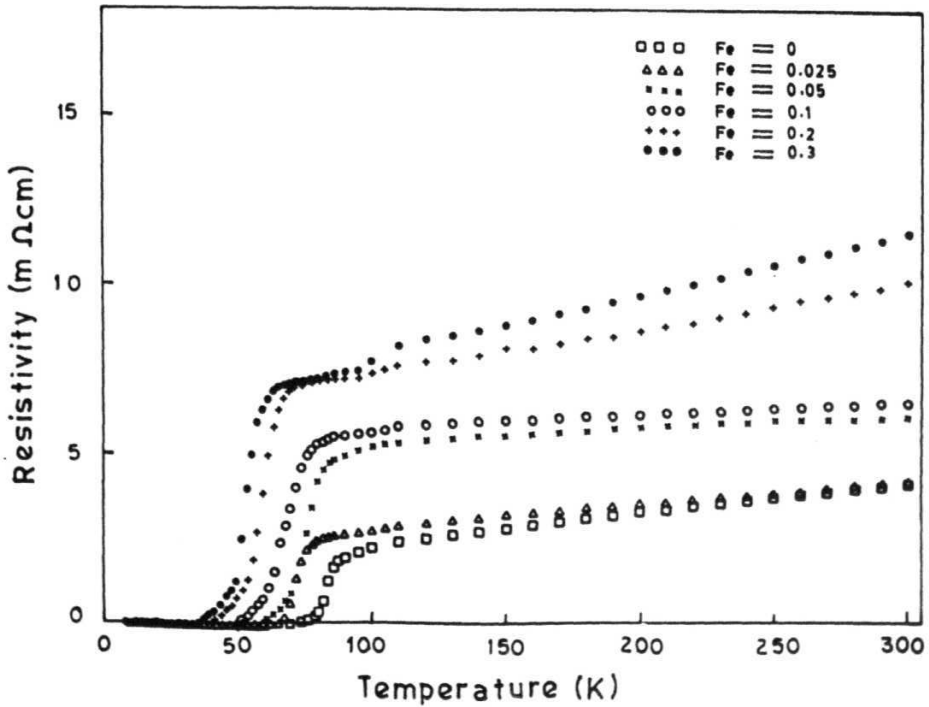


Fig-4.13 Resistivity versus temperature plot for the Fe doped 4334 superconductors in the temperature range 10–300 K.

increases followed by a sharp increase for x > 0.2. The increase in metallicity is accompanied by a kink in the $\rho(T)$ versus T plot at around 100 K. This kink is more pronounced for samples with x > 0.2. These observations can be considered as an artifact of phase separation and confirms our XRD results that solid solubility of Fe in 4334 is only up to x = 0.05. Similar kink is observed by Maeda et al for Fe concentration > 2 at.% in $Bi_2(Sr,Ca)_3(Cu_{1-x}Fe_x)_2O_y$ superconductors prepared by conventional solid state sintering process [148]. Fig-4.16 shows $T_{c(zero)}$ variations with x value. The $T_{c(zero)}$ is found to decrease rapidly as x changes from 0 to 0.05. As x increases from 0.05 to 0.3, the decrease in $T_{c(zero)}$ is slower. Within the solid solubility limit, i.e. for x < 0.05, $T_{c(onset)}$ remains unchanged.

Fig-4.14 shows resistivity versus temperature plots for $Bi_4Sr_3Ca_3Cu_{4-x}Cr_xO_z$ system with 0 < x < 0.2. The normal state resistivity varies linearly with temperature as per equation-4.4. The $\rho_{300}$ and $\rho_o$ are found to increase with increase in dopant concentration (table-4.4). The metallicity a does not however show a systematic variation with x. The $T_{c(onset)}$ does not change with Cr content. Fig-4.16 shows $T_{c(zero)}$ versus x. It decreases by about 3 K as x increases from 0 to 0.05. As x increases to 0.1, a sharp decrease in $T_{c(zero)}$ of about 20 K is observed. Further increase in x value to 0.2 decreases $T_{c(zero)}$ by only 4 K.

Fig-4.15 shows resistivity versus temperature plot for $Bi_4Sr_3Ca_3Cu_{4-x}Mn_xO_z$ system with 0 < x < 0.2. In the normal state, the resistivity versus temperature could be fitted to equation-4.4. $\rho_{300}$ and $\rho_o$ are found to increase gradually with increase in x (table-4.4). The metallicity a decreases with increase in x value. $T_{c(onset)}$ is found to be same for different dopant concentrations. $T_{c(zero)}$ versus x (fig-4.16) shows that $T_{c(zero)}$ decreases gradually by about 20 K as x increases for 0 to 0.2.

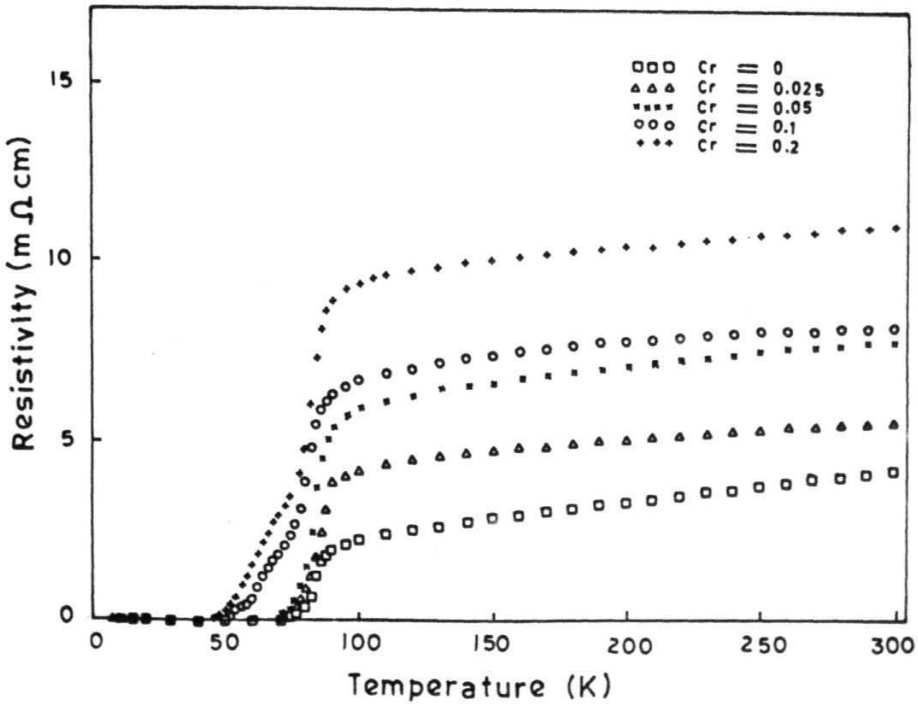


Fig-4.14 Resistivity versus temperature plot for the Cr doped 4334 superconductors in the temperature range 10–300 K.

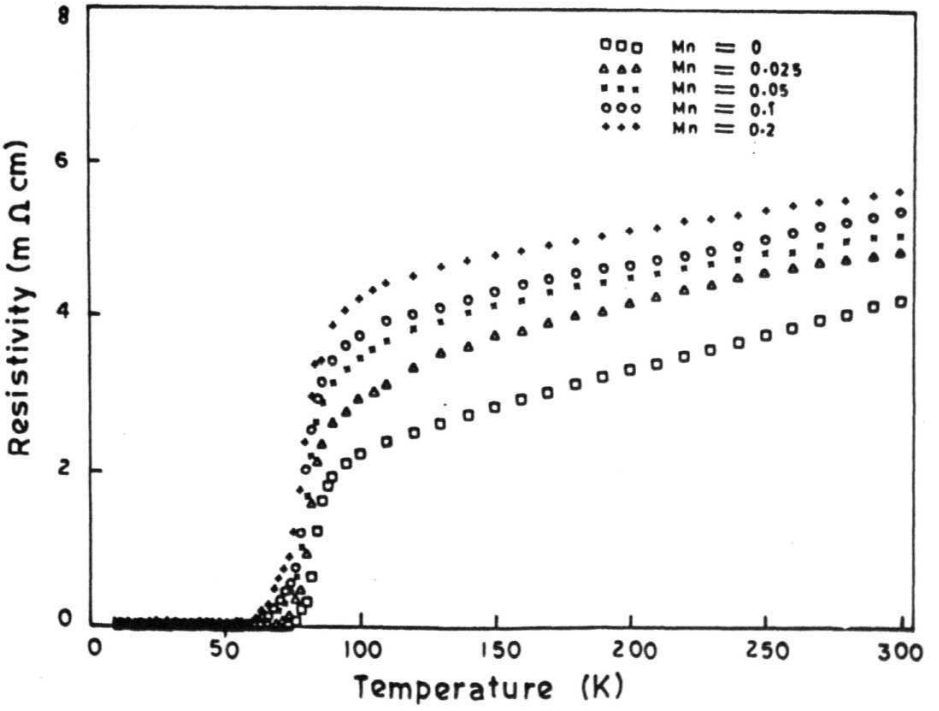


Fig-4.15 Resistivity versus temperature plot for the Mn doped 4334 superconductors in the temperature range 10–300 K.

A comparison of the $T_{c(zero)}$ depression as a function of dopant content for the three doped series of samples (fig-4.16) shows that the maximum depression rate is observed for Fe doping, followed by Cr and lastly by Mn doped samples.

### 4.4 ESR studies on doped and undoped glass ceramics:

ESR studies were carried out on the bulk and powders of doped and undoped ceramics heat treated at different temperatures for various durations. The ESR signal peak to peak intensity remained unaffected up to a heat treatment temperature of 300°C and decreased with further increase in temperature. The fully crystallized doped as well as undoped glass ceramics are found to be ESR silent. It is well known that pure superconductors are ESR silent and various theories have been put forward to explain the absence of ESR signal in high $T_c$ superconducting oxides and related materials [208, 216-218). It has been shown that in those reports where an ESR signal is observed, the signal has been attributed to the presence of impurity phases. The ESR silence in the case of the present 3d TM doped samples could imply that the 3d TM dopants are substituted at the Cu site and do not form precipitates. It is however possible that a small percentage of the dopant materials might go into the grain boundaries but cannot be detected when their concentration is beyond the sensitivity of the ESR spectrometer.

### 4.5 Discussion:

From the thermal analysis of the 4334 glasses, the crystallization activation energy estimated is consistent with several other reports by other groups [120, 122, 125]. Since there is no change in weight of the glass sample on first crystallization, and since the

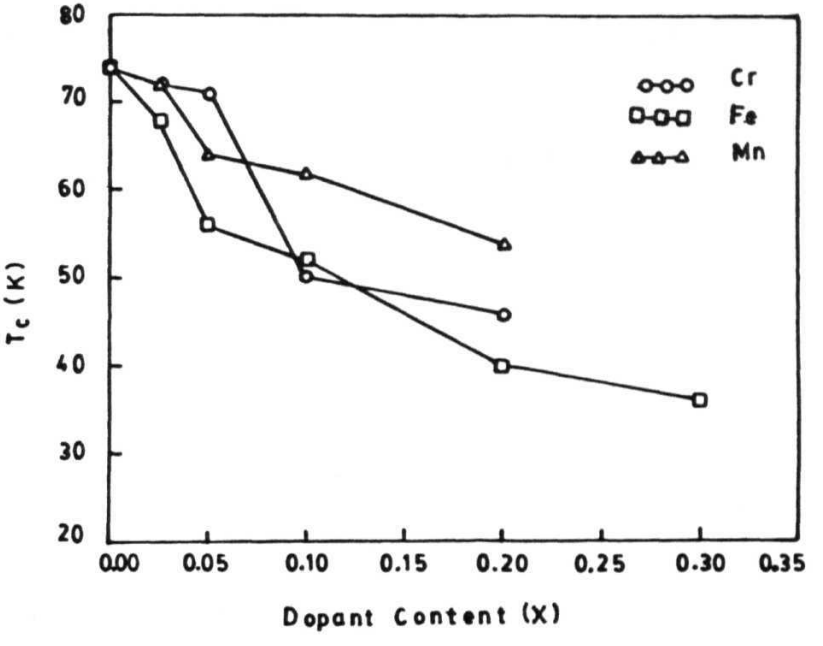


Fig-4.16 $T_{c(zero)}$ versus dopant content plots for Fe, Cr and Mn doped 4334 superconductors.

**first phase** formed is $Bi_2Sr_2CuO_y$ in which Cu ions exist almost completely as $Cu^{+2}$, the crystallization mechanism is an oxidation process involving absorption **of oxygen from** the glass matrix. Nassau et **al** [219] and Zheng et **al** [127] also reported **that the formation** of the first phase, $Bi_2Sr_2CuO_y$ does not require the absorption of **oxygen** from the atmosphere. Several groups have reported the formation of $Bi_2Sr_2CuO_y$ as the first phase on crystallization of other compositions of BSCCO and Pb-BSCCO glasses [72, 80, 83, 97, 108-111, 114, 116, 117].

A large decrease in the RT resistivity by about 8 orders of magnitude as the heat treatment temperature is raised from 500 to 650°C indicates that the devitrification reaction is very rapid in this temperature range. On crystallization, although the XRD pattern shows the growth of Bi-2201 phase, the sample still shows semiconducting behaviour down to the lowest temperature. This implies that there is no contact between the Bi-2201 superconducting crystallites and the semiconducting phase continue to dominate. Further increase in temperature to 820°C leads to the formation of Bi-2201 and Bi-2212 superconducting phases as indicated by the *p* vs. T plots. Using the XRD data it can be inferred that the Bi-2212 phase surrounds the Bi-2201 phase and forms a shell **around it.** Due to the oxygen uptake from the atmosphere **the density of this shell is greater than** the interior of the bulk sample as a consequence of which the devitrification rate slows down. The prolonged heat treatment at 820°C leads to the **growth** of Bi-2212 phase at the expense of Bi-2201 phase. If the glass is ground to a fine powder to facilitate oxygen absorption, one can obtain superconducting samples with metallic normal state resistivity for heat treatment duration of only 6 hours at 820°C. The heat treatment of the bulk glass sample at 850° for 24 hours indicate the formation of 110 K phase without significantly increasing the $T_{c(zero)}$. For phase purity **it is therefore advisable to use lower** heat treatment temperature preferably around 820°C.

The present studies show that the crystallization of these glasses is a bulk phenomenon and the devitrification reaction involves absorption of oxygen. The transformation of Bi-2201 to Bi-2212 superconducting phase is a slow process accompanied **by the uptake** of oxygen from the atmosphere. The bulk samples heat treated at 820°C show surface deformation. This can be considered as an indication of the melting of the interior of the sample and occur as a result of oxygen deficiency in the interior during devitrification. However, the presence of this liquid phase does not accelerate the Bi-2201 to Bi-2212 transformation. The transformation is accelerated on powdering the glass as the oxygen absorption rate in the case of powdered sample is enhanced because of larger surface area to volume ratio in comparison to the bulk sample. The glass powders heated to 820°C do not sinter implying that there is no liquid phase present. The transformation therefore is not mediated by a liquid phase as reported by Sato et al. [124] in the case of 2212 glass. The present results indicate that the phase transformation from Bi-2201 to Bi-22 2 involves the diffusion of Ca, Cu and 0 ions such that the elongation of *c*-axis takes place by adding $CaCuO_2$ units into Bi-2201 structure. The formation of $Cu_2O$ at around 650°C appears to play a significant role in this phase transformation. Matheis et al. [136] have also arrived at similar conclusions from the DTA and XRD studies of 2212 glass.

Other mechanisms of Bi-2212 phase formation have also been reported by other groups. Sato et al [124] reported a crystallization mechanism for $Bi_2Sr_2CaCu_2O_x$ glass. The Bi-2201 phase forms first until all the $Cu^{+2}$ is consumed; then $Bi_2Sr_{3-x}Ca_xO_y$ and $Cu_2O$ forms in the residual glass which contains almost only $Cu^{+1}$. When the sample is heated to 780°C, a liquid phase is formed related to the presence of $Cu_2O$; this liquid assists oxygen diffusion in converting $Cu^{+1}$ to $Cu^{42}$. De Guire et al [123] suggested **the**

formation of Bi-2212 as a result of reaction between Bi-2201, Raveau phase [220] and glass in the case of $Bi_{1.5}SrCaCu_2O_x$ glass. Holesinger et al [125] reported the crystallization of $Bi_2Sr_2CaCu_2O_x$ in $O_2$ occuring in two steps. In the first step Bi-2201 and $Cu_2O$ crystallized and then crystals of SrO, CaO and $Bi_2Sr_{3-x}Ca_xO_y$ were formed. Bi-2212 phase was formed as a dominant phase at 800°C.

The change in CuO content in the 433y composition with $3<y<6$ does not bring about large changes in the electrical properties and superconducting transition temperature. The $T_{c(zero)}$ ranges between 70-74 K for all the compositions studied. The superconducting glass ceramic obtained by heat treatment of the 4334 glass precursor has the highest $T_{c(zero)}$ and metallicity among all the compositions studied and is therefore of superior quality as compared to the other samples. The SEM results are in confirmity to this conclusion as the superconducting crystallites of this composition show better connectivity. The (0,0,/) reflection peaks are dominant in the XRD pattern of this sample indicating that the crystallites are preferentially oriented such that the *c*-axis is perpendicular to the sample surface. The XRD parameters do not change as a result of variation in CuO content. Excess CuO leads to the increase in intensity of $Cu_2O$ impurity reflection peak in the XRD patterns of the 433y glass ceramics (fig-4.9) but helps in the growth of uniform crystallites. These results and the small change in $T_{c(zero)}$ as a function of large variation in Cu content are found to be in agreement with the results obtained on the same compositions synthesised by conventional solid state reaction process by Tarascon et al. [213]. These results are also in accordance with the report that the 4334 glass crystallize into single phase Bi-2212 superconducting glass ceramic [77, 91, 94, 99].

XRD and resistivity versus temperature studies show that the solid solubility of 3d metal ions in the 4334 system is limited to x=0.05 in the case of Fe and Cr and x=0.1

in the case of Mn. The $T_{c(zero)}$ and c-lattice parameter are found to be systematically decreasing with increasing dopant concentration which shows that the 3d ion substitute at Cu site in the CuO plane. The normal state resistivity versus temperature plots are linear in the temperature range 100-300 K for all the compositions studied. The $\rho_{300}$ and $\rho_o$ are found to increase systematically with increasing dopant concentration.

A comparison of the results of the undoped and the doped samples show that the change in the structural and superconducting properties brought about by small concentration of the dopants are much larger than the changes introduced by large variation in Cu content in the case of undoped samples. Hence we conclude that the changes in superconducting properties of the doped samples are due to the substitution of 3d TM ions at the Cu site and not due to the variation in the microstructure like grain orientation, connectivity etc. in these materials.

The present studies suggest that the substitution of 3d transition metal ions at Cu-sites in CuO planes have significant and adverse effects on superconductivity and highlight the crucial importance of CuO planes for the occurance of superconductivity in the high-$T_c$ materials. A number of explanations like change in carrier density, inherent magnetic moment of the dopant, induced magnetic moments or the disorder created in the material due to inhomogenities have been provided to understand the $T_c$ depression as a result of 3d metal ion substitution at the Cu site in these materials [221, 222].

In Anderson's model of the linear resistivity [223], a dopant in the CuO planes is expected to introduce a temperature-independent magnetic scattering rate. Changes of $d\rho/dT$ can be due to changes in the charge carrier concentrations or the geometry of the Fermi surface.

Another important mechanism suggested to explain the suppression of $T_c$ is the disorder introduced by the substitutional elements. Since the superconductors are quasi-two-dimensional, scattering of the charge carriers by disorder can lead to a decrease in $T_c$ [224, 225].

The valence state of the 3d dopant ion is also one of the suggested parameter influencing $T_c$. Dopants existing in a single valence state do not alter the carrier density of the system, while mixed valent dopants vary the carrier density and suppress $T_c$ [226].

The inherent magnetic monient of the dopant is one of the reasons suggested for depression in $T_c$. The equally strong suppression of $T_c$ due to non-magnetic dopants like Zn is attributed to the change in magnetism of the neighbouring Cu spins due to induced localised magnetic moments which are responsible for pair breaking mechanism [227].

In recent theoretical attempts [228], it has been argued that $T_c$ depression can be understood to be due to the spin flip scattering within the Abrikosov-Gorkov theory [229] formulated for strong coupling situation if it is assumed that (a) $Cu^{+2}$ in CuO planes are highly localised and antiferromagnetically correlated even in the superconducting state and are therefore harmless and (b) the vacancy or an extra spin produced by a dopant acts as the magnetic scatterer.

The mixed valent 3d metallic dopants (Fe, Co, Ga) have been seen to affect the carrier density [26, 225]. But the observation of different $T_c$ depression rates cannot be explained on the basis of carrier density variation alone. The inherent magnetic moment of 3d dopants is also likely to play a role in the $T_c$ depression in these compounds. The

substitution of trivalent ions at $Cu^{+2}$ site shall lead to oxygen uptake and thus affect the local bonding and charge balance which consequently disturb the $Cu_{3d}$-$O_{2p}$ orbital hybridisation and thereby the superconducting properties. It has been recently demonstrated [230] that the in-plane superconducting correlation are enhanced by interlayer coupling. The recent experimental studies [231] also address the inplane and interlayer interplay and the implication of this interplay for the phenomenon of high $T_c$ superconductivity have been suggested. The 3d metallic dopant with different inherent magnetic moments and ionic sizes may affect the interplay between in-plane and interlayer behaviour of carriers in different magnitudes which may give rise to different $T_c$ depression rates.

All the doped and undoped superconducting glass-ceramics are ESR silent as is expected for pure superconductors. The possiblity of very small amounts of dopant ions precipitating is however not ruled out as the ESR does not detect very small concentrations of impurity.

# Chapter 5

## SUMMARY AND CONCLUSIONS

Glasses of composition $Bi_4Sr_3Ca_3Cu_yO_z$ (3<y<6) and $Bi_4Sr_3Ca_3Cu_{4-x}M_xO_z$ (M = Fe, Cr, Mn and 0<x<0.2) were synthesised by metal plate quench technique. The $T_x$ and the thermal stability AT = $T_x$-$T_g$ are highest for the glass with 4334 composition. IR studies show an absorption peak at 860 $cm^{-1}$ indicating the presence of $BiO_3$ units in these glasses. Susceptibility and $C=Cu^{+1}/Cu_{total}$ ratio for the 433y glasses are obtained from room temperature magnetic susceptibility studies. The susceptibility and the $Cu^{+2}$ concentration decrease with increase in CuO content upto y=5 and increases for the y=6 glass.

Detailed temperature dependence of DC electrical conductivity measurements were carried out in the temperature range 100-500 K. and the results analysed in view of various theoretical models available in the literature. The conductivity is found to increase with increase in CuO content. The high temperature conductivity data is explained in view of Mott's polaron model i.e. the conduction occurs by thermally activated small polaron hopping from the low valence state to the higher valence state of the transition metal ions (between $Cu^{+1}$ and $Cu^{+2}$ ions). From the analysis of data in view of Holstein and Emin's model, the conditions for formation of small polarons and adiabatic hopping is satisfied. The conduction in these glasses is by small polaron hopping in the adiabatic regime and activation energy dominates the factors which determine the conductivity. The phonon frequency $\nu_o$ and the Debye temperature $\theta_D$, obtained from the conductivity data are close to the values obtained from IR studies. The $\nu_o$ value obtained from Mott's

equation is close to the values obtained from conductivity plots and IR studies, after considering the polaron correlation effects. The polaron radius $r_p$ is found to be small indicating the formation of small polarons. The temperature dependence of electrical conductivity is found to be as per the theoretical predictions of Schnakenberg's model. The values of $\nu_o$ and $W_H$ (hopping activation energy) from the best fits of the theoretical curves are reasonable and consistent with the glass composition. The disorder activation energy $W_D$ value is close to the prediction of Miller-Abraham's theory. The conductivity parameters are not found to be significantly affected by 3d TM doping at Cu site and the conduction mechanism is essentially the same.

ESR studies on the doped and undoped Bi-Sr-Ca-Cu-0 glasses show that the spectras were all characteristic of $Cu^{+2}$ ions. The $Cu^{+2}$ concentration is found to be about 2 orders of magnitude smaller than that obtained from magnetic susceptibility studies. This is attributed to the presence of short range ordering of atomic scale in these glassesand the consequent presence of CuO square planar structures which are ESR silent. The existence of $Fe^{+3}$, $Mn^{+2}$ and $Cr^{+3}$ is inferred from the ESR spectra of the Fe, Mn and Cr doped glasses respectively.

Detailed and systematic studies were carried out on $Bi_4Sr_3Ca_3Cu_4O_x$ glasses using DSC, XRD and electrical resistivity measurements to understand the crystallization mechanism and phase formation in these glasses. The DSC studies on the 4334 glass shows a sharp exotherm at around 470°C and the crystallization activation energy is found to be 388 kJ/mole. The Avrami constant obtained is 3.69 which indicates that the crystallization in these glasses is a bulk phenomenon.

Three separate batches of glasses of 4334 composition were heat treated by scanning

the temperature from room temperature to 500, 650 and 820°C at a heating rate of 15°/min and quenched to room temperature in air. Parallel XRD and DC resistivity studies were carried out on the heat treated samples in order to understand the phase formation. The interior morphology of the samples was studied by carrying out XRD studies after acid-etching the surface of the heat treated samples. Weight changes in the samples as a result of heat treatment were also recorded.

The RT resistivity of the samples was found to decrease with increase in maximum scanning temperature. In comparison with the RT resistivity of the 4334 glass, the sample scanned to 500°C showed a drop of 2 orders of magnitude in the RT resistivity while the maximum drop in resistivity of about 8 orders of magnitude was observed for the sample scanned to 650°C implying that the rate of devitrification reaction is maximum in the 500-650°C temperature range. All the samples showed semiconducting behaviour in the resistivity versus temperature plots. The sample scanned to 820°C showed a superconducting onset at around 100 K. With prolonged heat treatment of the samples at 820°C, the samples continued to show weakly semiconducting behaviour in the 100-300 K temperature range and a superconductivity onset at 100 K. The RT resistivity continue to decrease with heat treatment duration. Insulator-Metal transition was observed after a heat treatment of 12 hrs for an RT resistivity of $10^{-2}$ Ω-cm. The samples heat treated for durations beyond 12 hrs show a metallic behaviour in the 100-300 K temperature range. The temperature dependence of the normal state resistivity *p(T)* at a temperature T is described by the equation $p(T) = \rho_o + \alpha T$, where the slope a = $d\rho/dT$ and $\rho_o$ are the measure of the metallicity and residual resistivity. With increase in heat treatment duration, the samples show an increase in $T_{c(zero)}$ and $\alpha$ and a decrease in *p(T)* and $\rho_o$ till a superconducting glass ceramic with $T_{c(zero)}$=74 K is obtained after 96 hrs heat treatment.

From the XRD studies on these samples (before and after acid-etching the surface) and from the weight changes as a result of heat treatment, it is seen that the first crystallization occurs at around 500°C and the phase formed is the Bi-2201. This is a bulk crystallization and does not involve the uptake of oxygen from the atmosphere. At 650°C formation of 2212 phase begins from the surface of the sample and is accompanied by the absorption of oxygen from the environment and the diffusion of Ca, Cu and O ions such that the elongation of c-axis takes place by adding $CaCuO_2$ units into Bi-2201 structure. Increase in temperature to 820°C is found to favour the growth of the 2212 phase and the prolonged heat treatment of the sample at 820°C shows the continuing growth of 2212 phase at the expense of the 2201 phase until an almost single phase 2212 sample is obtained after 96 hrs heat treatment.

Glasses of composition 433y are heat treated at 820°C for 96 hrs and furnace cooled. The XRD patterns showed well defined reflections all of which could be indexed on the basis of 2212 structure assuming pseudo tetragonal symmetry. The 4334 and the 4335 samples show highly intense [0,0, /] reflections indicating orientation of crystallites. Traces of $Cu_2O$ impurity was detected in samples with higher Cu content. The SEM of 433y ceramics show that the 4334 samples show larger inter-grain connectivity. The crystalline growth in the 4336 sample is however more uniform. This may be due to excess CuO acting as a flux for the growth of superconducting crystallites.

Electrical resistivity studies on the 433y samples as a function of temperature shows that all of them are superconductors with well defined metallic behaviour in the normal state and $T_{c(zero)}$ in the temperature range 70-74 K. The resistivity in the normal state varies linearly with temperature. The $\rho_{300}$ and $\rho_o$ are small for all the samples and do not show any systematic variation with CuO content. The $T_{c(zero)}$ is lower for the 4335

and 4336 samples. The 4334 sample show highest metallicity and lower superconducting transition width. Thus variations in CuO content do not bring about large changes in the superconducting properties. The 4334 starting composition is however found to be the optimum composition to obtain oriented and single phase 2212 superconductors. We also do not find any correlation between the c value of the glasses and the superconducting properties or the size and orientation of crystallites in the superconducting glass ceramics.

Mechanically processing of the samples give metallic normal state resistivity, smaller normal state resistivities and higher $T_{c(zero)}$ for smaller durations of heat treatment as campared to the bulk samples. This can be attributed to the larger oxygen absorption rate in the powdered sample because of larger surface area to volume ratio in comparison to the bulk sample.

Superconducting ceramics of $Bi_4Sr_3Ca_3Cu_{4-x}M_xO_z$ ( M = Fe, Cr and Mn and $0 < x < 0.2$) are prepared by heat treating the doped glasses at 820°C for 96 hrs. XRD studies on the doped samples shows single phase formation upto x = 0.05 for M = Fe and Cr and upto x = 0.1 for M = Mn. XRD patterns for higher values of x show traces of impurity and 2201 phase. The *a*-lattice parameter is $3.83\AA$ and does not vary significantly as a result of doping. The *c*-lattice parameter decreases with doping concentration for all the three doped series. c-lattice parameter change with dopant concentration for the three dopants show that Fe doping leads to a large decrease in *c*-axis in comparison to Cr, while Mn doping shows very small change. The c-lattice parameter does not change appreciably beyond solid solubility range for all the three dopants. From a consideration of the stability of the ions, the ionic radii and Mosbauer studies, we conclude that $Fe^{+3}$, $Mn^{+3}$ and $Cr^{+3}$ are the most probable ionic states of 3d dopants in these superconductors. The decrease in c- lattice parameter for the different dopants have been explained by

considering the ionic size differences between $Cu^{+2}$ and the dopant ions and the different Jahn-Teller effect of $Cu^{+2}$ and the dopant ions.

Resistivity versus temperature studies on the 3d doped superconductors in the temperature range 10-300 K show that all the doped samples are superconductors with metallic normal state resistivity. The $\rho_{300}$ and $\rho_o$ are found to increase with increase in dopant concentration. The $T_{c(onset)}$ remains the same for all the dopants and concentrations studied. The $T_{c(zero)}$ is found to decrease systematically with doping. A comparison of $T_{c(zero)}$ depression as a function of dopant concentration shows that the maximum depression rate is observed for Fe followed by Cr and Mn doped samples. The $T_{c(zero)}$ depression is found to follow the c-lattice parameter decrease showing that the $T_c$ depression is due to 3d ions substitution at Cu site in the CuO plane. A comparison of the results of the doped and undoped samples show that changes in structural and superconducting properties brought about by small concentration of dopants is much larger than changes introduced by large variation in Cu content in the case of undoped samples. Hence changes in superconducting properties of doped samples are due to substitution of 3d TM ions at Cu site and not due to variations in microstructure like grain orientation, connectivity etc.

A number of explanations like change in carrier density, inherent magnetic moment of the dopant, induced magnetic moments or condensation of a spinon and disorder created in the material due to inhomogenities have been provided to understand $T_c$ depression due to Cu site 3d doping. In recent theoretical studies, it has been argued that $T_c$ depression can be understood to be due to spin flip scattering within the Abrikosov-Gorkov theory by assuming that $Cu^{+2}$ in CuO planes are highly localised and antiferromagnetically correlated even in the superconducting state and that vacancy or extra spin

produced by a dopant acts as a scatterer. We have attempted to analyse our data on the basis of some of the above theories.

ESR studies on the doped and undoped samples show a decrease in amplitude of the spectra with increase in heat treatment duration and temperature above 300°C. The glass ceramic superconducting samples heat treated for 96 hrs are ESR silent.

## Conclusions

The dc electrical conductivities of $Bi_4Sr_3Ca_3Cu_yO_x$ ($3<y<6$) glasses are reported in the temperature range 100-500 K. The experimental results are analysed in view of various theoretical models. Mott's model of thermally activated small polaron hopping between the nearest neighbours is found to be consistent with the data in the high temperature range. At high temperatures the conduction in these glasses occurs by polaron hopping in the adiabatic regime. Schnakenberg's model is found to be consistent with the temperature dependence of conductivity. The model parameters estimated from the best fits are reasonable and consistent with the composition of the glass.

FT/IR studies on the 3d TM doped and undoped glasses show a peak at 860 $cm^{-1}$ indicating the existence of $BiO_3$ species as a part of $BiO_6$ octahedra with three Bi-0 bonds nearly equal and formed as a result of strong interaction with Sr. The fact that Bi-2201 is the first phase formed on crystallization indicates that Sr preferentially occupies the site near $BiO_6$ octahedra in these glasses. The broad absorption band at 500 $cm^{-1}$ corresponds to the phonon frequency of the glassses and does not alter appreciably with variation in composition or as a result of doping.

ESR studies on the BSCCO glasses show that only a small fraction of $Cu^{+2}$ ions are ESR active suggesting that most of the Cu ions could be present in square planar Cu-0 units. The formation of 2201 phase (having a single $CuO_2$ plane) as the first product of crystallization of these glasses strengthens this contention. Fe, Mn and Cr are present as $Fe^{+3}$, $Mn^{+2}$ and $Cr^{+3}$ ions in the Fe, Mn and Cr doped glasses respectively.

Studies on $Bi_4Sr_3Ca_3Cu_yO_x$ (433y) glasses ($3<y<6$) and corresponding glass ceramics show no definite correlation between the properties of the glasses and the superconducting glass ceramics. However, the 4334 glass shows the highest crystallization temperature and thermal stability; the corresponding glass-ceramic is almost a single phase sample with the highest $T_{c(zero)}$ and metallicity among all the glass-ceramics heat treated under identical conditions. The detailed studies, including Differential Scanning Calorimetric, Resistivity and X-ray diffraction, on 4334 glass and glass ceramics show that the activation energy for crystallization is 388 KJ/mol.; the devitrification reaction rate is maximum in the 500-650°C temperature range; $Bi_2Sr_2CuO_x$ (Bi-2201) is the first phase which crystallize from the glass and the crystallization is a bulk phenomenon. Metal-Insulator transition is observed for RT resistivity $10^{-2}\Omega$ cm. The $Bi_2Sr_2Ca_1Cu_2O_x$ (Bi-2212) phase formation starts above 650°C by a diffusion reaction between Bi-2201 phase, Ca, Cu and 0 at the sample surface.

The synthesis of glass ceramic superconductors of $Bi_4Sr_3Ca_3Cu_yO_w$ ($3<y<6$) and $Bi_4Sr_3Ca_3Cu_{4-x}M_xO_z$ (M = Fe, Cr, Mn and $0<x<0,2$) compositions is reported. X-ray diffraction studies indicate that the solid solubility of 3d metal ions in the 4334 system is limited to x=0.05 in the case of Fe and Cr and x=0.1 in the case of Mn. A systematic decrease in $T_c$ with increasing dopant concentration is observed from resistivity as well as from AC susceptibility measurements. $T_c$ depression rates, however are found to differ

**for different dopants. XRD studies indicate the decrease in *c* lattice parameter with increase in dopant content. The systematics of the superconducting transition is discussed in view of $T_c$ depression rates.**

List of Publications:

1. * Systematic studies on Bi-Sr-Ca-Cu-0 glasses and glass ceramics, authors- R. Singh and E. Zacharias, J. Phys. D: Appl. Phys. **23**, 199 (1990).

2. * Studies on Bi-Sr-Ca-Cu-0 glasses and superconducting ceramics, authors- R. Singh and E. Zacharias, Bull. Mat. Sci. 14(2), 343 (1991).

3. Structural and superconducting properties of $Bi_4Sr_3Ca_3Cu_yO_w$ and $Bi_4Sr_3Ca_3Cu_{4-x}M_xO_z$ (M = Fe, Cr and Mn) glass ceramics, authors- E. Zacharias and R. Singh, Int. J. Mod. Phys.B 9(1) (1995).

4. DC electrical conduction in $Bi_4Sr_3Ca_3Cu_yO_x$ ($3 < y < 6$) glasses, authors- E.Zacharias and R. Singh, Solid State Commun. 93(2), 135 (1995).

5. Crystallization and resistivity studies on $Bi_4Sr_3Ca_3Cu_yO_x$ glasses, authors- E. Zacharias and R. Singh, Physica C (resubmitted after implementing refree's suggestions).

6. Electrical properties of $Bi_4Sr_3Ca_3Cu_yO_x$ glasses, authors- R. Singh and E. Zacharias, Phys. Rev. B (communicated).

* -not part of the thesis.

## References


[1] H. Kammerlingh Onnes, Leiden Commun. **1206,** 1226 (1911).

[2] W. Meissner and R. Ochenfeld, Naturwiss **21,** 787 (1933).

[3] A. C. Rose-Innes and E. H. Rhoderick, Introduction to Superconductivity, p. 61, (Pergamon Press, UK) (1978).

[4] F. London and H. London, Physica 2, 341 (1935).

[5] J. Bardeen, L. N. Cooper and R. J. Schrieffer, Phys. Rev. **106,** 162 (1957); **108,** 1175 (1957); C. G. Kuper, An Introduction to the theory of Super conductivity, p.101, 105 & 184, (Clarendon Press, Oxford) (1968).

[6] C. E. Gough, M. S. Colclough, E. M. Forgan, R. G. Jordan, M. Keene, C. M. Muirhead, A. I. M. Rea, N. S. Thomas, J. S. A bell and S. Sutton, Nature **326,** 855 (1988).

[7] A. W. Sleight, J. L. Gillson and P. E. Bierstedt, Solid State Commun.**17**, 27 (1975).

[8] J. G. Bednorz and K. A. Miiller, Z. Phys. B Conden. Matter 64, 189 (1986).

[9] S. Uchida, H. Takagi, K. Kitagawa and S. Tanaka, Jpn. J. Appl. Phys. **26, L1** (1987).

[10] H. Takagi, S. Uchida, K. Kitazawa and S. Tanaka, Jpn. J. Appl. Phys. **26,** L123 (1987).

[11] J. D. Jorgensen, H. B. Schüttler, D. G. Hinks, D. W. Capone II, K. Zhang, M. B. Brodsky and D. J. Scalapino, Phys. Rev. Lett. 58, 1024 (1987).

[12] J. M. Tarascon, L. H. Greene, P. Barboux, W. R. McKinnon, G. W. Hull, T. P. Orlando, K. A. Delin, S. Foner and E. J. McNifT, Phys. Rev. B 36, 8393 (1987).

[13] G. Xiao, A. Bakhshai, M. Z. Cieplak, Z. Tesanovic and C. L. Chien, Phys. Rev. B 39, 315 (1989).

[14] M. X. Wu, J. R. Ashburn, C. J. Torng, P. H. Hor, R. I.Meng, L. Gao, Z. J. Huang, Y. Q. Wang and C. W. Chu, Phys. Rev. Lett. 58, 908 (1987).

[15] R. J. Cava, B. Batlogg, C. H. Chen, E. A. Rietman, S. M. Zahurak and D. Werder, Phys. Rev. B 36, 5719 (1987).

[16] P. K. Gallagher, H. M. O'Bryan, S. A. Sunshine, D. W. Murphy, Mat. Res. Bull **22,** 995 (1987).

[17] R. J. Cava, B. Batlogg, R. B. VanDover, D. \Y Murphy, S. Sunshine, T. Siegrist, J. P. Remeika, E. A. Rietman, S. Zahurak and G. P. Espinosa, Phys. Rev. Lett. 58, 1676 (1987).

[18] P. M. Grant, R. B. Beyers, E. M. Engler, G. Lim, S. S. P. Parkin, M. L. Ramirez, V. X. Lee, A. Nazzal, J. E. Vazquez and R. J. Savoy, Phys. Rev. B 35, 7242 (1987).

[19] R. M. Hazen, L. W. Finger, R. J. Angel, C. T. Prewitt, N. L. Ross, H. K. Mao, C. G. Hadidiacos, P. H. Hor, R. L. Meng and C. W. Chu, Phys. Rev. B 35, 7238 (1987).

[20] Y. LePage, W. R. McKinnon, J. M. Tarascon, L. H. Greene, G. W. Hull and D. M. Huang, Phys. Rev. B 35, 7245 (1987).

[21] P. H. Ho:, R. L. Meng, Y. Q. Wang, L. Gao, Z. J. Huang, J. Bechtold, K. Foster and C. W. Chu, Phys. Rev. Lett. 58, 1891 (1987).

[22] J. M. Tarascon, W. R. McKinnon, L. H. Greene, G. W. Hull and E. M. Vogel, Phys. Rev. B 36,226 (1987).

[23] Z. Fisk, J. D. Thompson, E. Zirngiebel, J. L. Smith and S. W. Cheong, Solid State Commun. 62, 743 (1987).

[24] S. Hasoya, S. I. Shamoto, M. K. Onoda and M. Sato, Jpn. J. Appl. Phys. 26, L325 (1987).

[25] D. W. Murphy, S. Sunshine, R. B. VanDover, R. J. Cava, B. Batlogg, S. M. Zahurak and L. F. Schneemeyer, Phys. Rev. Lett. 58, 1888 (1987).

[26] J. M. Tarascon, P. Barboux, P. F. Miceli, L. H. Greene and G. W. Hull, Phys. Rev. B **37**, 7458 (1988).

[27] G. Xiao, F. H. Streitz, A. Gavrin, Y. W. Du and C. L. Chien, Phys. Rev. B 35, 8782 (1987).

[28] Y. Maeno, T. Tomita, M. Kyogoku, S. Awaji, Y. A. Oki, K. Hoshino, A. A. Minami and T. Fujita, Nature **328,** 512 (1987).

[29] Y. K. Tao, J. S. Swinnea, A. Manthiram, J. S. Kim, J. B. Goodenough and H. Steinfink, J. Mater. Res. 3, 248 (1988).

[30] S. Mazumder, H. Rajagopal, A. Sequeira, J. Singh, A. K. Rajarajan, L. C. Gupta, and R. Vijaya Raghavan, Phase Trans. 19, 97 (1989).

**[31]** **H. Maeda**, A. Koizumi, N. **Bamba**, E. **Takayama**- Muromachi, **F. Izumi, H. Asano, K.** Shimizu, H. **Moriwaki**, H. **Maruyama**, Y. Kuroda and H. Yamakazi, Physica C **157,** 483 (1989).

[32] A. F. Marshall, R. W. Barton, K. Char, A. Kapitulnik, **B. Oh, R. H. Hammond** and S. S. **Laderman**, Phys. Rev. B 37, 9353 (1988).

[33] J. Karpinski, E. Kaldis, E. **Jilek**, S. Rusieeki and B. Bucher, **Nature S36, 660** (1988).

[34] R. J. Cava, J. J. Karajewski, W. F. Peck Jr., B. Batlogg, L. W. Pupp Jr., R. M. Fleming, A. C. W. P. James and P. Marsh, Nature **338,** 328 (1989).

[35] P. Bordet, C. Chaillout, J. Chenavas, J. L. Hodeau, M. Marezio, J. Karpinski and E. Kaldis, Nature **334,** 596 (1988).

[36] P. Marsh, R. M. Fleming, M. L. **Mandich**, A. M. De Santolo, J. Kwo, M. Hong and L. J. Martinez- Miranda, Nature **334,** 141 (1988).

[37] C. Michel, H. Hervieu, M. M. Borel, A. Gradin, F.Deslandes, J. Provst and B. Raveau, Z. Fur. Phys. Cond. Matt. 68, 421 (1987).

[38] H. Maeda, Y. Tanaka, M. Fukutomoi and T. Asano, Jpn. J. Appl. Phys. **27,** L209 (1988).

[39] H. W. **Zanbergen**, Y. K. Huang, M. J. V. Menken, Li, K. Kadouaki, **A. A. Menovsky,** G. Van Tendelooz and S. **Amelinckx**, Nature **332,** 620 (1988).

[40] R. **Ramesh**, C. J. D. Hetheringcon, G. Thomas, S. M. Green, C. Jiang, M. L. Pudee and H. L. Luo, Appl. Phys. Lett. 53, 615 (1988).

[41] J. L. Taloon, R. G. Buckley, P. W. Gilberd, M. R. Presland, I. M. Brown, M. E. Bowden, L. A. Christian and E. Goguel, Nature **333,** 153 (1988).

[42] J. M. Tarascon, W. R. McKinnon, P. Barboux, D. M. Huang, B. G. Badley, L. H. Green, G. W. Hull, Y. LePage, N. Stoffel and M. Giroud, Phys. Rev. B 38, 8885 (1988).

[43] S. A. Sunshine, T. Siegrist, L. F. **Schneemeyer**, D. W. Murphy, R. J. Cava, R. B. Van Dover, R. M. Fleming, **S.** H. **Glarum**, S. Nakahara, R. Farrow, J. J. Krajewski, S. M. Zahurak, J. V. Wasczak, J. H. Marshall, P. Marsh, **L. H. Rupp Jr., and W. F. Peck, Phys.** Rev. **B 38,** 893 (1988).

**[44]** **(a) M.** Takano, Nature **333,** 200 (1988); (b) R. J. Cava, B. Batlogg, S. A. **Sunshine,** P. T. Siegrist, E. M. Fleming, **R. Rabe,** L. F. Schneemeyer, G. W. Murphy, R. V. Van Dover, P. K. Gallagher, S. H. Glarum, S. Nakahara, R. C. Farrow, J. J. Krajewski, S. M. Zahurak, J. V. Waszcak, J. H. Marshall, **P.** Marsh, **L. W. Rupp** Jr., **W. F.** Peck and E. A. Rietman, Physica C **153-155,** 560 (1988).

[45] S. M. Green, C. Jiang, Yu. Mei, H. L. Luo and C. Politis, Phys. **Rev. B 38, 5016** (1988).

[46] E. Charira, R. Escudero, R. Rios-Jana and L. M. Leon, Phys. **Rev.** B 38, **9272** (1988).

[47] Y. Mei, S. M. Green, C. Jiang and H. L. Luo, J. Appl. Phys. **66,** 1777 (1989).

[48] L. Pierre, D. Morin, J. Schneck, J. C. Toledano, J. Primot, C. Dagnet, F. Glas, J. Etrillard and H. Savary, Solid State Commun. 69, 499 (1988).

[49] L. Hongbao, C. Lieyhao, Z. Ling, M. Zhiqiang, L. Xiaoxian, Y. U. Zhidong, M. **Yue** Bai, M. Xianglei, Z. Guien, R. Yaozhong, C. Zhaojia and Z. Yuheng, Solid State Commun. 69, 867 (1988).

[50] A. K. Sarkar and I. Maartense, Solid State Commun. **77,** 121 (1991).

[51] Z. Z. Sheng and A. M. Herman, Nature **332,** 55 (1988).

[52] R. M. Hazen, L. W. Finger, R. J. Angel, C. T. Prewitt, N. L. Ross, C. G. Hadidiacos, P. J. Heaney, D. R. Veblen, Z. Z. Sheng, A. El Ali and A. M. Hermann, Phys. Rev. Lett. **60,** 1657 (1988).

[53] M. A. Subramanian, J. C. Calabrese, C. C. Torardi, J. Gopalakrishnan, T. R. Askew, R. B. Flippen, K. J. Morrissey, V. Chowdhry and A. W. Sleight, Nature **332,** 420 (1988).

[54] C. C. Torardi, M. A. Subramanian, J. C. Calabrese, J. Gopalakrishnan, K. J. Morrissey, T. R. Askew, R. B. Flippen, U. Chowdhry and A. W. Sleight, Science **240,** 631 (1988).

[55] S. S. P. Parkin, V. Y. Lee, E. M. Engler, A. I. Nazzal, **T.** C. **Huang, G. Gorman, R. Savoy and R.** Beyers, Phys. Rev. Lett. **60,** 2539 (1988).

**[56]** S. S. P. Parkin, V. X. Lee, A. 1. Nazzal, R. Savoy, **R. Beyers and** S. **La Placa, Phys. Rev. Lett. 61,** 750 (1988).

**[57]** M. A. Subramanian, J. B. Parise, J. C. Calabrese, C. C. **Torardi, J. Gopalakrishnan and A. W.** Sleight, J. Solid State Chem. **77,** 192 (1988),

[58] M. A. Subramanian, C. C. Torardi, J. Gopalakrishnan, P. L. Gai, J. C. Calabrese, T. R. Askew, R. B. Flippen and A. W. Sleight, Science **242**, 249 (1988).

[59] R. J. Cava, B. Batlogg, J. J. Krajewski, L. W. Rupp, L. F. Schneemeyer, T. Siegrist, R. B. Van Dover, P. Marsh, W. F. Peck Jr., P. K. Gallagher, S. H. Glarum, J. H. Marshall, R. C. Farrow, J. V. Waszczak, R. Hull and P. Trevor, Nature **336**, 211 (1988).

[60] Y. Tokura, H. Takagi and S. Uchida, Nature **337,** 345 (1989).

[61] A. F. Herbard et al., Nature **350,** 600 (1991).

[62] K. Tanigaki, T. W. Ebbesen, S. Saito, J. Mizuki, J. S. Tsai, Y. Kulo and S. Kuroshima, Nature 352, (1991).

[63] S. N. Putillin, E. V. Antipov, 0. Chmaissem and M. Marezio, Nature **362,** 226 (1993).

[64] A. Schilling, M. Cantoni, J. D Guo and H. R. Ott, Nature 363, 56 (1993).

[65] C. C. Torardi, M. A. Subramanian, J. C. Calabrese, J. Gopalakrishnan, E. M. McCarron, K. J. Morrissey, T. R. Askew, R. B. Flippen, V. Chowdhry and A. W. Sleight, Phys. Rev. B 38, 225 (1988).

[66] K. Imai, I. Nakai, T. Kawashima, S. Sueno and A. Ono, Jpn. J. Appl. Phys. 27, L1661 (1988).

[67] M. Onoda and M. Sato, Solid State Commun. 67, 799 (1988).

[68] R. M. Hazen, C. T. Prewitt, R. J. Angel, N. L. Ross, L. W. Finger, C. G. Hadidiacos, D. R. Veblon, P. J. Heaney, P. H. Hor, Z. J. Huang, L. Gao, J. Bechtold and C. W. Chu, Phys. Rev. Lett. 60, 1174 (1988).

[69] J. M. Tarascon, Y. Le Page, P. Barboux, B. G. Bagley, L. H. Greene, W. R. McKinnon, G. W. Hull, M. Giroud and D. M. Hwang, Phys. Rev. B 37, 9382 (1988).

[70] J. K. Liang, S. S. Xie, G. C. Che, J. Q. Huang, Y. L. Zhang and Z. X. Zhao, Mod. Phys. Lett. B 2, 483 (1988).

[71] H. Maeda, Y. Tanaka, M. Fukumori and T. Asano, Jpn. **J. Appl. Phys. 27,** L209 (1988).

[72] M. Yoshimura, T. H. Sung, Z. Nakagawa and T. Nakamura, Jpn. J. Appl. Phys. 27, L1877 (1988).

[73] M. Tatsumisago, C. A. Angell, S. Tsuboi, **V. Akamatsu, N. Tohge and T. Minami, Appl.** Phys. Lett. **54,** 2269 **(1989).**

**[74] T. Komatsu, C. Hirose, R. Sato** and **K. Matusita, J. Non-Cryst. Solids, 126,** 273 (1990).

**[75] T.** Komatsu, C. Hirose, T. Ohki, R. Sato, K. Matusita **and** T. **Yamashita, Appl.** Phys. Lett. 57, 183 (1990).

[76] S. E. LeBeau, J. Righi, J. E. Ostenson, S. C. **Saunders and D. K. Finnemore, Appl.** Phys. Lett. **55,** 292 (1989).

[77] H. Zheng, Yi Hu and J. D. Mackenzie, Appl. Phys. Lett. 58, 1679 (1991).

[78] Y. Abe, H. Honsono, M. Hosoe, J. Iwase and Y. Kubo, Appl. Phys. **Lett. 53, 1341** (1988).

[79] Y. Abe, H. Arakawa, M. Hosoe, Y. Hikichi, J. Iwase, H. Honsono and Y. Kubo, Jpn. J. Appl. Phys. 28, L1929 (1989).

[80] W. H. Lee and Y. Abe, Jpn. J. Appl. Phys. **30,** L697 (1991).

[81] Y. Abe, K. Hirata, H. Honsono and Y. Kubo, J. Mater. Res. 7, **1599** (1992).

[82] R. Wang, L. Sun and A. Liu, Mod. Phys. Lett. 7, 389 (1993).

[83] Y. Abe, H. Honsono W. H. Lee, M. Hosoe K. Nakamura and E. **Inukai, J. Mater.** Res. **8, 1** (1993).

[84] T. Komatsu, R.Sato, K. Imai, K.Matusita and T. Yamashita, Jpn. J. Appl. Phys. 27, L550 (1988).

[85] T. Komatsu, T. Ohki, K. Matusita and T. Yamashita, Nippon Seram. Kyokai Gakuj. Ronbun, 97, 251 (1989).

[86] N. Tohge, S. Tsuboi. Y. Akamatsu, M. Tatsumisago and T. Minami, **Nippon** Seram. Kyokai Gakuj. Ronbun, 97, 334 (1989).

**[87] T. Komatsu, K. Imai, R.** Sato, K. Matusita and T. Yamashita, **Jpn. J. Appl. Phys. 27, L533 (1988).**

**[88] T. Minami, Y. Akamatsu, M. Tatsumisago, N. Tohge and Y. Kowada, Jpn. J. Appl. Phys. 27, L777 (1988).**

**[89] D. G. Hink, L. Soderholm, D. W. Capone II, B. Dabrowski, A. W. Mitchell and D. Shi, Appl. Phys. Lett. 53, 423 (1988).**

[90] A. Inoue, H. Kimura, K. Matsuzaki, A. Tsai and T. Masumoto, Jpn. J. Appl. Phys. 27, L941 (1988).

[91] H. Zheng and J. D. Mackenzie, Phys Rev. B 38 7166 (1988).

[92] F. H. Garzon, J. G. Beery and I. D. Raistrick, Appl. Phys. Lett. **53**, 805 (1988).

[93] K. B. R. Varma, G. N. Subbana, T. V. Ramakrishnan and C. N. R. Rao, J. Appl. Phys. 55, 75 (1989).

[94] R. Singh and E. Zacharias, J. phys. D: Appl. Phys. 23, 199 (1990).

[95] R. Singh and E. Zacharias, Bull. Mat. Sci. 14 343 (1991).

[96] Y. Abe, H. Hosono, M. Hosoe, J. Iwase and Y. Osaka, J. Non-Cryst. Solids **105**, 185(1988).

[97] T. Kasuga and Y. Abe, J. Amer. Ceram. Soc. 76, 1885 (1993).

[98] W. H. Lee, H. Hosono and Y. Abe, Proc. 16th. Int. Congr. on Glass, Madrid, Spain, Vol.4. Sociedad Espanola de Ceramica y Vidrio, Madrid, Spain (1992).

[99] R. C.Baker, W. M. Hurg and H. Steinfink, Appl. Phys. lett. 54, 371 (1989).

[100] A. Bhargava, R. L. Snyder and A. K. Varshneya, Mater. Lett. 8, 425 (1989).

[101] A. Asthana, P. D. Han, Z. Xu, L. Chang, D. A. Payne and P. J. Gilbert, Mat. Res. Soc. Symp. Proc. 169, 329 (1990).

[102] A. Asthana, P. D. Han, Z. Xu, L. Chang, D. A. Payne and P. J. Gilbert, Physica C **174,** 33 (1991).

[103] A. E. Miller, K. Nassau and D. J. Werder, J. Mater. Res. 8, 973 (1992).

[104] C. J. Kim, M. R. DeGuire and N. P. Bansal, High temp. Superconductors: Fundamental Properties and Novel Materials Processing, MRS proceeding, (Ed. J. Narayan, C. W. Chu, L. F. Schneermeyer and D. K. Christen), **169,** 333 (1992).

[105] T. Kanai, T. Kumagai, A. Soeta, T. Suzuki, K. Aihara, T. Kamo and S. Matsuda, Jpn. J. Appl. Phys.27, L1435 (1988).

[106] T. Kasuga and Y. Abe, J. Amer. Ceram. Soc.76, 1885 (1993).

[107] K. B. R. Verma, G. N. Subbana, T. V. Ramakrishna and C. N. **R. Rao, J. Appl.** Phys. 55 75 (1989).

[108] A. Asthana, P. D. Han, L. Chang and D. A. Payne, Mat. Lett. 8 286 (1989).

**[109]** **W.** Wong-Ng, C. K. Chiang, S. W. Freiman, L. **P.** Cook **and M. D. Hill, Ceram. Bull.** August, 1261 (1992).

**[110]** **W.** Wong-Ng, C. K. Chiang, S. W. Freiman, L. P. Cook, N. **M. Hwang and M. D. Hill,** Superconductivity, Proc. First Int. Ceramic Science **and** Technology Congr., Anahem, Calif., U.S.A p.115 (1990).

[111] W. Wong-Ng, C. K. Chiang, S. W. Freiman, L. P. Cook, N. **M. Hwang and M. D. Hill,** Mater. Res. Soc. Symp. Proc. **169,** 123 (1990).

[112] Y. Massalker, A. N. Sembira and J. Baram, J. Mater. Res. 8, 2445 (1993).

**[113]** J. Danusantoso and T. K. Chaki, Supercond. Sci. Technol. **4,** 509 **(1991).**

[114] T. Komatsu and K. Matusita, Thermochim. Acta. **174,** 131 (1991).

[115] I. Matsubara, H. Kageyama, H. Tanigawa, T. Ogura, H. Yamashita and T. Kawai, Jpn. J. Appl. Phys. **28**. L1121 (1989).

[116] T. Komatsu, T. Ohki, C. Hirose and K. Matusita, J. Non-Cryst. Solids. **113,** 274 (1989).

[117] Y. Ibara, H. Nasu and T. Imura, Jpn. J. Appl. Phys. **28,** 274 (1989).

[118] R. Sato, T. Komatsu, K. Matushita and T. Yamashita, Jpn. J. Appl. Phys. **28,** L583 (1989).

[119] C. K. Chiang, W. Wong-Ng, L. P. Cook, S. W. Freiman, N. M. **Hwang** and M. D. Hill, Advances in Mater. Sci. and Appl. of High Temp. Supercond., NASA Conf. Publ. 3100, p.127 (1990).

[120] M. Tatsumisago, C. A. Angell, Y. Akamatsu, S. Tsuboi, N. Toghe and T. Minarni, Appl. Phys. Lett. 55 600 (1989).

[121] T. Komatsu, R. Sato, Y. Kuken and K. Matusita, J. Amer. Ceram. Soc. **76,** 2795 (1993).

**[122]** H. Zheng and J. D. Mackenzie, Phys. Rev. B **43** 3048 (1991).

**[123]** M. R. DeGuire, N. P. Bansal and C. J. Kim, J Amer. Ceram. Soc. **73, 1165 (1990).**

**[124]** **R. Sato, T.** Komatsu, Y. Kuken, K. Matusita, K.Sawada **and M. Hiraoka, J. Non. Cryst.** Solids **152** 150 (1993).

**[125]** **T. G. Holesinger, D. J. Miller and L. S. Chumbley, J. Mater. Res. 7, 1658 (1992).**

[126] H. Nobumasa, K. Shimizu, Y. Kitano and T. Kawai, Jpn. J. Appl. Phys. 27, L846 (1988).

[127] H. Zheng, M. W. Colby and J. D. Mackenzie J. Non. Cryst. Solids **127** 143 (1991).

[128] N. P. Bansal, J. Appl. Phys. 68, 114 (1990).

[129] Y. L. Chen and R. Stevens, J. Amer. Ceram. Soc. 75, 1142 (1992).

[130] Y. L. Chen and R. Stevens, J. Amer. Ceram. Soc. 75, 1150 (1992).

[131] Y. L. Chen and R. Stevens, J. Amer. Ceram. Soc. 75, 1160 (1992).

[132] J. S. Luo, N. Merchant, V. A. Maroni, D. M. Gruen, B. S. Tani, W. L. Carter and G. N. Riley, J. Appl. Supercond. Sci. Technol. 1, 101 (1993).

[133] H. Takei, M. Koike, H. Takeya, K. Suzuki and M. Ichihara, Jpn. J. Appl. Phys. **28,** L1193 (1989).

[134] U. Endo, S. Koyama and T. Kawai, Jpn. J. Appl. Phys. 28, 1190 (1989).

[135] Y. Oka, N. Yamamoto, H. Kitaguchi, K. Oda and J. Takada, Jpn. J. Appl. Phys. 28, L213 (1989).

[136] D. P. Matheis, S. T. Misture and R. L. Snyder, Physica C **207,** 134 (1993) and references herein.

[137] L. D. Bolgomolova, M. P. Glasova, V. M. Kalygina, S. I. Reiman, S. N. Spasibkina and I. V. Filatova, J. Non. Cryst. Solids 58, 71 (1983).

[138] L. D. Bolgomolova, M. P. Glasova, V. M. Kalygina, S. I. Reiman, S. N. Spasibkina and I. V. Filatova, J. Non. Cryst. Solids 85, 170 (1986).

[139] R. Singh and K. Sethupathi, J. Phys. D: Appl. Phys. 22, L709 (1989).

[140] L. H. Greene and B. G. Bagley, in 'Physical properties of High Temp. Supercond. II' edited: D. M. Ginsberg (World Scientific, Singapore) (1990).

[141] A. V. Narlikar, C. V. Narasimha Rao and S. K. Agarwal, in 'Studies on High Temp. Supercond.' Vol.1 edited: A. V. Narlikar (Nova Science, NY) p.341 (1989).

[142] K. Wasterholt, M. Arndt, H. J. Weller et al, Physica C **153-155,** 862 (1988).

[143] F. Izumi, H. Asano, T. Ishigaki, E. Takayama, Muromachi, Y. Uchida, W. Watanabe and T. Nishikawa, Jpn. J. Appl. Phys. 26, L649 (1987).

[144] R. S. Howland, T. H. Gaballe, S. S. Laderman, A. Fischer-Colbrie, M. Scott, J. M. Tarascon and P. Barboux, Phys. Rev. B 39, 9017 (1989).

[145] F. Bridges, J. B. Boyce, T. Claeson, T. H. Gaballe and J. M. Tarascon, Phys. Rev. B 42, 2137 (1990).

[146] K. Uchinokura, T. Yabe, S. Takebayashi, M. Hase and A, Maeda, Physica C **162-**164,981 (1989).

[147] T. E. Jones, P. M. Thibado, W. C. Mcginnis, R. D. Boss, J. W. Schindler and S. Oseroff, Physica C **162-164,** 25 (1989).

[148] A. Maeda, T. Yabe, S. Takebayashi, M. Hase and K. Uchinokura, Phys. Rev. B 41,4112 (1990).

[149] S. K. Agarwal, V. N. Moorthy, G. L. Bhalla, V. P. S. Awana and A. V. Narlikar, Ind. J. Pure and Appl. Phys. 30, 586 (1992).

[150] P. S. Prabhu, M. S. R. Rao and G. V. S. Rao, Physica C **211,** 279 (1993).

[151] M. G. Britton, 'Glass as an engineering material' (Wiley Interscience, New York), (1972).

[152] Turnbel and M. H. Cohen, J. Chem. Phys. 29, 1049 (1958).

[153] Rawson, 'Inorganic glass forming systems' (1967).

[154] W. H. Zachariason, J. Arner. Chem. Soc. 54, 3841 (1932).

[155] H. Hirashima, Y. Watanabe and T. Yoshida, J. Non, Cryst. Solids **95-96,** 825 (1987).

[156] Y. Sakurai and J. Yamaki, J. Electrochem. Soc. **132,** 512 (1985).

[157] N. F. Mott, J. Non-Cryst. Solids 1, 1 (1968).

[158] I. G. Austin and N. F. Mott, Adv. Phys. 18, 41 (1969).

[159] J. D. Mackenzie, 'Modern aspects of vitreous state', vol.3 (Washington, Butterworth) 126 (1964).

[160] L. Murawski, C. H. Chung and J. D. Mackenzie, J. Non-Cryst. Solids **32, 91** (1979).

[161] M. Munakata, Solid State Electron. 1, 159 (1960).

[162] A. P. Schmid, J. Appl. Phys. 39, 3140 (1968); 40, 4128 (1969).

**[163] G. S. Linsley, A. E. Owen and F. M. Hayatee, J. Non-Cryst. Solids 4, 208 (1970).**

**[164] G. W. Anderson and W. D. Compton, J. Chem. Phys. 52, 6166 (1970).**

**[165] M. Sayer, A. Mansingh, J. M. Reyes and G. Rosenblatt, J. Appl. Phys. 42, 2857 (1971).**

**[166] M. Sayer and A. Mansingh, Phys. Rev. B 6, 4629 (1972).**

**[167] C. H. Chung** and **J. D. Mackenzie, Rev.** Chim. **Min 16, 308 (1979).**

**[168] V. K. Dhawan,** A. Mansingh and **M.** Sayer, J. Non-Cryst. Solids **51, 87 (1982).**

**[169]** L. **Murawski, J.** Mat. Sci. **17, 2155** (1982).

**[170] R. Singh, J.** Phys. **D: Appl.** Phys. **17,** L57 (1984).

**[171] K. W.** Hansen, **J.** Electrochern. Soc. **112, 10** (1965); **113, 9 (1966).**

**[172] D. L. Kinser, J.** Electrochem. Soc. **117,** 546 **(1970); 117, 1586 (1970).**

[173] E. **J.** Friebele, **I** . K. Wilson, A. K. Dozier and **D. L.** Kinser, Phys. **Status. Solidi. 45,323 (1971).**

**[174] R. H.** Caley and **J.** Can, Ceram. Soc. **39,** 7 (1970).

**[175] A. Mansingh, J. K.** Vaid and **R. P.** Tandon, **J.** Phys. C: **Solid State Phys. 10, 4061 (1977).**

**[176]** A. Mansingh, A. Dhawan, **R.** P. Tandon and J. K. Vaid, J. **Non-Cryst.** Solids **27, 309** (1978)

**[177]** A. Mansingh,R. P. Tandon and J. K. Vaid, Phys. Rev. **B 21, 4829 (1980).**

**[178] A. Ghosh, Philosophical Magazine B 61, 87 (1990).**

**[179] R. Singh and J. S.** Chakravarthi, Phys. Rev. **B (1995) (in press)**

**[180] A. Duran, J. R.** Jurado **and J. M. F. Navarro, J. Non-Cryst. Solids 79, 333 (1986).**

**[181] A. Ghosh, J. Phys. Condens. Matter 1, 7819 (1989).**

**[182] A. Ghosh and D. Chakravorty, J. Phys. Condens. Matter 2, 931 (1990).**

**[183] C. F. Drake,I. F. Scalan and A. Angel, Phys. Stat. Solidi 32, 193 (1969).**

**[184] T. Komatsu, R. Sato, K. Matusita and T. Yaashita, Appl. Phys. Lett. 54, 1169 (1989).**

[185] A. Bishay and C. Maghrabi, Phys. and Chem. of Glasses 10, 1 (1969).

[186] H. Zheng, R. Xu and J. D. Mackenzie, J. Mater. Res. 4, 911 (1989).

[187] F. Miyaji, T. Yoko and S. Sakka, J. Non-Cryst. Solids, 126, 170 (1990).

[188] G. Malmros, Acta. Chem. Scand. **24**, 384 (1970).

[189] D. J. Segal, R. P. Santoro and R. E. Newham, Z. Kristallogr. **118,** 291 (1963).

[190] J. Schnakenberg, Phys Stat. Solidi 28, 623 (1968).

[191] N. F. Mott and E. A. Davis, Electronic process in Non-Crystalline Solids $2^{nd}$ ed. (Clarendon Press. Oxford) (1979).

[192] T. Holstein, Ann. Phys., 8, 343 (1959).

[193] D. Emin and T. Holstein, Ann. Phys., 53, 439 (1969).

[194] L. Friedman and T. Holstein, Ann. Phys (NY) 21, 494 (1963).

[195] G.N. Greaves, J. Non-Cryst. Solids 11, 427 (1973); 51, 87 (1982).

[196] G. P. Triberis and L. R. Friedman, J. Phys. C: Solid State Phys. 14, 4631 (1985).

[197] G. P. Triberis and L. R. Friedman, J. Phys. C: Solid State Phys. 18, 2281 (1981).

[198] G. P. Triberis, J. Non-Cryst. Solids **104,** 135 (1988).

[199] V. N. Bogomolova, E. K. Kudinov and Y. A. Frisov, Sov. Phys.-Solid State 9, 3175 (1967).

[200] A. Miller and S. Abrahams, Phys. Rev. **120,** 745 (1960).

[201] J. Appel, Solid State Phys. 21, 193 (1968).

[202] P. J. Bray et al, 'Glass Science and Technology' editor: D. R. Uhlmann and N. J. Kreidl, voUB p.188 (1990).

[203] P. J. Bray et al, 'Glass Science and Technology' editor: D. R. Uhlmann and N. J. Kreidl, voUB p.182 (1990).

[204] P. J. Bray et al, 'Glass Science and Technology' editor: D. R. Uhlmann and N. J. Kreidl, voUB p.180 (1990).

[205] D. L. Griscom, J. Non-Cryst. Solids 40, 211 (1980).

[206] Imagawa, Phys. Stat. Sol. 30, 469 (1968).

[207] D. Vier et al, Phys Rev. B 36, 8888 (1987) and references therein; P. Simon et al, Phys Rev. B 48, 4216 (1993) and references therein.

[208] F. Mehran and P. W. Anderson, Solid State Commun. 71, 29 (1989).

[209] F. Mehran et al, Solid State Commun. 67, 1187 (1988); F. Mehran et al, ibid. 76, 55 (1988); R. Janes, K. K. Singh, S. D. Burnside and P. P. Edwards, Solid State Commun. 79,241 (1991).

[210] D. Loveridge and S. Parke, Phys. Chem. Glasses 12, 19 (1971).

[211] C. Hirayama, J. G. Castle and M. Kuriyama, Phys. Chem. Glasses 9, 109 (1968).

[212] N. P. Bansal, R. H.Doremus, A. J. Bruce and C. T. Moynihan, J. Amer. Ceram. Soc. 66 (1983) 233.

[213] J. M. Tarascon, Y. Le Page, P. Barboux, B. G. Bagley, L. H. Greene, W. R. McKinnon, G. W. Hull, M. Girond and D. M. Hwang, Phys. Rev. B 37 (1988) 9382.

[214] M. Ruzhang, Li Yang, C. Guohui, F. Yongrong and L. Weidong, Solid State Commun. 75,53 (1990).

[215] K. Remschnig, J. M. Tarascon, P. F. Miceli, G. W. Hull and W. R. McKinnon, Phys. Rev. B 43, 5481 (1991).

[216] S. Chakravarty and R. Orbach, Phys. Rev. Lett. 64, 224 (1990).

[217] A. V. Lazuta, Physica C 181, 127 (1991).

[218] S. A. Kivelson et al, Phys. Rev. B 35, 8865 (1987); K. W. H. Stevens, Czech. J. Phys. 41, 819 (1991); W. R. McKinnon et al, 66, 1093 (1988).

[219] K. Nassau, A. E. Miller, E. M. Gyorgy and T. Siegrist, J. Mat. Res. 4 (1989) 1330.

[220] R. S. Roth, C. Rawn, B. P. Burton and F. Beech, J. Res. Natnl. Inst. Stand. Technol. 95,291 (1990).

[221] M. Mehbod, W. Biberaker, A. G. M. Jansen *et. al.*, Phys. Rev. B 38, 1181 (1988).

[222] J. B. Torrance, Y. Tokura, N. I. Nazzal *et. al.*, Phys. Rev. Lett. 61, 1127 (1988).

[223] P. W. Anderson, Phys. Rev. Lett. 67, 2092 (1991).

[224] H. Fukuyama, Physica B+C, 126B, 306 (1984).

[225] W. Brenig, M. A. Paalanen, A. F. Hebard and P. Wolfe, Phys Rev. B. 33, 1691 (1986).

[226] R. Yoshizaki, J. Fujikama, T. Ishigaki and H.Asano, Physica C 171, 315 (1990).

[227] H. Alloul, P. Mendels, H. Casalta, J. F. Marucco and J. Arabski, Phys. Rev. Lett. 67,3140(1991).

[228] Y. 0. Nakamura, N. Matsuda and Y. Shiina, Solid State Commun. **81**, 923 (1992).

[229] A.A. Abrikosov and L. P. Gorkov, Zh. Eksperimi. Toer. Fiz. 39, 1781 (1960); Sov. Phys. JETP 12, 1243 (1961)

[230] M. Arpinwadkar, G. Bhaskaran, R. Basu and V. N. Muthukumar, Phys. Rev. Lett. 70,674 (1993).

[231] S. L. Cooper, P. Nythus, D. Reznik, M. V. Klein, W. C. Lee, D. M. Ginsberg, B. W. Veal, A. P. Paulikas and B. Dabrowski, Phys. Rev. Lett. 70, 1533 (1993).